Dynamics of Ice Sheets and Glaciers

Ralf Greve

Institute of Low Temperature Science

Hokkaido University

Lecture Notes

Sapporo 2010

These lecture notes are largely based on the textbook

- Greve, R. and H. Blatter. 2009. *Dynamics of Ice Sheets and Glaciers.* Springer, Berlin, Germany etc. ISBN 978-3-642-03414-5.

Further recommended textbooks are:

- Hooke, R. LeB. 2005. *Principles of Glacier Mechanics.* Cambridge University Press, Cambridge, UK and New York, NY, USA, 2nd edition.
- Paterson, W. S. B. 1994. *The Physics of Glaciers.* Pergamon Press, Oxford, UK etc., 3rd edition.
- Van der Veen, C. J. 1999. *Fundamentals of Glacier Dynamics.* A. A. Balkema, Rotterdam, The Netherlands.

Contents

1 Introduction

General Definitions

- *(Inland-) Ice sheets*
  → land-based ice masses of continental size, area > 50,000 km^2 (Antarctica, Greenland).
- *Ice shelves*
  → floating ice masses, connected to an ice sheet (Antarctica).

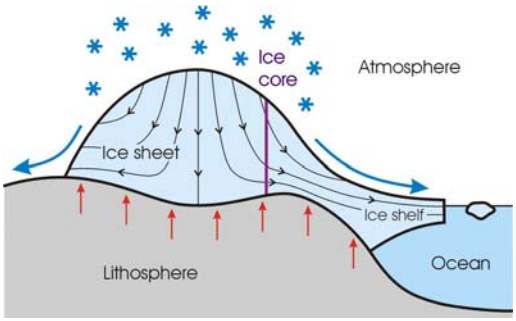

General Definitions

- *Ice caps*
  → extended land-based ice masses, area < 50,000 km^2 (Austfonna, Vatnajökull, North/South Patagonian Icefields...).
- *Glaciers*
  → small land-based ice masses in mountainous regions, constrained by topographical features.

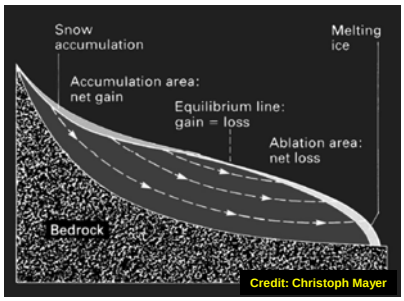

Remark: “Glacier” is sometimes also used as an umbrella term for all land-based ice bodies (ice sheets, ice caps and glaciers as defined above).

Ice Sheets

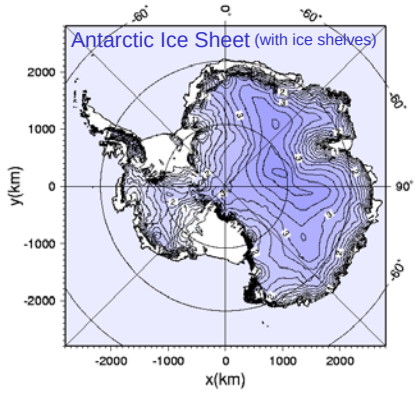

Volume 25.4×10^6 km^3,
area 13.8×10^6 km^2.

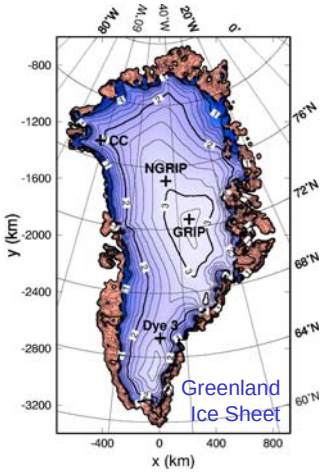

Volume 2.9×10^6 km^3,
area 1.7×10^6 km^2.

Glaciers and Ice Caps

- Can be found on every continent (polar/subpolar areas, mountains).
- Number: > 160,000 (~ 70 ice caps).
- Many different types:
  Valley glaciers, cirque glaciers, hanging glaciers, tidewater glaciers, rock glaciers…

Photo credit: www.glaciers-online.net

Ice Inventory

	Glaciers and ice caps	Greenland Ice Sheet	Antarctic Ice Sheet (+ shelves)
Area (10^6 km^2)	0.51 - 0.54	1.7	12.3 (+ 1.5)
Volume (10^6 km^3)	0.05 - 0.13	2.9	24.7 (+ 0.7)
Sea level equivalent (m)	0.15 - 0.37	7.3	56.6 (+ 0)
Sea level rise 1993 - 2003 (mm/a)	0.77 ± 0.22	0.21 ± 0.07	0.21 ± 0.35

Sources: Lemke et al. (2007) [IPCC AR4 Ch. 4], Bindoff et al. (2007) [IPCC AR4 Ch. 5].

Spatial Scales and Response Times

Source: Lemke et al. (2007) [IPCC AR4 Ch. 4]

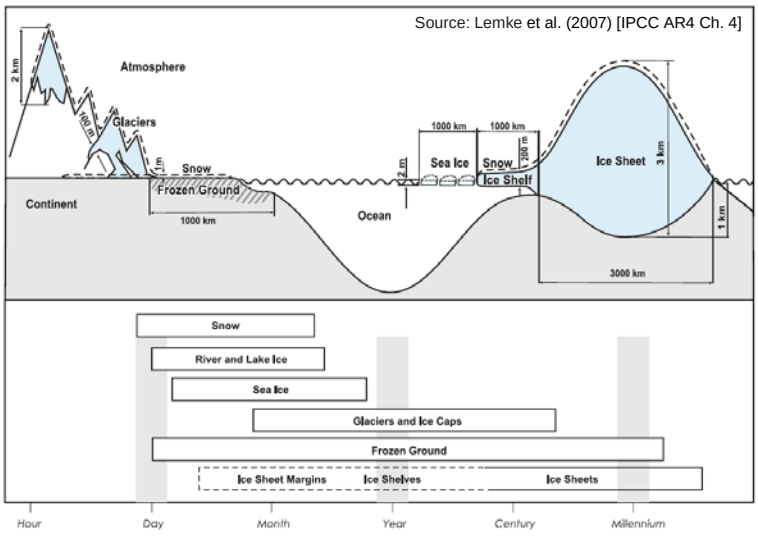

2 Elements of Continuum Mechanics

2.1 Bodies and Configurations

Continuum mechanics is concerned with the motion and deformation of continuous *bodies* (for instance, a glacier). A body consists of an infinite number of material elements, called *particles*. For any time t, each particle is identified by a position vector $\mathbf{x}$ (relative to a prescribed origin O) in the physical space $\mathcal{E}$, and the continuous set of position vectors for all particles of the body is called a *configuration* κ of the body. If t is the actual time, the corresponding configuration is called the *present configuration* κ_t. In addition, we define a *reference configuration* κ_r which refers to a fixed (or initial) time t_0. Position vectors in the reference configuration will be written in capitals, for example as $\mathbf{X}$; they can be used for identifying the individual particles of the body, independent of the actual time. Note that different sets of basis vectors ($\{\mathbf{E}_A\}_{A=1,2,3}$, $\{\mathbf{e}_i\}_{i=1,2,3}$) and different origins may be used in the two configurations (Fig. 2.1).

The mapping $\boldsymbol{\chi}$ which provides the position $\mathbf{x}$ of each particle at time t as a function of its reference position $\mathbf{X}$ is called the *motion* of the body,

$$\begin{aligned} \boldsymbol{\chi}: \quad & \kappa_r \to \kappa_t \\ & \mathbf{X} \to \mathbf{x} = \mathbf{x}(\mathbf{X}, t)\,. \end{aligned} \tag{2.1}$$

It is assumed that the motion $\mathbf{x}(\mathbf{X}, t)$ is continuously differentiable in the entire body (with the possible exception of discrete singular lines or surfaces), and that the inverse mapping

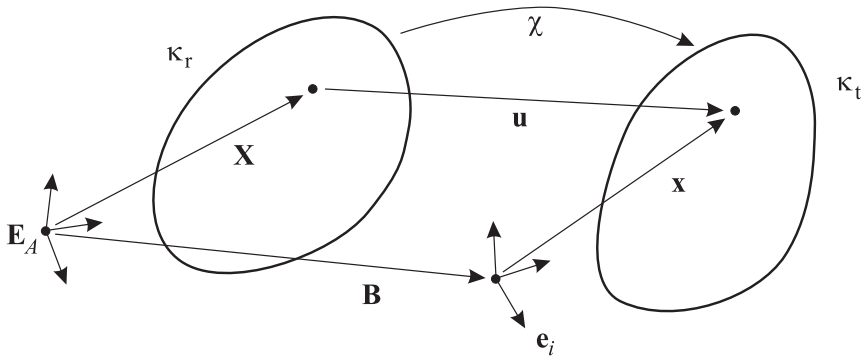

Figure 2.1: Bodies, reference configuration κ_r and present configuration κ_t.

$\boldsymbol{\chi}^{-1}$ exists:

$$\boldsymbol{\chi}^{-1}: \quad \begin{array}{l} \kappa_t \to \kappa_r \\ \mathbf{x} \to \mathbf{X} = \mathbf{X}(\mathbf{x}, t)\,. \end{array} \tag{2.2}$$

The *displacement* is defined as the connecting vector between a given particle in the reference and present configuration. If the connecting vector between the two origins of the basis systems is denoted by $\mathbf{B}$, then

$$\mathbf{u} = \mathbf{x} - \mathbf{X} + \mathbf{B} \tag{2.3}$$

holds. The above relations are illustrated in Fig. 2.1.

Of course, in a deformable body the displacement at time t will in general be different for different particles, so that it can be written as the vector field $\mathbf{u} = \mathbf{u}(\mathbf{X}, t)$. However, this is not the only possibility. Equation (2.2) shows that $\mathbf{X}$ can be expressed in terms of $\mathbf{x}$ and t, so that we can also assume the displacement field as a function of $\mathbf{x}$ and t, that is, $\mathbf{u} = \mathbf{u}(\mathbf{x}, t)$. These two possibilities also hold for other field quantities ψ (density, temperature, velocity etc.), and we call $\psi(\mathbf{X}, t)$ the *Lagrangian* or *material description*, whereas $\psi(\mathbf{x}, t)$ is referred to as the *Eulerian* or *spatial description*. Most frequently, for solid bodies the Lagrangian description is used, whereas the Eulerian description is more appropriate for problems of fluid dynamics (like glacier flow).

2.2 Kinematics

2.2.1 Deformation Gradient

The *deformation gradient* F is defined as the material gradient (gradient with respect to $\mathbf{X}$) of the motion (2.1),

$$\mathsf{F} = \operatorname{Grad} \mathbf{x}(\mathbf{X}, t)\,, \tag{2.4}$$

or in components

$$F_{iA} = \frac{\partial x_i(\mathbf{X}, t)}{\partial X_A} = x_{i,A}\,, \tag{2.5}$$

where $\mathsf{F} = F_{iA}\, \mathbf{e}_i\, \mathbf{E}_A$, the operator $\operatorname{Grad}(\cdot)$ is the material gradient, and the notation $(\cdot)_{,A}$ means the partial derivative $\partial(\cdot)/\partial X_A$. Note that small indices generally refer to the present configuration and capital indices to the reference configuration. The deformation gradient is a tensor field of order 2.

According to definition (2.4), the deformation gradient F can be interpreted as the functional matrix of the motion function (2.1). It transforms line elements from the reference configuration ($\mathrm{d}\mathbf{X}$) to the present configuration ($\mathrm{d}\mathbf{x}$),

$$\mathrm{d}\mathbf{x} = \mathsf{F} \cdot \mathrm{d}\mathbf{X}\,, \quad \text{or} \quad \mathrm{d}x_i = F_{iA}\, \mathrm{d}X_A\,, \tag{2.6}$$

which is illustrated in Fig. 2.2.

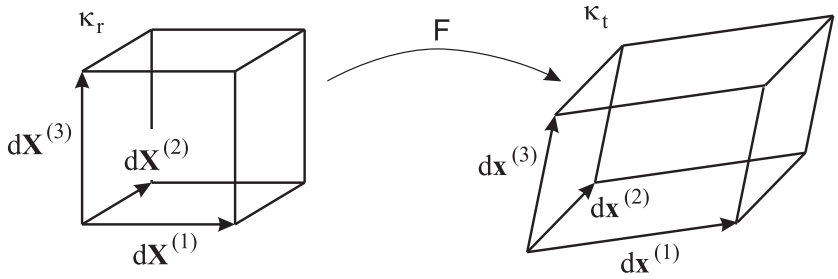

Figure 2.2: Deformation gradient: Transformation between line and volume elements in the reference and present configuration.

The determinant of the deformation gradient, called the *Jacobian*, is given by

$$J = \det \mathsf{F}\,, \quad \text{or} \quad J = \tfrac{1}{6}\varepsilon_{ijk}\varepsilon_{ABC}F_{iA}F_{jB}F_{kC}\,; \tag{2.7}$$

for the component form on the right see Eq. (A.43). Since we have ensured that the motion function is invertible, J must be different from zero, and the inverse deformation gradient F^{-1} exists. Further, real motions cannot invert the orientation, so that

$$J > 0 \tag{2.8}$$

must hold. The Jacobian determines the local volume change due to the motion,

$$\mathrm{d}v = J\,\mathrm{d}V\,, \tag{2.9}$$

where $\mathrm{d}V$ is the volume element in the reference configuration which may be spanned by three line elements $\mathrm{d}\mathbf{X}^{(1)}$, $\mathrm{d}\mathbf{X}^{(2)}$, $\mathrm{d}\mathbf{X}^{(3)}$, and $\mathrm{d}v$ is the volume element in the present configuration spanned by $\mathrm{d}\mathbf{x}^{(1)}$, $\mathrm{d}\mathbf{x}^{(2)}$, $\mathrm{d}\mathbf{x}^{(3)}$ (Fig. 2.2).

2.2.2 Velocity, Acceleration, Velocity Gradient

As usual, we define the *velocity* $\mathbf{v}$ as the first time derivative of the position $\mathbf{x}$ [motion (2.1)],

$$\mathbf{v} = \mathbf{v}(\mathbf{X}, t) = \frac{\partial \mathbf{x}(\mathbf{X}, t)}{\partial t}\,, \tag{2.10}$$

and the *acceleration* $\mathbf{a}$ as its second time derivative,

$$\mathbf{a} = \mathbf{a}(\mathbf{X}, t) = \frac{\partial^2 \mathbf{x}(\mathbf{X}, t)}{\partial t^2} = \frac{\partial \mathbf{v}(\mathbf{X}, t)}{\partial t}\,. \tag{2.11}$$

Evidently, this yields the velocity and acceleration fields in Lagrangian description. By inserting the inverse motion (2.2) one can readily obtain the corresponding Eulerian descriptions $\mathbf{v}(\mathbf{x}, t)$ and $\mathbf{a}(\mathbf{x}, t)$.

The time derivatives in Eqs. (2.10) and (2.11) are taken for fixed material position vectors $\mathbf{X}$. We will call this the *material time derivative*, denoted briefly by the operators $\mathrm{d}(\bullet)/\mathrm{d}t$ or $(\bullet)^{\cdot}$. Therefore, for any field quantity ψ,

$$\dot{\psi} = \frac{\mathrm{d}\psi}{\mathrm{d}t} = \frac{\partial \psi(\mathbf{X}, t)}{\partial t} \,. \tag{2.12}$$

For example, Eqs. (2.10) and (2.11) read

$$\mathbf{v} = \dot{\mathbf{x}} = \frac{\mathrm{d}\mathbf{x}}{\mathrm{d}t} \,, \qquad \mathbf{a} = \ddot{\mathbf{x}} = \frac{\mathrm{d}^2\mathbf{x}}{\mathrm{d}t^2} = \dot{\mathbf{v}} = \frac{\mathrm{d}\mathbf{v}}{\mathrm{d}t} \,. \tag{2.13}$$

By contrast, the operator $\partial(\bullet)/\partial t$ denotes the *local time derivative* for fixed spatial position vector $\mathbf{x}$,

$$\frac{\partial \psi}{\partial t} = \frac{\partial \psi(\mathbf{x}, t)}{\partial t} \,. \tag{2.14}$$

With the chain rule, the relation between the material and local time derivative is

$$\begin{aligned} \frac{\mathrm{d}\psi}{\mathrm{d}t} &= \frac{\mathrm{d}}{\mathrm{d}t} \psi(\mathbf{x}(\mathbf{X}, t), t) \\ &= \frac{\partial \psi(\mathbf{x}, t)}{\partial t} + \operatorname{grad} \psi(\mathbf{x}, t) \cdot \frac{\mathrm{d}\mathbf{x}(\mathbf{X}, t)}{\mathrm{d}t} \\ &= \frac{\partial \psi}{\partial t} + (\operatorname{grad} \psi) \cdot \mathbf{v} \,, \end{aligned} \tag{2.15}$$

where the operator $\operatorname{grad}(\cdot)$ is the spatial gradient, of which the components are the partial derivatives $(\cdot)_{,i} = \partial(\cdot)/\partial x_i$. One says that the material time derivative $\mathrm{d}\psi/\mathrm{d}t$ is composed of a local part $\partial\psi/\partial t$ and an advective part $(\operatorname{grad}\psi) \cdot \mathbf{v}$.

Relation (2.15) is equally valid if ψ is a vector or tensor field. Therefore, for the acceleration expressed by Eq. $(2.13)_2$,

$$\mathbf{a} = \frac{\partial \mathbf{v}}{\partial t} + (\operatorname{grad} \mathbf{v}) \cdot \mathbf{v} \,. \tag{2.16}$$

The tensor quantity

$$\mathsf{L} = \operatorname{grad} \mathbf{v} = \frac{\partial v_i}{\partial x_j} \, \mathbf{e}_i \, \mathbf{e}_j = v_{i,j} \, \mathbf{e}_i \, \mathbf{e}_j \tag{2.17}$$

which appears in Eq. (2.16) is called the *velocity gradient*. It is related to the material time derivative of the deformation gradient as follows,

$$\begin{aligned} &\dot{F}_{iA} = \frac{\partial^2 x_i(\mathbf{X}, t)}{\partial t \, \partial X_A} = \frac{\partial v_i(\mathbf{X}, t)}{\partial X_A} = \frac{\partial v_i(\mathbf{x}, t)}{\partial x_j} \frac{\partial x_j(\mathbf{X}, t)}{\partial X_A} = \frac{\partial v_i(\mathbf{x}, t)}{\partial x_j} \, F_{jA} \\ &\Rightarrow \; \dot{\mathsf{F}} = \mathsf{L} \cdot \mathsf{F} \,, \quad \text{or} \quad \mathsf{L} = \dot{\mathsf{F}} \cdot \mathsf{F}^{-1} \,. \end{aligned} \tag{2.18}$$

Without proof, we note that the material time derivative of the Jacobian is

$$\dot{J} = J \operatorname{div} \mathbf{v} = J \operatorname{tr} \mathsf{L} \tag{2.19}$$

[$\operatorname{div}\mathbf{v} = v_{i,i} = L_{ii} = \operatorname{tr}\mathsf{L}$; for the definition of the trace of a tensor see Eq. $(A.42)_1$]. In words, the divergence of the velocity field determines local volume changes [see also Eq. (2.9)], which is a very intuitive result.

Like any arbitrary tensor, the velocity gradient can be additively decomposed into unique symmetric and antisymmetric parts,

$$\mathsf{L} = \mathsf{D} + \mathsf{W}\,, \tag{2.20}$$

with

$$\begin{aligned} \mathsf{D} &= \tfrac{1}{2}(\mathsf{L} + \mathsf{L}^{\mathrm{T}}) \qquad (\text{“strain-rate tensor” or “stretching tensor”})\,, \\ \mathsf{W} &= \tfrac{1}{2}(\mathsf{L} - \mathsf{L}^{\mathrm{T}}) \qquad (\text{“spin tensor”})\,. \end{aligned} \tag{2.21}$$

Evidently, $\mathsf{D} = \mathsf{D}^{\mathrm{T}}$ (symmetry) and $\mathsf{W} = -\mathsf{W}^{\mathrm{T}}$ (antisymmetry) are fulfilled.

In order to give an interpretation of the elements of the matrix of the strain-rate tensor D (with respect to a given orthonormal basis $\{\mathbf{e}_i\}$), we now compute the material time derivative of line elements $\mathrm{d}\mathbf{x}$ in the present configuration:

$$(\mathrm{d}\mathbf{x})^{\cdot} = \dot{\mathsf{F}} \cdot \mathrm{d}\mathbf{X} = \mathsf{L} \cdot \mathsf{F} \cdot \mathrm{d}\mathbf{X} = \mathsf{L} \cdot \mathrm{d}\mathbf{x} \tag{2.22}$$

[where Eqs. (2.6), (2.18) and $(\mathrm{d}\mathbf{X})^{\cdot} = \mathbf{0}$ were used]. For the scalar product between two line elements $\mathrm{d}\mathbf{x}^{(1)}$ and $\mathrm{d}\mathbf{x}^{(2)}$, this yields

$$\begin{aligned} (\mathrm{d}\mathbf{x}^{(1)} \cdot \mathrm{d}\mathbf{x}^{(2)})^{\cdot} &= (\mathrm{d}\mathbf{x}^{(1)})^{\cdot} \cdot \mathrm{d}\mathbf{x}^{(2)} + \mathrm{d}\mathbf{x}^{(1)} \cdot (\mathrm{d}\mathbf{x}^{(2)})^{\cdot} \\ &= (\mathsf{L} \cdot \mathrm{d}\mathbf{x}^{(1)}) \cdot \mathrm{d}\mathbf{x}^{(2)} + \mathrm{d}\mathbf{x}^{(1)} \cdot (\mathsf{L} \cdot \mathrm{d}\mathbf{x}^{(2)}) \\ &= \mathrm{d}\mathbf{x}^{(1)} \cdot \mathsf{L}^{\mathrm{T}} \cdot \mathrm{d}\mathbf{x}^{(2)} + \mathrm{d}\mathbf{x}^{(1)} \cdot \mathsf{L} \cdot \mathrm{d}\mathbf{x}^{(2)} \\ &= 2\,\mathrm{d}\mathbf{x}^{(1)} \cdot \mathsf{D} \cdot \mathrm{d}\mathbf{x}^{(2)}\,. \end{aligned} \tag{2.23}$$

Let us assume

$$\begin{aligned} \mathrm{d}\mathbf{x}^{(1)} &= \mathbf{n}^{(1)}\mathrm{d}s^{(1)}\,, \\ \mathrm{d}\mathbf{x}^{(2)} &= \mathbf{n}^{(2)}\mathrm{d}s^{(2)}\,, \end{aligned} \qquad \mathbf{n}^{(1)} \cdot \mathbf{n}^{(2)} = \cos((\pi/2) - \gamma) = \sin\gamma\,, \tag{2.24}$$

where $\mathbf{n}^{(1)}$, $\mathbf{n}^{(2)}$ are unit vectors, and γ is the deviation of the angle between $\mathbf{n}^{(1)}$ and $\mathbf{n}^{(2)}$ from a right angle. Equation (2.23) then reads

$$\begin{aligned} &(\sin\gamma\,\mathrm{d}s^{(1)}\mathrm{d}s^{(2)})^{\cdot} = 2\mathrm{d}s^{(1)}\mathrm{d}s^{(2)}\,\mathbf{n}^{(1)} \cdot \mathsf{D} \cdot \mathbf{n}^{(2)} \\ &\Rightarrow\ \dot{\gamma}\cos\gamma + \sin\gamma\left(\frac{(\mathrm{d}s^{(1)})^{\cdot}}{\mathrm{d}s^{(1)}} + \frac{(\mathrm{d}s^{(2)})^{\cdot}}{\mathrm{d}s^{(2)}}\right) = 2\mathbf{n}^{(1)} \cdot \mathsf{D} \cdot \mathbf{n}^{(2)}\,. \end{aligned} \tag{2.25}$$

We first make the special choice $\mathbf{n}^{(1)} = \mathbf{n}^{(2)} = \mathbf{e}_x$ ($\gamma = 90°$) and $\mathrm{d}s^{(1)} = \mathrm{d}s^{(2)} = \mathrm{d}s$ (Fig. 2.3, left). Then,

$$2\frac{(\mathrm{d}s)^{\cdot}}{\mathrm{d}s} = 2\mathbf{e}_x \cdot \mathsf{D} \cdot \mathbf{e}_x \quad \Rightarrow \quad D_{xx} = \frac{(\mathrm{d}s)^{\cdot}}{\mathrm{d}s}\,. \tag{2.26}$$

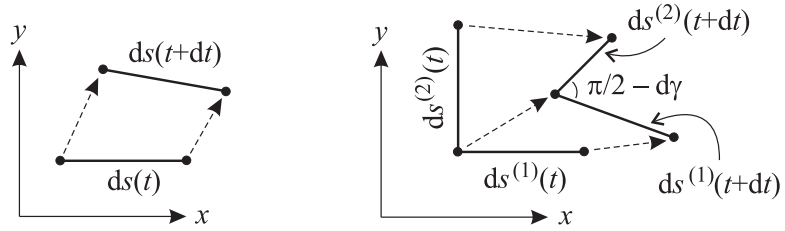

Figure 2.3: Dilatation (left) and shear (right) of line elements in the present configuration.

Analogous results are found for the y- and z-directions. Therefore, the elements D_{xx}, D_{yy}, D_{zz} on the main diagonal of the matrix of D are equal to the *dilatation rates* in the x-, y- and z-direction, respectively.

Second, we choose $\mathbf{n}^{(1)} = \mathbf{e}_x$ and $\mathbf{n}^{(2)} = \mathbf{e}_y$, so that $\gamma = 0$ (Fig. 2.3, right). This yields

$$\dot{\gamma} = 2\mathbf{e}_x \cdot \mathsf{D} \cdot \mathbf{e}_y \quad \Rightarrow \quad D_{xy} = \frac{\dot{\gamma}}{2}\,. \tag{2.27}$$

Analogous relations can be obtained for the two other off-diagonal elements D_{xz} and D_{yz}. Therefore, $2D_{xy}$, $2D_{xz}$ and $2D_{yz}$ denote the *shear rates* $\dot{\gamma}_{xy}$, $\dot{\gamma}_{xz}$ and $\dot{\gamma}_{yz}$, that is, the temporal changes of right angles formed by the respective coordinate directions.

As for the spin tensor W, we note that its matrix has only three independent elements (this holds for any antisymmetric tensor). Without loss of generality, it can therefore be written as

$$\mathsf{W} = \begin{pmatrix} 0 & -w_3 & w_2 \\ w_3 & 0 & -w_1 \\ -w_2 & w_1 & 0 \end{pmatrix} \tag{2.28}$$

[see also Eq. (A.18) and the discussion there]. The w_i arranged in the above form are the components of the *dual vector*

$$\mathbf{w} = \operatorname{dual} \mathsf{W} = \begin{pmatrix} w_1 \\ w_2 \\ w_3 \end{pmatrix}\,, \tag{2.29}$$

with which the linear transformation $\mathsf{W} \cdot \mathbf{a}$ (arbitrary vector $\mathbf{a}$) can be expressed as a cross product,

$$\mathsf{W} \cdot \mathbf{a} = \mathbf{w} \times \mathbf{a}\,. \tag{2.30}$$

Thus, Eq. (2.22) yields

$$(\mathrm{d}\mathbf{x})^{\cdot} = \mathsf{D} \cdot \mathrm{d}\mathbf{x} + \mathbf{w} \times \mathrm{d}\mathbf{x}\,. \tag{2.31}$$

The first summand on the right-hand side describes the strain (deformation) part of the motion, the second summand the local rigid body rotation with angular velocity $\mathbf{w}$. This justifies the names "strain-rate tensor" and "spin tensor" for D and W, respectively.

2.3 Balance Equations

2.3.1 Reynolds' Transport Theorem

We consider a material volume $\omega \subset \kappa_t$ in the present configuration. "Material" means that the volume consists of the same particles for all times, $\partial\omega$ denotes the boundary of ω, $\mathbf{v}$ the velocity field of the body and $\mathbf{n}$ the unit normal vector on $\partial\omega$ (see Fig. 2.4). For an arbitrary scalar, vector or tensor field quantity $\psi(\mathbf{x}, t)$, we now calculate the term $(\mathrm{d}/\mathrm{d}t) \int_\omega \psi \, \mathrm{d}v$, that is, the temporal change of the field quantity integrated over the volume ω.

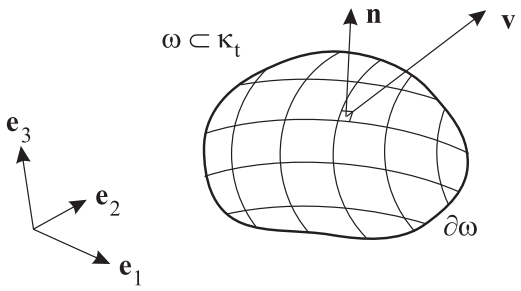

Figure 2.4: On the Reynolds' transport theorem: Material volume ω with boundary $\partial\omega$ in the present configuration κ_t.

To this end, we transform the integration variable to material coordinates $\mathbf{X}$, which changes the integration domain ω to the volume $\Omega \subset \kappa_r$ in the reference configuration as

$$\frac{\mathrm{d}}{\mathrm{d}t} \int_\omega \psi(\mathbf{x}, t) \, \mathrm{d}v = \frac{\mathrm{d}}{\mathrm{d}t} \int_\Omega \psi(\mathbf{x}(\mathbf{X}, t), t) \, J(\mathbf{X}, t) \mathrm{d}V \, . \tag{2.32}$$

For the transformation of the volume element Eq. (2.9) was used. Since Ω, as a material volume in the reference configuration, is time-independent, differentiation and integration can be exchanged on the right-hand side, provided that the fields ψ, J and $\mathbf{v}$ are sufficiently smooth:

$$\begin{aligned} \frac{\mathrm{d}}{\mathrm{d}t} \int_\omega \psi(\mathbf{x}, t) \, \mathrm{d}v &= \int_\Omega (\dot{\psi} J + \psi \dot{J}) \, \mathrm{d}V \\ &= \int_\Omega (\dot{\psi} + \psi \, \mathrm{div}\, \mathbf{v}) \, J \mathrm{d}V \\ &= \int_\omega (\dot{\psi} + \psi \, \mathrm{div}\, \mathbf{v}) \, \mathrm{d}v \, . \end{aligned} \tag{2.33}$$

In the second step, Eq. (2.19) was used, and in the last step the integral was transformed back to spatial coordinates. The result can be further rewritten as

$$\begin{aligned} \frac{\mathrm{d}}{\mathrm{d}t} \int_\omega \psi(\mathbf{x}, t) \, \mathrm{d}v &= \int_\omega \left(\frac{\partial \psi}{\partial t} + (\mathrm{grad}\, \psi) \cdot \mathbf{v} + \psi \, \mathrm{div}\, \mathbf{v} \right) \mathrm{d}v \\ &= \int_\omega \left(\frac{\partial \psi}{\partial t} + \mathrm{div}\, (\psi \mathbf{v}) \right) \mathrm{d}v \, . \end{aligned} \tag{2.34}$$

By using the divergence theorem (A.63), we now obtain

$$\frac{\mathrm{d}}{\mathrm{d}t}\int_\omega \psi(\mathbf{x},t)\,\mathrm{d}v = \int_\omega \frac{\partial\psi}{\partial t}\,\mathrm{d}v + \oint_{\partial\omega} \psi\mathbf{v}\cdot\mathbf{n}\,\mathrm{d}a\,, \tag{2.35}$$

which is known as *Reynolds' transport theorem*. It says that the temporal change of the integral $\int_\omega \psi\,\mathrm{d}v$ over the material volume ω is composed of two parts, (i) the local change $\partial\psi/\partial t$ within ω, and (ii) the advective flux $\psi\mathbf{v}$ in the normal direction $\mathbf{n}$ across the boundary $\partial\omega$. Note that, if ψ is a tensor field of order $r \geq 1$, $\psi\mathbf{v}$ is a tensor product which yields a tensor of order $r+1$.

2.3.2 General Balance Equation

Let $\mathcal{G}(\omega,t)$ be a physical quantity of the entire material volume ω, which is supposed to be additive over subsets of ω (e.g., mass, momentum or internal energy, but not temperature or velocity). We assume that the change of $\mathcal{G}$ with time may be due to three different processes, namely

- the *flux* $\mathcal{F}(\partial\omega,t)$ of $\mathcal{G}$ across the boundary $\partial\omega$,
- the *production* $\mathcal{P}(\omega,t)$ of $\mathcal{G}$ within the volume ω,
- the *supply* $\mathcal{S}(\omega,t)$ of $\mathcal{G}$ within the volume ω.

Therefore, we can balance $\mathrm{d}\mathcal{G}/\mathrm{d}t$ as follows:

$$\frac{\mathrm{d}}{\mathrm{d}t}\mathcal{G}(\omega,t) = -\mathcal{F}(\partial\omega,t) + \mathcal{P}(\omega,t) + \mathcal{S}(\omega,t)\,, \tag{2.36}$$

where positive fluxes have been defined as outflows from the volume, so that the flux term has a negative sign.

The idea behind distinguishing between the mathematically equivalent quantities production and supply is that production is due to internal processes (within the volume ω) only, whereas supply has an external source. *Conserved quantities* are characterised by a vanishing production.

In order to reformulate the statement (2.36), we assume that $\mathcal{G}$, $\mathcal{P}$ and $\mathcal{S}$ can be expressed as volume integrals of corresponding *densities* g, p and s,

$$\begin{aligned}
\mathcal{G}(\omega,t) &= \textstyle\int_\omega g(\mathbf{x},t)\,\mathrm{d}v\,, \qquad g:\ \text{density of the quantity } \mathcal{G}\,,\\
\mathcal{P}(\omega,t) &= \textstyle\int_\omega p(\mathbf{x},t)\,\mathrm{d}v\,, \qquad p:\ \text{production density of } \mathcal{G}\,,\\
\mathcal{S}(\omega,t) &= \textstyle\int_\omega s(\mathbf{x},t)\,\mathrm{d}v\,, \qquad s:\ \text{supply density of } \mathcal{G}\,,
\end{aligned} \tag{2.37}$$

and that $\mathcal{F}$ can be obtained as the surface integral of a *flux density* $\boldsymbol{\phi}$,

$$\mathcal{F}(\partial\omega,t) = \oint_{\partial\omega} \boldsymbol{\phi}(\mathbf{x},t)\cdot\mathbf{n}\,\mathrm{d}a\,, \tag{2.38}$$

where $\mathrm{d}a$ is the scalar surface element. Note that, if $\mathcal{G}$ is a tensor quantity of order $r \geq 0$ (scalar, vector etc.), then the order of g, p and s is also equal to r, whereas the order of $\boldsymbol{\phi}$ is $r+1$.

Inserting the expressions (2.37) and (2.38) in Eq. (2.36) yields the *general balance equation in integral form*,

$$\begin{aligned} \frac{\mathrm{d}}{\mathrm{d}t}\int_\omega g(\mathbf{x},t)\,\mathrm{d}v &= -\oint_{\partial\omega}\boldsymbol{\phi}(\mathbf{x},t)\cdot\mathbf{n}\,\mathrm{d}a \\ &\quad + \int_\omega p(\mathbf{x},t)\,\mathrm{d}v + \int_\omega s(\mathbf{x},t)\,\mathrm{d}v\,. \end{aligned} \tag{2.39}$$

Provided that all fields in this equation are sufficiently smooth, it can be localised as follows. We apply Reynolds' transport theorem (2.35) to the left-hand side (with $\psi = g$), transform all surface integrals to volume integrals with the divergence theorem (A.63) and assemble all terms on the left-hand side:

$$\int_\omega \left(\frac{\partial g}{\partial t} + \operatorname{div}(g\mathbf{v}) + \operatorname{div}\boldsymbol{\phi} - p - s \right) \mathrm{d}v = 0\,. \tag{2.40}$$

This relation must hold for any arbitrary material volume ω, which is only possible if the integrand itself vanishes. Thus,

$$\frac{\partial g}{\partial t} = -\operatorname{div}(\boldsymbol{\phi} + g\mathbf{v}) + p + s\,, \tag{2.41}$$

which is the *general balance equation in local form*. It balances the local change of the density g with the production and supply densities and the negative divergence of two flux terms, the actual flux density $\boldsymbol{\phi}$ and the advective (or convective) flux density $g\mathbf{v}$.

2.3.3 General Jump Condition

The local balance equation (2.41) is only valid for those parts of the material volume ω for which all fields are sufficiently smooth. We now consider the case that there exists an oriented *singular surface* σ within ω for which this is not fulfilled. In particular, the density g may be discontinuous on σ. Denote the unit normal vector on σ by $\mathbf{n}$, the side of ω into which $\mathbf{n}$ points by ω^+ and the other side by ω^-. The singular surface need not be material, that is to say, it may travel with its own velocity $\mathbf{w}$ which may differ from the particle velocity $\mathbf{v}$ (Fig. 2.5).

The values which a field quantity $\psi(\mathbf{x},t)$ assumes when the point $\mathbf{x} \in \sigma$ (on the singular surface) is approached on an arbitrary path in ω^- or ω^+ are denoted by ψ^- and ψ^+, respectively:

$$\begin{aligned} \forall \mathbf{x} \in \sigma : \qquad \psi^-(\mathbf{x},t) &= \lim\nolimits_{\mathbf{y}\to\mathbf{x},\,\mathbf{y}\in\omega^-} \psi(\mathbf{y},t)\,, \\ \psi^+(\mathbf{x},t) &= \lim\nolimits_{\mathbf{y}\to\mathbf{x},\,\mathbf{y}\in\omega^+} \psi(\mathbf{y},t)\,. \end{aligned} \tag{2.42}$$

Of course, this requires that the limits exist and are finite. We define the *jump* $[\![\psi]\!]$ of ψ on σ as

$$\forall \mathbf{x} \in \sigma : \quad [\![\psi]\!](\mathbf{x},t) = \psi^+(\mathbf{x},t) - \psi^-(\mathbf{x},t)\,. \tag{2.43}$$

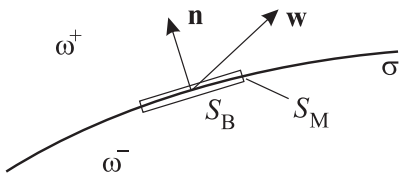

Figure 2.5: Singular surface σ within the material volume ω.

If $[\![\psi]\!] \neq 0$, the quantity ψ experiences a discontinuity on the singular surface.

We now motivate a balance equation similar to Eq. (2.39) for the pill-box volume ν around the singular surface σ with basal area S_B und mantle area S_M, which is also indicated in Fig. 2.5. It is hereby assumed that S_B and S_M are very small, so that the curvature of σ can be neglected. This entails a very small volume of the pill-box, so that the three volume integrals in Eq. (2.39) are negligible compared to the surface integral of the flux density $\boldsymbol{\phi}$ (provided that all integrands are bounded). So the first guess for the balance equation of the pill-box volume ν would be $\oint_{\partial\nu} \boldsymbol{\phi}(\mathbf{x},t)\cdot\mathbf{n}\,\mathrm{d}a = 0$. However, in general we are concerned with a non-material volume here, so that, in addition to the actual flux density $\boldsymbol{\phi}$ an advective flux density $g(\mathbf{v}-\mathbf{w})$ due to the particle motion (velocity $\mathbf{v}$) relative to the motion of the singular surface (velocity $\mathbf{w}$) must be taken into account. Thus, the correct form of the balance equation is

$$\oint_{\partial\nu} (\boldsymbol{\phi} + g(\mathbf{v}-\mathbf{w}))\cdot\mathbf{n}\,\mathrm{d}a = 0\,. \tag{2.44}$$

The geometry of the pill-box volume is such that $S_\mathrm{M} \ll S_\mathrm{B}$, so that all fluxes through S_M can be neglected in comparison with fluxes through S_B. Therefore, only the basal surfaces with area S_B on the ω^+ and ω^- side of σ (denoted as S_B^+ and S_B^-, respectively) contribute to the surface integral (2.44):

$$\int_{S_\mathrm{B}^+} (\boldsymbol{\phi} + g(\mathbf{v}-\mathbf{w}))\cdot\mathbf{n}\,\mathrm{d}a + \int_{S_\mathrm{B}^-} (\boldsymbol{\phi} + g(\mathbf{v}-\mathbf{w}))\cdot(-\mathbf{n})\,\mathrm{d}a = 0 \tag{2.45}$$

(note that the outer unit normal vector is $\mathbf{n}$ on S_B^+ and $-\mathbf{n}$ on S_B^-). Since all field quantities are virtually constant on the very small surfaces S_B^+ and S_B^-, this can be written as

$$\begin{aligned} &S_\mathrm{B}\,(\boldsymbol{\phi}^+ + g^+(\mathbf{v}^+-\mathbf{w}))\cdot\mathbf{n} + S_\mathrm{B}\,(\boldsymbol{\phi}^- + g^-(\mathbf{v}^--\mathbf{w}))\cdot(-\mathbf{n}) = 0 \\ &\Rightarrow\ \boldsymbol{\phi}^+\cdot\mathbf{n} - \boldsymbol{\phi}^-\cdot\mathbf{n} + (g^+(\mathbf{v}^+-\mathbf{w}))\cdot\mathbf{n} - (g^-(\mathbf{v}^--\mathbf{w}))\cdot\mathbf{n} = 0\,, \end{aligned} \tag{2.46}$$

and with definition (2.43) we obtain

$$[\![\boldsymbol{\phi}\cdot\mathbf{n}]\!] + [\![g\,((\mathbf{v}-\mathbf{w})\cdot\mathbf{n})]\!] = 0\,. \tag{2.47}$$

This is the *general jump condition on singular surfaces*. For a formal derivation of this jump condition see, e.g., Liu (2002), Hutter and Jöhnk (2004).

2.3.4 Mass Balance

If the physical quantity $\mathcal{G}$ is identified with the total mass M of the material volume ω, it is clear that $\mathrm{d}M/\mathrm{d}t = 0$, because the mass of a material volume cannot change. With the (mass) density ρ this can be expressed as

$$\frac{\mathrm{d}}{\mathrm{d}t}\int_\omega \rho \,\mathrm{d}v = 0\,. \tag{2.48}$$

By comparison with the general balance equation (2.39) we find immediately

$$g = \rho\,, \quad \boldsymbol{\phi} = \mathbf{0}\,, \quad p = 0\,, \quad s = 0\,. \tag{2.49}$$

With these densities, the local balance equation (2.41) reads

$$\frac{\partial \rho}{\partial t} + \operatorname{div}(\rho \mathbf{v}) = 0\,. \tag{2.50}$$

This is the *mass balance*, also known as the *continuity equation*. An equivalent form can be derived by differentiating the product,

$$\begin{aligned} &\frac{\partial \rho}{\partial t} + (\operatorname{grad}\rho)\cdot\mathbf{v} + \rho \operatorname{div}\mathbf{v} = 0 \\ &\Rightarrow\ \dot{\rho} + \rho \operatorname{div}\mathbf{v} = 0\,. \end{aligned} \tag{2.51}$$

An important special case is that of an *incompressible* material, defined by a constant density, that is, $\rho = \text{const}$ or $\dot{\rho} = 0$. For this case, Eq. (2.51) simplifies to

$$\operatorname{div}\mathbf{v} = 0\,, \tag{2.52}$$

which is the mass balance or continuity equation for incompressible materials. Evidently, the corresponding velocity field is source-free (solenoidal).

By inserting the densities (2.49) in the general jump condition (2.47), we obtain the *mass jump condition* on singular surfaces as

$$[\![\rho\,((\mathbf{v} - \mathbf{w})\cdot\mathbf{n})]\!] = 0\,. \tag{2.53}$$

It simply states that the mass inflow at one side of the singular surface must equal the mass outflow at the other side.

Let us come back to the general balance equation (2.41) and write the density g as

$$g = \rho g_\mathrm{s}\,, \tag{2.54}$$

where g_s denotes the physical quantity under consideration *per unit mass* (which, of course, only makes sense if the quantity is not the mass itself). This yields

$$\begin{aligned}
&\frac{\partial(\rho g_s)}{\partial t} + \operatorname{div}(\boldsymbol{\phi} + \rho g_s \mathbf{v}) = p + s \\
\Rightarrow\ &\rho \frac{\partial g_s}{\partial t} + g_s \frac{\partial \rho}{\partial t} + \operatorname{div} \boldsymbol{\phi} + g_s \operatorname{div}(\rho \mathbf{v}) + (\operatorname{grad} g_s) \cdot \rho \mathbf{v} = p + s \\
\Rightarrow\ &\rho \left\{ \frac{\partial g_s}{\partial t} + (\operatorname{grad} g_s) \cdot \mathbf{v} \right\} + g_s \left\{ \frac{\partial \rho}{\partial t} + \operatorname{div}(\rho \mathbf{v}) \right\} \\
&\qquad\qquad = -\operatorname{div} \boldsymbol{\phi} + p + s \,. \qquad (2.55)
\end{aligned}$$

The first term in curly brackets is the material time derivative of g [see Eq. (2.15)], the second term vanishes because of the mass balance (2.50). It remains

$$\rho \frac{\mathrm{d} g_s}{\mathrm{d} t} = -\operatorname{div} \boldsymbol{\phi} + p + s \qquad (2.56)$$

as an alternative representation of the general balance equation, which can be used for any quantity except mass.

2.3.5 Momentum Balance

Let us now identify the physical quantity $\mathcal{G}$ with the total momentum $\mathbf{P}$ (vector!) of the material volume ω. Since momentum is equal to mass times velocity, the momentum density can be expressed as mass density times velocity,

$$g = \rho \mathbf{v} \,, \qquad (2.57)$$

and the total momentum $\mathbf{P}$ is equal to $\int_\omega \rho \mathbf{v} \, \mathrm{d}v$. Following Newton's Second Law, its temporal change $\mathrm{d}\mathbf{P}/\mathrm{d}t$ must be given by the sum of all forces $\mathbf{F}$ which act on the volume ω. These forces can either be external *volume forces* $\mathbf{f}(\mathbf{x}, t)$ acting on any volume element within ω (e.g., the gravity field), or internal *stresses* (surface forces) $\mathbf{t}_\mathbf{n}(\mathbf{x}, t)$ acting on the boundary surface $\partial\omega$ (Fig. 2.6). The latter do not only depend on position $\mathbf{x}$ and time t, but also on the orientation of the surface, expressed by the unit normal vector $\mathbf{n}$.

The total force acting on the material volume ω is therefore

$$\mathbf{F} = \oint_{\partial\omega} \mathbf{t}_\mathbf{n}(\mathbf{x}, t) \, \mathrm{d}a + \int_\omega \mathbf{f}(\mathbf{x}, t) \, \mathrm{d}v \,, \qquad (2.58)$$

and Newton's Second Law reads

$$\frac{\mathrm{d}}{\mathrm{d}t} \int_\omega \rho(\mathbf{x}, t) \mathbf{v}(\mathbf{x}, t) \, \mathrm{d}v = \oint_{\partial\omega} \mathbf{t}_\mathbf{n}(\mathbf{x}, t) \, \mathrm{d}a + \int_\omega \mathbf{f}(\mathbf{x}, t) \, \mathrm{d}v \,. \qquad (2.59)$$

Except for the surface integral (flux term), this has the form of the general balance equation (2.39). By comparing the flux terms, we infer that the stress vector $\mathbf{t}_\mathbf{n}$ must be a *linear* function of $\mathbf{n}$, that is,

$$\mathbf{t}_\mathbf{n}(\mathbf{x}, t) = \mathsf{t}(\mathbf{x}, t) \cdot \mathbf{n} \,, \qquad (2.60)$$

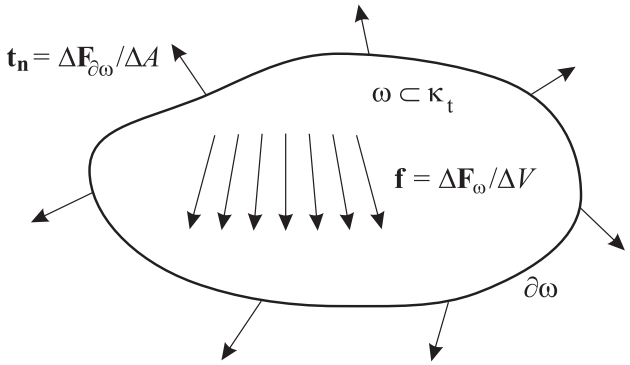

Figure 2.6: Volume forces $\mathbf{f}$ and surface forces $\mathbf{t_n}$ which act on a material volume ω and its surface $\partial\omega$ in the present configuration κ_t.

where $\mathsf{t}(\mathbf{x}, t)$ is a tensor field of order 2 which is called the *Cauchy stress tensor*. Now we can identify

$$g = \rho\mathbf{v}\,, \quad \boldsymbol{\phi} = -\mathsf{t}\,, \quad p = \mathbf{0}\,, \quad s = \mathbf{f} \tag{2.61}$$

(the volume force is interpreted as a supply term and not a production term because it is assumed to have an external source), and from Eq. (2.41) we obtain the local form of the *momentum balance* as

$$\frac{\partial(\rho\mathbf{v})}{\partial t} + \operatorname{div}(\rho\mathbf{v}\,\mathbf{v}) = \operatorname{div}\mathsf{t} + \mathbf{f}\,. \tag{2.62}$$

With the specific momentum (momentum per unit mass)

$$g_{\mathrm{s}} = \frac{g}{\rho} = \mathbf{v} \tag{2.63}$$

and the representation (2.56) of the general balance equation, an equivalent form of the momentum balance is

$$\rho\frac{\mathrm{d}\mathbf{v}}{\mathrm{d}t} = \operatorname{div}\mathsf{t} + \mathbf{f}\,. \tag{2.64}$$

Note that, if the momentum balance is formulated in a non-inertial system (for instance, the rotating Earth), the volume force $\mathbf{f}$ contains contributions from inertial forces (centrifugal force, Coriolis force etc.).

The *momentum jump condition* on singular surfaces is readily obtained from Eqs. (2.47) and (2.61),

$$[\![\mathsf{t}\cdot\mathbf{n}]\!] - [\![\rho\mathbf{v}\,((\mathbf{v}-\mathbf{w})\cdot\mathbf{n})]\!] = \mathbf{0}\,. \tag{2.65}$$

It relates the jump of the stress vector $(\mathsf{t}\cdot\mathbf{n})$ to the jump of the advective momentum flux across the interface. In the case of a *material singular surface* $(\mathbf{v}^+\cdot\mathbf{n} = \mathbf{v}^-\cdot\mathbf{n} = \mathbf{w}\cdot\mathbf{n})$ the stress vector is continuous,

$$[\![\mathsf{t}\cdot\mathbf{n}]\!] = \mathbf{0}\,. \tag{2.66}$$

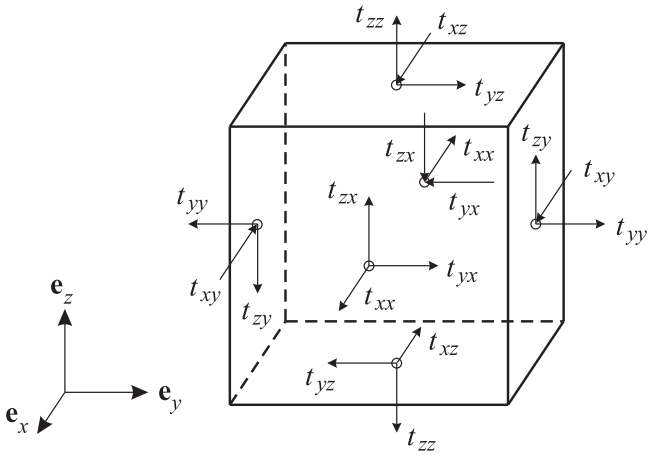

Figure 2.7: Components of the Cauchy stress tensor.

With respect to a given orthonormal basis $\{\mathbf{e}_i\}$, the matrix of the Cauchy stress tensor t defined by Eq. (2.60) is

$$\mathsf{t} = \begin{pmatrix} t_{xx} & t_{xy} & t_{xz} \\ t_{yx} & t_{yy} & t_{yz} \\ t_{zx} & t_{zy} & t_{zz} \end{pmatrix} . \tag{2.67}$$

The elements of this matrix can be interpreted as follows. For a cut along the xy plane, that is, with unit normal vector $\mathbf{n} = \pm\mathbf{e}_z$ (the sign depends on the orientation of the plane), the stress vector

$$\mathbf{t}_{\pm\mathbf{e}_z} = \pm\mathsf{t}\cdot\mathbf{e}_z = \pm \begin{pmatrix} t_{xz} \\ t_{yz} \\ t_{zz} \end{pmatrix} \tag{2.68}$$

is obtained. Evidently, the diagonal element t_{zz} is perpendicular to the cut plane, whereas the off-diagonal elements t_{xz} and t_{yz} are parallel to the plane. The same result is found for cuts along the xz and yz planes. Therefore, the three diagonal elements (t_{xx}, t_{yy}, t_{zz}) are referred to as *normal stresses*, and the six off-diagonal elements (t_{xy}, t_{yx}, t_{xz}, t_{zx}, t_{yz}, t_{zy}) are called *shear stresses*. The meaning of these components is illustrated in Fig. 2.7.

2.3.6 Balance of Angular Momentum

In point mechanics, the angular momentum $\mathbf{L}$ of a mass point is given by $\mathbf{L} = \mathbf{x}\times\mathbf{P}$ (cross product of position vector and momentum), and the torque $\mathbf{M}$ is defined as $\mathbf{M} = \mathbf{x}\times\mathbf{F}$ (cross product of position vector and force acting on the mass point). In view of the momentum densities (2.61) for the continuous body, this motivates the following identities for the densities of angular momentum:

$$g = \mathbf{x}\times\rho\mathbf{v}\,, \quad \boldsymbol{\phi} = -\mathbf{x}\times\mathsf{t}\,, \quad p = \mathbf{0}\,, \quad s = \mathbf{x}\times\mathbf{f}\,. \tag{2.69}$$

Inserting these identities in Eq. (2.41) yields the *balance of angular momentum*,

$$\frac{\partial(\mathbf{x}\times\rho\mathbf{v})}{\partial t}+\operatorname{div}\left[(\mathbf{x}\times\rho\mathbf{v})\,\mathbf{v}\right]=\operatorname{div}\left(\mathbf{x}\times\mathsf{t}\right)+\mathbf{x}\times\mathbf{f}\,. \tag{2.70}$$

Using the momentum balance (2.62), this can be drastically simplified. By subtracting $\mathbf{x}\times$(2.62) from the balance of angular momentum (2.70), it reduces to the statement that the *Cauchy stress tensor is symmetric*,

$$\mathsf{t}=\mathsf{t}^{\mathrm{T}},\quad \text{or}\quad t_{ij}=t_{ji} \tag{2.71}$$

[the computation is demonstrated in detail by Greve and Blatter (2009)]. By contrast, an independent jump condition of angular momentum does not exist; it is equivalent to the momentum jump condition (2.65).

2.3.7 Energy Balance

Balance of Kinetic Energy

We now compute the dot product of the momentum balance (2.64) and the velocity $\mathbf{v}$. Expressed in index notation, this is

$$\begin{aligned}
&\rho v_k\frac{\mathrm{d}v_k}{\mathrm{d}t}=t_{kl,l}v_k+f_kv_k\\
&\Rightarrow\ \rho\frac{\mathrm{d}}{\mathrm{d}t}\left(\frac{v_kv_k}{2}\right)=(t_{kl}v_k)_{,l}-t_{kl}v_{k,l}+f_kv_k\\
&\qquad\qquad=(\mathsf{t}\cdot\mathbf{v})_{l,l}-(\mathsf{t}\cdot\mathsf{L})_{ll}+f_kv_k\\
&\Rightarrow\ \rho\frac{\mathrm{d}}{\mathrm{d}t}\left(\frac{v^2}{2}\right)=\operatorname{div}(\mathsf{t}\cdot\mathbf{v})-\operatorname{tr}(\mathsf{t}\cdot\mathsf{L})+\mathbf{f}\cdot\mathbf{v}
\end{aligned} \tag{2.72}$$

[in the step from line 2 to 3 the symmetry of t, Eq. (2.71), has been used, and in the last line we have introduced the *speed* $v=|\mathbf{v}|$, which is the absolute value of the velocity]. For the second summand on the right-hand side, $\operatorname{tr}(\mathsf{t}\cdot\mathsf{L})$, we apply the decomposition (2.20) of L, the symmetry of t and the antisymmetry of W,

$$\begin{aligned}
\operatorname{tr}(\mathsf{t}\cdot\mathsf{L}) &= \operatorname{tr}(\mathsf{t}\cdot\mathsf{D})+\operatorname{tr}(\mathsf{t}\cdot\mathsf{W})\\
&= \operatorname{tr}(\mathsf{t}\cdot\mathsf{D})+t_{ij}W_{ji}\\
&= \operatorname{tr}(\mathsf{t}\cdot\mathsf{D})+\tfrac{1}{2}(t_{ij}W_{ji}+t_{ji}W_{ij})\\
&= \operatorname{tr}(\mathsf{t}\cdot\mathsf{D})+\tfrac{1}{2}(t_{ij}W_{ji}-t_{ij}W_{ji})=\operatorname{tr}(\mathsf{t}\cdot\mathsf{D})\,,
\end{aligned} \tag{2.73}$$

so that

$$\rho\frac{\mathrm{d}}{\mathrm{d}t}\left(\frac{v^2}{2}\right)=\operatorname{div}(\mathsf{t}\cdot\mathbf{v})-\operatorname{tr}(\mathsf{t}\cdot\mathsf{D})+\mathbf{f}\cdot\mathbf{v}\,. \tag{2.74}$$

Since the kinetic energy of a mass m is given by $mv^2/2$, the term $v^2/2$ denotes the specific kinetic energy (per unit mass) of a continuous body. Comparison of the above result with the general balance equation (2.56) shows that it can be interpreted as the *balance of kinetic energy*, where

$$\begin{array}{lcll} g & = & \rho v^2/2 & \text{(kinetic energy density)}\,, \\ g_s & = & v^2/2 & \text{(specific kinetic energy)}\,, \\ \boldsymbol{\phi} & = & -\mathsf{t}\cdot\mathbf{v} & \text{(power of stresses)}\,, \\ p & = & -\mathrm{tr}\,(\mathsf{t}\cdot\mathsf{D}) & (-p\text{: dissipation power})\,, \\ s & = & \mathbf{f}\cdot\mathbf{v} & \text{(power of volume forces)}\,. \end{array} \tag{2.75}$$

The attribution of the dissipation power as a production term and the power of volume forces as a supply term was done because the former is only due to intrinsic quantities, whereas in the latter the volume force occurs which has an external source. Thus, in contrast to mass, momentum and angular momentum, the kinetic energy has a non-zero production density, which means that it is not a conserved quantity.

Energy Balance, Balance of Internal Energy

The balance of kinetic energy, Eq. (2.74), is not an independent statement, but a mere consequence of the momentum balance (2.64). However, classical mechanics and thermodynamics tells us that the kinetic energy is only one part of the total energy of a system (here: continuous body), and that the total energy is a conserved quantity (no production). In order to formulate the (total) energy balance, we thus extend Eq. (2.75) by introducing an internal energy, a heat flux and a radiation power and setting the production to zero:

$$\begin{array}{lcll} g & = & \rho(u+v^2/2) & (u\text{: specific internal energy})\,, \\ g_s & = & u+v^2/2\,, & \\ \boldsymbol{\phi} & = & \mathbf{q}-\mathsf{t}\cdot\mathbf{v} & (\mathbf{q}\text{: heat flux})\,, \\ p & = & 0\,, & \\ s & = & \rho r+\mathbf{f}\cdot\mathbf{v} & (r\text{: specific radiation power})\,. \end{array} \tag{2.76}$$

By inserting these densities in Eq. (2.41), the *energy balance*

$$\begin{aligned} \frac{\partial}{\partial t}\left[\rho\Big(u+\frac{v^2}{2}\Big)\right] + \mathrm{div}\,\left[\rho\Big(u+\frac{v^2}{2}\Big)\,\mathbf{v}\right] \\ = -\mathrm{div}\,\mathbf{q} + \mathrm{div}\,(\mathsf{t}\cdot\mathbf{v}) + \rho r + \mathbf{f}\cdot\mathbf{v} \end{aligned} \tag{2.77}$$

is obtained, which is also known as the *First Law of Thermodynamics*. An alternative form follows from Eq. (2.56),

$$\rho\frac{\mathrm{d}}{\mathrm{d}t}\Big(u+\frac{v^2}{2}\Big) = -\mathrm{div}\,\mathbf{q} + \mathrm{div}\,(\mathsf{t}\cdot\mathbf{v}) + \rho r + \mathbf{f}\cdot\mathbf{v}\,. \tag{2.78}$$

This can be simplified further:

$$\begin{aligned}\rho\frac{\mathrm{d}u}{\mathrm{d}t} + \rho v_k\frac{\mathrm{d}v_k}{\mathrm{d}t} &= -q_{k,k} + (t_{kl}v_k)_{,l} + \rho r + f_k v_k \\ &= -q_{k,k} + t_{kl,l}v_k + t_{kl}v_{k,l} + \rho r + f_k v_k \\ \Rightarrow\ \rho\frac{\mathrm{d}u}{\mathrm{d}t} + v_k\left\{\rho\frac{\mathrm{d}v_k}{\mathrm{d}t} - t_{kl,l} - f_k\right\} &= -q_{k,k} + t_{lk}L_{kl} + \rho r\,. \end{aligned} \tag{2.79}$$

The term in curly brackets vanishes because of the momentum balance (2.64), and the term $t_{lk}L_{kl} = \mathrm{tr}\,(\mathsf{t}\cdot\mathsf{L})$ can again be replaced by $\mathrm{tr}\,(\mathsf{t}\cdot\mathsf{D})$ [see Eq. (2.73)], so that we obtain

$$\rho\frac{\mathrm{d}u}{\mathrm{d}t} = -\mathrm{div}\,\mathbf{q} + \mathrm{tr}\,(\mathsf{t}\cdot\mathsf{D}) + \rho r\,. \tag{2.80}$$

Evidently, this is the *balance of internal energy* in the form (2.56), with the corresponding densities

$$\begin{array}{lcll} g & = & \rho u\,, & \\ g_s & = & u & \text{(specific internal energy)}\,, \\ \boldsymbol{\phi} & = & \mathbf{q} & \text{(heat flux)}\,, \\ p & = & \mathrm{tr}\,(\mathsf{t}\cdot\mathsf{D}) & \text{(dissipation power)}\,, \\ s & = & \rho r & (r\text{: specific radiation power})\,. \end{array} \tag{2.81}$$

In contrast to the total energy, the internal energy is not a conserved quantity. Its production density is equal to the dissipation power, which already appeared in the balance of kinetic energy (2.74) with a negative sign. The name "dissipation power" results from the fact that it annihilates kinetic energy and changes it into internal energy. In other words, macroscopic mechanical energy is transformed into heat (microscopic, unordered motion). Therefore, the dissipation power can also be interpreted as heat production due to internal friction.

From Eqs. (2.47) and (2.76) we obtain the *energy jump condition*

$$[\![\mathbf{q}\cdot\mathbf{n}]\!] - [\![\mathbf{v}\cdot\mathsf{t}\cdot\mathbf{n}]\!] + \left[\!\left[\rho\left(u + \tfrac{1}{2}v^2\right)\,((\mathbf{v}-\mathbf{w})\cdot\mathbf{n})\right]\!\right] = 0\,. \tag{2.82}$$

In case of a *material singular surface* ($\mathbf{v}^+\cdot\mathbf{n} = \mathbf{v}^-\cdot\mathbf{n} = \mathbf{w}\cdot\mathbf{n}$) the third summand vanishes, and because of the continuity of the stress vector $\mathsf{t}\cdot\mathbf{n}$ [Eq. (2.66)] it can be factored out in the second summand:

$$\begin{aligned} &[\![\mathbf{q}\cdot\mathbf{n}]\!] - [\![\mathbf{v}]\!]\cdot\mathsf{t}\cdot\mathbf{n} = 0 \\ \Rightarrow\ &[\![\mathbf{q}\cdot\mathbf{n}]\!] - [\![\mathbf{v}_\perp]\!]\cdot\mathsf{t}\cdot\mathbf{n} - \left[\!\left[\mathbf{v}_\parallel\right]\!\right]\cdot\mathsf{t}\cdot\mathbf{n} = 0 \\ \Rightarrow\ &[\![\mathbf{q}\cdot\mathbf{n}]\!] - \left[\!\left[\mathbf{v}_\parallel\right]\!\right]\cdot\mathsf{t}\cdot\mathbf{n} = 0 \end{aligned} \tag{2.83}$$

[where $\mathbf{v} = \mathbf{v}_\perp + \mathbf{v}_\parallel$, with the normal component $\mathbf{v}_\perp = (\mathbf{v}\cdot\mathbf{n})\mathbf{n}$ and the tangential component $\mathbf{v}_\parallel = \mathbf{v} - (\mathbf{v}\cdot\mathbf{n})\mathbf{n}$; the jump of $\mathbf{v}_\perp$ vanishes because of $\mathbf{v}^+\cdot\mathbf{n} = \mathbf{v}^-\cdot\mathbf{n}$]. Only under the additional assumption of a *no-slip condition*, that is, $\left[\!\left[\mathbf{v}_\parallel\right]\!\right] = \mathbf{0}$, does the normal component of the heat flux $(\mathbf{q}\cdot\mathbf{n})$ become continuous.

2.4 Constitutive Equations

2.4.1 Homogeneous Viscous Thermoelastic Bodies

The balance equations of mass, momentum and internal energy derived in Sect. 2.3 read

$$\frac{\mathrm{d}\rho}{\mathrm{d}t} = -\rho \operatorname{div} \mathbf{v}\,, \tag{2.84}$$

$$\rho \frac{\mathrm{d}\mathbf{v}}{\mathrm{d}t} = \operatorname{div} \mathsf{t} + \mathbf{f}\,, \tag{2.85}$$

$$\rho \frac{\mathrm{d}u}{\mathrm{d}t} = -\operatorname{div} \mathbf{q} + \operatorname{tr}(\mathsf{t} \cdot \mathsf{D}) + \rho r \tag{2.86}$$

[see Eqs. (2.51), (2.64) and (2.80); the balance of angular momentum is implicitly included in the symmetry of t]. They constitute *evolution equations* for the unknown fields ρ, $\mathbf{v}$ and u; however, on the right-hand sides the fields t and $\mathbf{q}$ are also unknown. The supply terms $\mathbf{f}$ and r are assumed to be prescribed as external forcings. Thus, in component form we have $1+3+1=5$ equations (mass balance: scalar equation, momentum balance: vector equation, energy balance: scalar equation) for the $1+3+6+1+3=14$ unknown fields ρ (scalar), $\mathbf{v}$ (vector), t (symmetric tensor), u (scalar) and $\mathbf{q}$ (vector), and the system is highly under-determined. Therefore, additional *closure relations* between the field quantities are required. These closure relations describe the specific behaviour of the different materials (whereas the balance equations are universally valid), and they are called *constitutive equations* or *material equations*.

The general theory of constitutive equations is beyond the scope of this text [see e.g. Liu (2002), Hutter and Jöhnk (2004)]. Here, we confine ourselves to a simple class of materials, the so-called *homogeneous viscous thermoelastic bodies*. This will be sufficient for our purpose of describing ice-dynamic processes.

A homogeneous viscous thermoelastic body is defined as a material whose constitutive equations are functions of the form

$$\begin{aligned} \mathsf{t} &= \mathsf{t}(\mathsf{F}, \dot{\mathsf{F}}, T, \operatorname{grad} T)\,, \\ \mathbf{q} &= \mathbf{q}(\mathsf{F}, \dot{\mathsf{F}}, T, \operatorname{grad} T)\,, \\ u &= u(\mathsf{F}, \dot{\mathsf{F}}, T, \operatorname{grad} T)\,, \end{aligned} \tag{2.87}$$

where the *temperature* $T(\mathbf{x}, t)$ has been introduced as an additional scalar field quantity. Hence, the Cauchy stress tensor t, the heat flux $\mathbf{q}$ and the specific internal energy u are understood as the dependent *material quantities*, and the material shows neither non-local nor memory effects. Note that due to Eq. (2.18) the dependency on $\dot{\mathsf{F}}$ can also be expressed as a dependency on the velocity gradient L. In the following, we will discuss an example of a homogeneous viscous thermoelastic body relevant for ice dynamics, namely the Newtonian fluid.

2.4.2 Newtonian Fluid

Compressible Newtonian Fluid

A material is called *viscous* if the material function $(2.87)_1$ for the stress tensor t contains an explicit dependency on $\dot{\mathsf{F}}$ or L. The most important realisation of a viscous material is the *Newtonian fluid* (also called *linear viscous fluid*), which can either be compressible or incompressible. For the compressible case, t depends linearly on the strain-rate tensor D (symmetric part of L), the density ρ and the temperature T, through the following material function,

$$\mathsf{t} = -p(\rho, T)\,\mathsf{I} + (\lambda\,\mathrm{tr}\,\mathsf{D})\,\mathsf{I} + 2\eta\,\mathsf{D}\,, \tag{2.88}$$

where p is the *thermodynamic pressure*, which is a function of the density ρ and the temperature T ("thermal equation of state"), and λ and η are the *coefficients of viscosity*. In principle, λ and η can also depend on ρ and T, but for simplicity we assume that they are constant.

For the divergence of the stress tensor (2.88) we find

$$\begin{aligned}
(\mathrm{div}\,\mathsf{t})_i = t_{ij,j} &= (p\,\delta_{ij} + \lambda\,D_{kk}\,\delta_{ij} + 2\eta\,D_{ij})_{,j} \\
&= (p\,\delta_{ij})_{,j} + (\lambda\,v_{k,k}\delta_{ij})_{,j} + \eta\,v_{i,jj} + \eta\,v_{j,ij} \\
&= p_{,j}\delta_{ij} + \lambda\,v_{k,kj}\delta_{ij} + \eta\,v_{i,jj} + \eta\,v_{j,ji} \\
&= p_{,i} + (\lambda+\eta)\,v_{k,ki} + \eta\,v_{i,jj} \\
\Rightarrow\ \mathrm{div}\,\mathsf{t} &= -\mathrm{grad}\,p(\rho,T) + (\lambda+\eta)\,\mathrm{grad}\,\mathrm{div}\,\mathbf{v} + \eta\,\Delta\mathbf{v}\,,
\end{aligned} \tag{2.89}$$

where Δ is the Laplacian introduced in Eqs. (A.57) and (A.62). With this result, the momentum balance (2.85) yields the equation of motion

$$\rho\frac{\mathrm{d}\mathbf{v}}{\mathrm{d}t} = -\mathrm{grad}\,p(\rho,T) + (\lambda+\eta)\,\mathrm{grad}\,\mathrm{div}\,\mathbf{v} + \eta\,\Delta\mathbf{v} + \mathbf{f}\,, \tag{2.90}$$

which is the *Navier-Stokes equation* for the case of a compressible Newtonian fluid. If we assume that the temperature of the system is known (for instance, nearly isothermal conditions), then, together with the mass balance (2.84), we have four component equations for the four unknown field components v_x, v_y, v_z and ρ, which is again a closed system.

Incompressible Newtonian Fluid

For the incompressible Newtonian fluid, $\rho = \mathrm{const}$ holds, so that the mass balance reduces to

$$\mathrm{div}\,\mathbf{v} = 0 \tag{2.91}$$

[see Eq. (2.52)]. It is then convenient to split the stress tensor as

$$\mathsf{t} = -p\,\mathsf{I} + \mathsf{t}^{\mathrm{D}}\,, \tag{2.92}$$

where

$$p = -\tfrac{1}{3}\,\mathrm{tr}\,\mathsf{t} \tag{2.93}$$

denotes the pressure, and t^{D} is the traceless *stress deviator* ($\operatorname{tr}\mathsf{t}^{\mathrm{D}} = 0$). Now the material function $(2.87)_1$ only determines the stress deviator t^{D} and reads

$$\mathsf{t}^{\mathrm{D}} = 2\eta\,\mathsf{D}\,, \tag{2.94}$$

where the coefficient η is again the *shear viscosity* (or simply the *viscosity*). Note also that the mass balance (2.91) is equivalent to $\operatorname{tr}\mathsf{D} = 0$, so that the strain-rate tensor is equal to its deviatoric part, that is, $\mathsf{D} = \mathsf{D}^{\mathrm{D}}$.

In order to derive the equation of motion for the incompressible case, we compute the divergence of the stress tensor with the decomposition (2.92), the material function (2.94) and the mass balance (2.91),

$$\operatorname{div}\mathsf{t} = -\operatorname{grad} p + \operatorname{div}\mathsf{t}^{\mathrm{D}}\,, \tag{2.95}$$

where

$$\begin{aligned}(\operatorname{div}\mathsf{t}^{\mathrm{D}})_i &= 2\eta\, D_{ij,j} = \eta\,(v_{i,jj} + v_{j,ij}) = \eta\,(v_{i,jj} + v_{j,ji}) \\ &= \eta\,[v_{i,jj} + (\operatorname{div}\mathbf{v})_{,i}] = \eta\, v_{i,jj} = \eta\,(\Delta\mathbf{v})_i\,. \end{aligned} \tag{2.96}$$

Insertion of these results in the momentum balance (2.85) yields the *Navier-Stokes equation* for the incompressible Newtonian fluid,

$$\rho\frac{\mathrm{d}\mathbf{v}}{\mathrm{d}t} = -\operatorname{grad} p + \eta\,\Delta\mathbf{v} + \mathbf{f}\,. \tag{2.97}$$

Note that, in contrast to the compressible case, there is only a single pressure p involved. It appears as a free field, so that we have the four component equations (2.91) and (2.97) for the four unknown field components v_x, v_y, v_z and p.

If the viscosity η is temperature-dependent and the temperature is not known *a priori*, then a *thermo-mechanically coupled problem* is obtained, for which the energy balance (2.86) must additionally be solved. This requires that the material functions $(2.87)_2$ and $(2.87)_3$ for the heat flux and the internal energy be specified. Insertion in the energy balance yields the missing evolution equation for the temperature. For instance, let the heat flow be given by *Fourier's law of heat conduction*,

$$\mathbf{q} = -\kappa\operatorname{grad} T\,, \tag{2.98}$$

and the internal energy depend linearly on temperature,

$$u = u_0 + c(T - T_0)\,, \tag{2.99}$$

where κ is the heat conductivity, c the specific heat, u_0 a fixed reference value for u and T_0 a fixed reference value for T [such that $u(T_0) = u_0$]. Then the energy balance (2.86) results in

$$\begin{aligned}\rho c\frac{\mathrm{d}T}{\mathrm{d}t} &= \kappa\operatorname{div}\operatorname{grad} T + \operatorname{tr}\left[(-p\,\mathsf{I} + 2\eta\mathsf{D})\cdot\mathsf{D}\right] + \rho r \\ &= \kappa\,\Delta T - p\operatorname{tr}\mathsf{D} + 2\eta\operatorname{tr}\mathsf{D}^2 + \rho r \\ \Rightarrow\ \rho c\frac{\mathrm{d}T}{\mathrm{d}t} &= \kappa\,\Delta T + 2\eta\operatorname{tr}\mathsf{D}^2 + \rho r \end{aligned} \tag{2.100}$$

(note that $\operatorname{tr}\mathsf{D} = \operatorname{div}\mathbf{v} = 0$). Now we have the five equations (2.91), (2.97) and (2.100) which govern the evolution of the five fields v_x, v_y, v_z, p and T.

Gravity-Driven Thin Film Flow

Let us consider a thin film (thickness H) of an incompressible Newtonian fluid (density ρ, viscosity η), which flows down an impenetrable plane (inclination angle α) under the influence of gravity (acceleration due to gravity $\mathbf{g}$); see Fig. 2.8. The film is uniform and of infinite extent in the x (downhill) and y (lateral) directions. At the contact between the fluid and the underlying plane, no-slip conditions prevail, and the free surface is stress-free. Further, steady-state conditions are assumed.

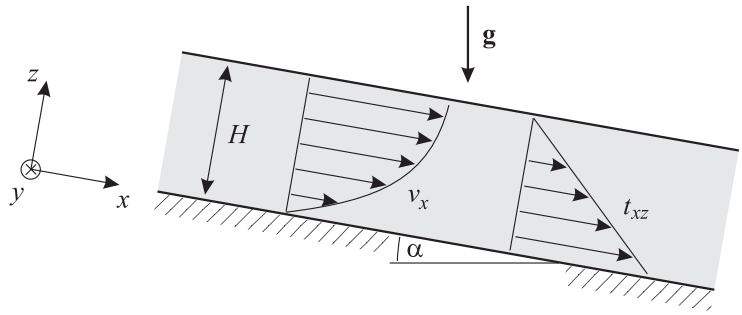

Figure 2.8: Gravity-driven thin film flow of an incompressible Newtonian fluid.

This problem is a realisation of *plane strain*: due to the uniformity in the y (lateral) direction, the velocity component v_y and the strain-rate components D_{xy}, D_{yy} and D_{yz} vanish, and all field quantities are independent of y. Further, the uniformity in the x (downhill) direction and the steady-state assumption imply that dependencies on x and t will not occur either, so that only dependence on the vertical coordinate z remains. Moreover, due to the impenetrable basal plane, there will be no vertical velocity component v_z, and the only remaining velocity component is $v_x(z)$.

Taking into account $\mathbf{f} = \rho\mathbf{g}$ and $\mathbf{g} = g\sin\alpha\,\mathbf{e}_x - g\cos\alpha\,\mathbf{e}_z$, we note the x-component of the Navier-Stokes equation (2.97),

$$\begin{aligned}\rho\frac{\mathrm{d}v_x}{\mathrm{d}t} &= \rho\left(\frac{\partial v_x}{\partial t} + v_x\frac{\partial v_x}{\partial x} + v_y\frac{\partial v_x}{\partial y} + v_z\frac{\partial v_x}{\partial z}\right)\\ &= -\frac{\partial p}{\partial x} + \eta\left(\frac{\partial^2 v_x}{\partial x^2} + \frac{\partial^2 v_x}{\partial y^2} + \frac{\partial^2 v_x}{\partial z^2}\right) + \rho g\sin\alpha\,. \end{aligned} \tag{2.101}$$

Owing to the above arguments, all terms except the last two vanish, and the equation simplifies to

$$\eta\frac{\partial^2 v_x}{\partial z^2} = -\rho g\sin\alpha\,. \tag{2.102}$$

This can readily be integrated,

$$\eta \frac{\partial v_x}{\partial z} = C_1 - \rho g z \sin\alpha \,, \tag{2.103}$$

where C_1 is an integration constant. Its value can be determined by noting that, due to the material function (2.94), the left-hand side is equal to the shear stress t_{xz},

$$t_{xz} = \eta \frac{\partial v_x}{\partial z} = C_1 - \rho g z \sin\alpha \,, \tag{2.104}$$

which vanishes at the free surface ($z = H$) as a consequence of the stress-free boundary condition. Thus,

$$t_{xz}|_{z=H} = C_1 - \rho g H \sin\alpha = 0 \quad \Rightarrow \quad C_1 = \rho g H \sin\alpha \,, \tag{2.105}$$

and we obtain for the shear stress the linear profile

$$t_{xz} = \eta \frac{\partial v_x}{\partial z} = \rho g (H - z) \sin\alpha \,. \tag{2.106}$$

A further integration yields the velocity,

$$v_x = \frac{\rho g}{\eta} \left(H z - \frac{z^2}{2} \right) \sin\alpha + C_2 \,, \tag{2.107}$$

and the integration constant C_2 is evidently equal to zero due to the no-slip condition $v_x|_{z=0} = 0$. Therefore, the solution for the downhill velocity is the parabolic profile

$$v_x = \frac{\rho g H \sin\alpha}{\eta} \left(z - \frac{z^2}{2H} \right) . \tag{2.108}$$

The solutions (2.106) and (2.108) are also shown in Fig. 2.8.

Analogous to Eq. (2.101), the z-component of the Navier-Stokes equation (2.97) reads

$$\begin{aligned} \rho \frac{\mathrm{d}v_z}{\mathrm{d}t} &= \rho \left(\frac{\partial v_z}{\partial t} + v_x \frac{\partial v_z}{\partial x} + v_y \frac{\partial v_z}{\partial y} + v_z \frac{\partial v_z}{\partial z} \right) \\ &= -\frac{\partial p}{\partial z} + \eta \left(\frac{\partial^2 v_z}{\partial x^2} + \frac{\partial^2 v_z}{\partial y^2} + \frac{\partial^2 v_z}{\partial z^2} \right) - \rho g \cos\alpha \,, \end{aligned} \tag{2.109}$$

and simplifies for the thin film problem to

$$\frac{\partial p}{\partial z} = -\rho g \cos\alpha \,. \tag{2.110}$$

The integral of this equation is

$$p = C_3 - \rho g z \cos\alpha \,, \tag{2.111}$$

and the integration constant C_3 follows from the stress-free boundary condition at the surface,

$$p|_{z=H} = C_3 - \rho g H \cos\alpha = 0 \quad \Rightarrow \quad C_3 = \rho g H \cos\alpha \,. \tag{2.112}$$

Thus, we obtain

$$p = \rho g (H - z) \cos\alpha \,, \tag{2.113}$$

which is a hydrostatic pressure profile, that is, the pressure at any point in the thin film equals the weight of the overburden fluid.

While one may think first of an oil film ($\eta \sim 0.1\,\mathrm{Pa\,s}$) thinner than one millimetre flowing down some substrate as a realisation of gravity-driven thin film flow, we can also make the film 100 metres thick and assume a viscosity as large as $\eta \sim 10^{14}\,\mathrm{Pa\,s}$. Then we already have a very simple model of a flowing glacier. However, for a realistic description of glacier ice the incompressible Newtonian fluid is not sufficient. In the next chapter we will formulate more appropriate constitutive equations for glacier ice.

3 Constitutive Equations for Polycrystalline Ice

3.1 Microstructure of Ice

The phase of H_2O ice which exists at pressure and temperature conditions encountered in ice sheets and glaciers is called *ice Ih*. It forms hexagonal crystals, that is, the water molecules are arranged in layers of hexagonal rings (Fig. 3.1). The plane of such a layer is called the *basal plane*, which actually consists of two planes shifted slightly (by 0.0923 nm) against each other. The direction perpendicular to the basal planes is the *optic axis* or *c-axis*, and the distance between two adjacent basal planes is 0.276 nm.

Owing to this relatively large distance, the basal planes can glide on each other when a shear stress is applied, comparable to the deformation of a deck of cards. To a much lesser extent, gliding is also possible in the prismatic and pyramidal planes (see Fig. 3.2). This means that the ice crystal responds to an applied shear stress with a continuous deformation, which goes on as long as the stress is applied (*creep*, fluid-like behaviour) and depends on the direction of the stress relative to the crystal planes (*anisotropy*).

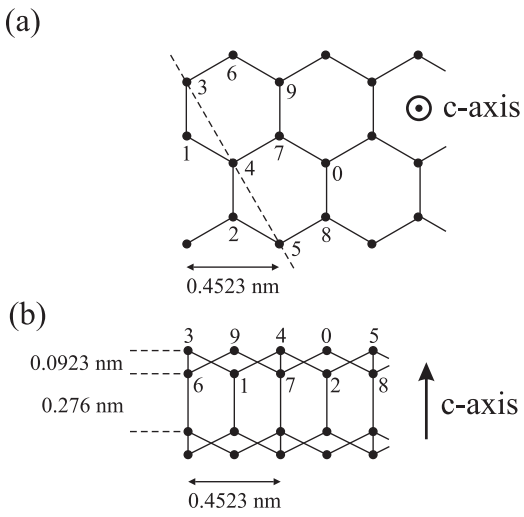

Figure 3.1: Structure of an ice crystal. The circles denote the oxygen atoms of the H_2O molecules. (a) Projection on the basal plane. (b) Projection on plane indicated by the broken line in (a). Adapted from Paterson (1994), © Elsevier.

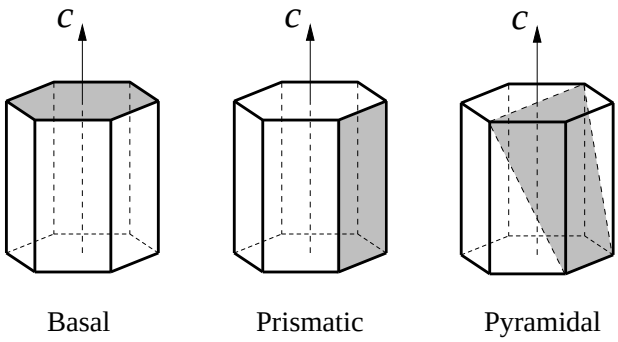

Figure 3.2: Basal, prismatic and pyramidal glide planes in the hexagonal ice Ih crystal. Reproduced from Faria (2003), © S. H. Faria.

Measurements have shown that ice crystals show some creep even for very low stresses. In a perfect crystal such a behaviour would not be expected. However, in real crystals *dislocations* occur, which are defects in its structure. These imperfections make the crystal much more easily deformable, and this is enhanced even more by the fact that during creep additional dislocations are generated. This creep mechanism is consequently called *dislocation creep*.

3.2 Creep of Polycrystalline Ice

Naturally, ice which occurs in ice sheets and glaciers does not consist of a single ice crystal. Rather, it is composed of a vast number of *crystallites* (also called *grains*), the typical size of which is of the order of millimetres to centimetres. Such a compound is called *polycrystalline ice*. An example is shown in Fig. 3.3.

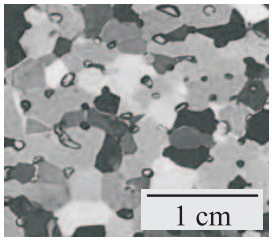

Figure 3.3: Thin-section of polycrystalline glacier ice regarded between crossed polarisation filters. The crystallites (grains) are clearly visible, and their apparent colours depend on the c-axis orientation.

The c-axis orientations of the crystallites in polycrystalline ice differ from one another. In the following, we will assume that the orientation distribution is completely random.

In this case, the anisotropy of the crystallites averages out in the compound, so that its macroscopic behaviour will be *isotropic*. In other words, the material properties of polycrystalline ice do not show any directional dependence.

Let us assume to conduct a shear experiment with a small sample of polycrystalline ice as sketched in Fig. 3.4 (left panel). The shear stress τ is assumed to be held constant, and the shear angle γ is measured as a function of time. The resulting creep curve $\gamma(t)$ is shown schematically in Fig. 3.4 (right panel). An initial, instantaneous *elastic deformation* of the polycrystalline aggregate is followed by a phase called *primary creep* during which the shear rate $\dot{\gamma}$ decreases continuously. This behaviour is related to the increasing geometric incompatibilities of the deforming crystallites with different orientations. After some time, a minimum shear rate is reached which remains constant subsequently, so that the shear angle increases linearly with time. This phase is known as *secondary creep*. In the case of rather high temperatures and/or high stresses, at a later stage *dynamic recrystallisation* (nucleation and growth of crystallites which are favourably oriented for deformation; also known as *migration recrystallisation*) sets in, which leads to accelerated creep and finally a constant shear rate (linear increase of the shear angle with time) significantly larger than that of the secondary creep. This is called *tertiary creep*.

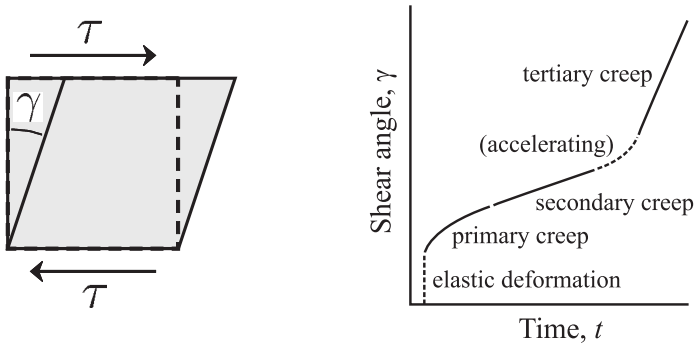

Figure 3.4: Shear experiment for a sample of polycrystalline ice. τ denotes the applied shear stress, γ the shear angle and t the time.

3.3 Flow Relation

3.3.1 Glen's Flow Law

From the above considerations it becomes clear that the shear rate $\dot{\gamma}$ for secondary (minimum) creep of isotropic polycrystalline ice under the simple-shear conditions illustrated in Fig. 3.4 can be expressed as a unique function of the shear stress τ, the ice temperature T and the pressure p,

$$\dot{\gamma} = \dot{\gamma}(\tau, T, p)\,. \tag{3.1}$$

Numerous laboratory experiments and field measurements suggest that the concrete relation is that of a non-linearly viscous fluid,

$$\dot{\gamma} = \frac{1}{\eta(T, p, |\tau|)}\,\tau\,, \tag{3.2}$$

where η denotes the shear viscosity. The inverse $1/\eta$ is called *fluidity*, and its dependence on the temperature T, the pressure p and the absolute value of the shear stress $|\tau|$ can be factorised as

$$\frac{1}{\eta(T, p, |\tau|)} = 2A(T, p)\, f(|\tau|)\,, \tag{3.3}$$

where $A(T, p)$ is the *rate factor* and $f(|\tau|)$ the *creep function*. These are usually expressed in the form of an *Arrhenius law*

$$A(T, p) = A_0\, e^{-(Q+pV)/RT}\,, \tag{3.4}$$

[A_0: pre-exponential constant, Q: activation energy, V: activation volume, R: universal gas constant ($= 8.314$ J mol^{-1} K^{-1})], and a *power law*,

$$f(|\tau|) = |\tau|^{n-1} \tag{3.5}$$

(n: stress exponent), respectively.

Let us now generalise the non-linearly viscous flow law (3.2) for secondary creep to arbitrary deformations and stresses. To a good approximation, ice can be described as incompressible, so that the pressure p will be a free field, and the three-dimensional flow law will relate the strain-rate tensor D and the stress deviator t^{D} (compare Sect. 2.4.2). If we define a Cartesian coordinate system such that the plane of Fig. 3.4 (left panel) falls on the x-z plane (where x is the horizontal and z the vertical coordinate), then we can identify $\dot{\gamma} = 2D_{xz}$ [see Eq. (2.27)] and $\tau = t_{xz}$ (see Fig. 2.7), so that (3.2) becomes

$$D_{xz} = \frac{1}{2\eta(T, p, |t_{xz}|)}\, t_{xz}\,. \tag{3.6}$$

Since D_{xz} is the x-z component of D and t_{xz} the x-z component of t^{D}, this suggests that the general flow law reads

$$\mathsf{D} = \frac{1}{2\eta(T, p, \sigma_{\mathrm{e}})}\, \mathsf{t}^{\mathrm{D}}\,. \tag{3.7}$$

The only non-straightforward point is the question how the $|t_{xz}|$ in Eq. (3.6) translates to the newly introduced scalar σ_{e} (*effective stress*). As a relation between two tensors, Eq. (3.7) must be independent of any particular basis (coordinate system). Therefore, the effective stress σ_{e} cannot be equal to a single element like $|t_{xz}|$, but it must be a *scalar invariant* of t^{D}. An order 2 tensor in three-dimensional space has only three independent invariants [see Eq. (A.42)], which are for t^{D}

$$\begin{aligned} I_{\mathsf{t}^{\mathrm{D}}} &= \operatorname{tr} \mathsf{t}^{\mathrm{D}} = 0\,, \\ II_{\mathsf{t}^{\mathrm{D}}} &= \tfrac{1}{2}\left[\operatorname{tr}(\mathsf{t}^{\mathrm{D}})^2 - (\operatorname{tr}\mathsf{t}^{\mathrm{D}})^2\right] = \tfrac{1}{2}\operatorname{tr}(\mathsf{t}^{\mathrm{D}})^2 \\ &= \tfrac{1}{2}\left[(t^{\mathrm{D}}_{xx})^2 + (t^{\mathrm{D}}_{yy})^2 + (t^{\mathrm{D}}_{zz})^2\right] + t^2_{xy} + t^2_{xz} + t^2_{yz}\,, \\ III_{\mathsf{t}^{\mathrm{D}}} &= \det \mathsf{t}^{\mathrm{D}} \end{aligned} \tag{3.8}$$

(note that $t_{ij} = t^{\mathrm{D}}_{ij}$ for $i \neq j$). If we choose

$$\sigma_{\mathrm{e}} = \sqrt{II_{\mathsf{t}^{\mathrm{D}}}} = \sqrt{\tfrac{1}{2}\,\mathrm{tr}\,(\mathsf{t}^{\mathrm{D}})^2}\,, \tag{3.9}$$

then we have found an invariant quantity which simplifies to $|t_{xz}|$ for the simple-shear conditions of (3.6). It is therefore reasonable to assume that (3.9) is the correct expression for the effective stress in the flow law (3.7).

As for the fluidity $1/\eta$ in Eq. (3.7), we can directly infer its functional dependence on T, p and σ_{e} from Eqs. (3.3), (3.4) and (3.5):

$$\frac{1}{\eta(T, p, \sigma_{\mathrm{e}})} = 2A(T, p)\, f(\sigma_{\mathrm{e}}) \tag{3.10}$$

[rate factor $A(T, p)$, creep function $f(\sigma_{\mathrm{e}})$], with the Arrhenius law

$$A(T, p) = A_0\, e^{-(Q+pV)/RT} \tag{3.11}$$

and the power law

$$f(\sigma_{\mathrm{e}}) = \sigma_{\mathrm{e}}^{n-1}\,. \tag{3.12}$$

The optimum value for the stress exponent n has been a matter of continuous debate, but most frequently $n = 3$ is used (Paterson 1994, van der Veen 1999, and references therein).

The melting temperature of ice, T_{m}, is pressure-dependent. For low pressures ($p \lesssim 100\,\mathrm{kPa}$), $T_{\mathrm{m}} = T_0 = 273.15\,\mathrm{K}$, and for pressures which occur typically in ice sheets and glaciers ($p \lesssim 50\,\mathrm{MPa}$) the linear relation

$$T_{\mathrm{m}} = T_0 - \beta\, p \tag{3.13}$$

holds. For pure ice, the *Clausius-Clapeyron constant* β has the value $\beta = 7.42{\times}10^{-8}\,\mathrm{K\,Pa^{-1}}$, but under realistic conditions the value for air-saturated ice, $\beta = 9.8 \times 10^{-8}\,\mathrm{K\,Pa^{-1}}$, is preferable (Hooke 2005). Under hydrostatic conditions, this leads to a melting-point lowering of 0.87 K per kilometre of ice thickness. With (3.13), the *temperature relative to the pressure melting point* is defined as

$$T' = T - T_{\mathrm{m}} + T_0 = T + \beta\, p\,, \tag{3.14}$$

so that the pressure melting point always corresponds to $T' = T_0 = 273.15\,\mathrm{K}$ (or 0°C). Measurements have shown that the pressure dependence in the Arrhenius law (3.11) is accounted for satisfactorily if the absolute temperature is replaced by the temperature relative to the pressure melting point, that is

$$A(T, p) = A(T') = A_0\, e^{-Q/RT'}\,. \tag{3.15}$$

Recommended values for the pre-exponential constant and the activation energy are listed in Table 3.1. The larger activation energy for $T' > 263.15\,\mathrm{K}$ is probably due to grain boundary sliding and the presence of liquid water at grain boundaries which contribute

Parameter	Value	
Stress exponent, n	3	
Pre-exponential constant, A_0	$3.985 \times 10^{-13}\,\mathrm{s^{-1}\,Pa^{-3}}$	(for $T' \leq 263.15\,\mathrm{K}$)
	$1.916 \times 10^{3}\,\mathrm{s^{-1}\,Pa^{-3}}$	(for $T' > 263.15\,\mathrm{K}$)
Activation energy, Q	$60\,\mathrm{kJ\,mol^{-1}}$	(for $T' \leq 263.15\,\mathrm{K}$)
	$139\,\mathrm{kJ\,mol^{-1}}$	(for $T' > 263.15\,\mathrm{K}$)

Table 3.1: Stress exponent and parameters for the Arrhenius law (3.15) (Paterson 1994).

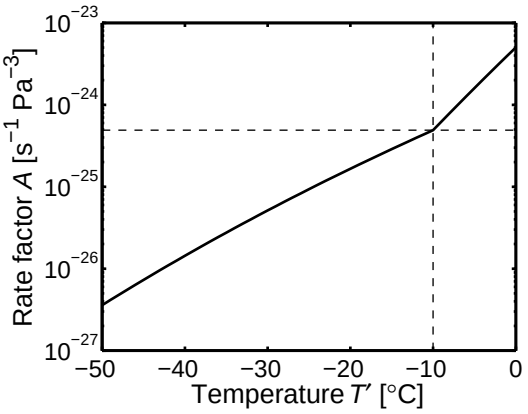

Figure 3.5: Rate factor $A(T')$ for the temperature range from $-50°\mathrm{C}$ to $0°\mathrm{C}$ (relative to the pressure melting point) according to the Arrhenius law (3.15). The kink at $-10°\mathrm{C}$ is due to the piecewise definition of the pre-exponential constant A_0 and the activation energy Q.

to creep in this temperature range [see the discussion by Paterson (1994), and references therein]. The two values of the pre-exponential constant yield $A(T' = 263.15\ \mathrm{K}) = 4.9 \times 10^{-25}\,\mathrm{s^{-1}\,Pa^{-3}}$ for both regimes, so that the function is continuous (Fig. 3.5). Note that these values are only reasonable for $n = 3$.

Equation (3.7) together with (3.10), (3.12) and (3.15) reads

$$\mathsf{D} = A(T')\,\sigma_{\mathrm{e}}^{n-1}\,\mathsf{t}^{\mathrm{D}}\,, \tag{3.16}$$

which is called *Nye's generalisation of Glen's flow law*, or *Glen's flow law* for short (Glen 1955, Nye 1957). Figure 3.6 shows the corresponding viscosity

$$\eta(T', \sigma_{\mathrm{e}}) = \frac{1}{2A(T')\,\sigma_{\mathrm{e}}^{n-1}} \tag{3.17}$$

for different stresses and temperatures. Evidently, the viscosity of polycrystalline ice is much larger than that of viscous fluids of everyday life. For instance, the viscosity of motor oil is of the order of $0.1\,\mathrm{Pa\,s}$, compared to $\sim 10^{13}\,\mathrm{Pa\,s}$ for ice at $T' = 0°\mathrm{C}$ and

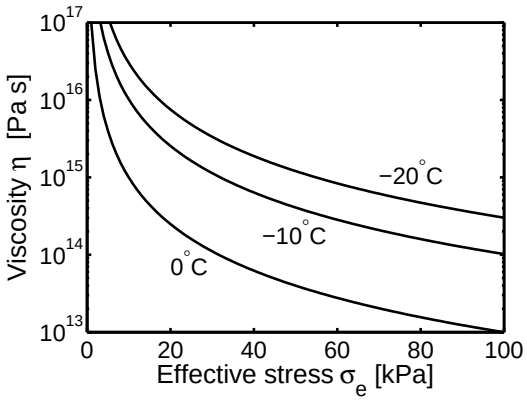

Figure 3.6: Viscosity (3.17) for a stress exponent $n = 3$, effective stresses up to 100 kPa (1 bar) and temperatures between $-20°\mathrm{C}$ and $0°\mathrm{C}$ (relative to the pressure melting point).

$\sigma_\mathrm{e} = 100\,\mathrm{kPa}$ (1 bar). On the other hand, the upper mantle of the Earth has a viscosity of the order of $10^{21}\,\mathrm{Pa\,s}$, which is further eight orders of magnitude stiffer, but still considered to be a fluid on geological time-scales.

In order to derive the inverse form of Glen's flow law, we define the *effective strain rate*

$$d_\mathrm{e} = \sqrt{\tfrac{1}{2}\,\mathrm{tr}\,\mathsf{D}^2}\,, \tag{3.18}$$

[square root of the second invariant of the strain-rate tensor, compare to (3.9)], for which we obtain, by inserting (3.16)

$$d_\mathrm{e} = A(T')\,\sigma_\mathrm{e}^{n-1}\,\sigma_\mathrm{e} = A(T')\,\sigma_\mathrm{e}^n \quad \Leftrightarrow \quad \sigma_\mathrm{e} = A(T')^{-1/n}\,d_\mathrm{e}^{1/n}\,. \tag{3.19}$$

Solving (3.16) for t^D and using (3.19) yields

$$\begin{aligned}\mathsf{t}^\mathrm{D} &= A(T')^{-1}\,\sigma_\mathrm{e}^{-(n-1)}\mathsf{D}\\ &= A(T')^{-1}\,A(T')^{(n-1)/n}\,d_\mathrm{e}^{-(n-1)/n}\mathsf{D}\\ &= A(T')^{-1/n}\,d_\mathrm{e}^{-(1-1/n)}\mathsf{D}\\ \Rightarrow\quad \mathsf{t}^\mathrm{D} &= B(T')\,d_\mathrm{e}^{-(1-1/n)}\mathsf{D}\,,\end{aligned} \tag{3.20}$$

where the *associated rate factor* $B(T') = A(T')^{-1/n}$ has been introduced. We may write this with the shear viscosity η as

$$\mathsf{t}^\mathrm{D} = 2\eta(T', d_\mathrm{e})\,\mathsf{D} \tag{3.21}$$

[see (3.7)], where

$$\eta(T', d_\mathrm{e}) = \frac{1}{2}B(T')\,d_\mathrm{e}^{-(1-1/n)}\,. \tag{3.22}$$

Evidently, the flow law for polycrystalline ice in the form of (3.7) or (3.21) is very similar to that of the incompressible Newtonian fluid which was discussed in Sect. 2.4.2 [see Eq. (2.94)]. The difference is that here we deal with a *non-linear* flow law, in that the viscosity depends on the effective stress or the effective strain rate.

3.3.2 Flow Enhancement Factor

The flow law of Sect. 3.3.1 is valid for secondary creep of isotropic polycrystalline ice. However, as we have discussed in Sect. 3.2, in regions of flowing ice sheets and glaciers with relatively high temperatures and/or stresses, tertiary creep may prevail, which goes along with the formation of an anisotropic fabric (non-uniform orientation distribution of the c-axes) favourable for the deformation regime at hand.

A crude, but very common way of including this effect in the flow law is by multiplying the isotropic ice fluidity for secondary creep by a *flow enhancement factor* $E > 1$ (Hooke 2005). This can be conveniently achieved by replacing the rate factor $A(T')$ for the Glen flow law by

$$A(T') \to EA(T') \,. \tag{3.23}$$

Suggested values for the flow enhancement factor vary and depend on the deformation regime; however, in practice often an overall constant value somewhere between 1 and 10 for the considered ice sheet or glacier is chosen.

In case of Glen's flow law, we have seen that an analytical inversion is possible. Equation (3.23) yields for the associated rate factor introduced in Eq. (3.20)

$$B(T') = A(T')^{-1/n} \;\to\; [EA(T')]^{-1/n} = E_{\mathrm{s}} B(T') \,, \tag{3.24}$$

where $E_{\mathrm{s}} = E^{-1/n}$ is the *stress enhancement factor*.

3.4 Heat Flux and Internal Energy

The heat flux $\mathbf{q}$ in polycrystalline ice can be described well by Fourier's law of heat conduction [see (2.98)],

$$\mathbf{q} = -\kappa(T) \operatorname{grad} T \,, \tag{3.25}$$

with the temperature-dependent heat conductivity

$$\kappa(T) = 9.828\, e^{-0.0057\, T[\mathrm{K}]}\, \mathrm{W\,m^{-1}K^{-1}} \tag{3.26}$$

(Ritz 1987). For $T = T_0 = 273.15\,\mathrm{K}$ this yields a value of $2.07\,\mathrm{W\,m^{-1}K^{-1}}$, and it increases with decreasing temperature (Fig. 3.7, top panel).

The caloric equation of state (constitutive equation for the internal energy) is given by

$$u = \int_{T_0}^{T} c(\bar{T})\, \mathrm{d}\bar{T} \,, \tag{3.27}$$

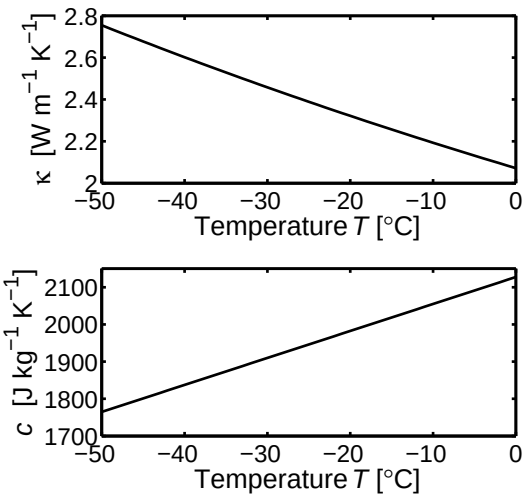

Figure 3.7: Heat conductivity κ and specific heat c for the temperature range from $-50°$C until $0°$C.

which is a generalisation of Eq. (2.99) with the temperature-dependent specific heat

$$c(T) = (146.3 + 7.253\,T[\mathrm{K}])\,\mathrm{J\,kg^{-1}K^{-1}} \tag{3.28}$$

(Ritz 1987). According to this formula, at $T = T_0 = 273.15\,\mathrm{K}$ one obtains $2127.5\,\mathrm{J\,kg^{-1}K^{-1}}$. Contrary to the heat conductivity, the specific heat decreases with decreasing temperature (Fig. 3.7, bottom panel).

4 Large-Scale Dynamics of Ice Sheets

4.1 Full Stokes Flow Problem

4.1.1 Field Equations

With the constitutive equations given in Sects. 3.3 and 3.4, we are now able to formulate the mechanical and thermodynamical field equations for the flow of ice in an ice sheet. Figure 4.1 shows the typical geometry (cross section) of a grounded ice sheet with attached floating ice shelf (the latter will be treated in Chap. 5), as well as its interactions with the atmosphere (snowfall, melting), the lithosphere (geothermal heat flux, isostasy) and the ocean (melting, calving). Also, a Cartesian coordinate system is introduced, where x and y lie in the horizontal plane, and z is positive upward. These coordinates are naturally associated with the set of basis vectors $\{\mathbf{e}_x, \mathbf{e}_y, \mathbf{e}_z\}$. The free surface (ice-atmosphere interface) is given by the function $z = h(x, y, t)$, the ice base by $z = b(x, y, t)$ and the lithosphere surface by $z = z_{\mathrm{l}}(x, y, t)$. Note that for the grounded ice sheet the ice base and the lithosphere surface fall together ($b = z_{\mathrm{l}}$) and form the ice-lithosphere interface.

By introducing the Cartesian coordinates x, y, z, we have tacitly assumed a flat Earth. For the vertical direction, this simplification is justified because the vertical extent of ice sheets (as well as ice shelves and glaciers) is always much smaller than the mean radius of the Earth ($R_{\mathrm{e}} = 6371\,\mathrm{km}$), so that curvature effects are negligible. In the horizontal, the flattening can be achieved by a suitable map projection. For ice sheets, often the polar stereographic projection is used, which is illustrated in Fig. 4.2. It preserves angles, but not distances and areas. The distortions are negligible for most practical applications, though. Even for the entire Antarctic Ice Sheet (situated between $\sim 63°\mathrm{S}$ and $90°\mathrm{S}$), the distortion of the length scale nowhere exceeds 3% if the standard parallel is chosen as $\varphi_0 = 71°\mathrm{S}$.

Since we have assumed ice to be an incompressible material, the mass balance (2.52) applies,

$$\operatorname{div} \mathbf{v} = 0\,. \tag{4.1}$$

The flow law in the form (3.21) yields for the divergence of the stress deviator [note that, contrary to (2.96), η is not constant]

$$\begin{aligned}
(\operatorname{div} \mathsf{t}^{\mathrm{D}})_i &= 2(\eta\, D_{ij})_{,j} = 2\eta\, D_{ij,j} + 2D_{ij}\,\eta_{,j} \\
&= \eta\,(v_{i,jj} + v_{j,ij}) + (v_{i,j} + v_{j,i})\,\eta_{,j} \\
&= \eta\,[(\Delta \mathbf{v})_i + (\operatorname{div} \mathbf{v})_{,i}] + \Big[\Big(\operatorname{grad} \mathbf{v} + (\operatorname{grad} \mathbf{v})^{\mathrm{T}}\Big) \cdot \operatorname{grad} \eta\Big]_i \\
&= \eta\,(\Delta \mathbf{v})_i + \Big[\Big(\operatorname{grad} \mathbf{v} + (\operatorname{grad} \mathbf{v})^{\mathrm{T}}\Big) \cdot \operatorname{grad} \eta\Big]_i\,.
\end{aligned} \tag{4.2}$$

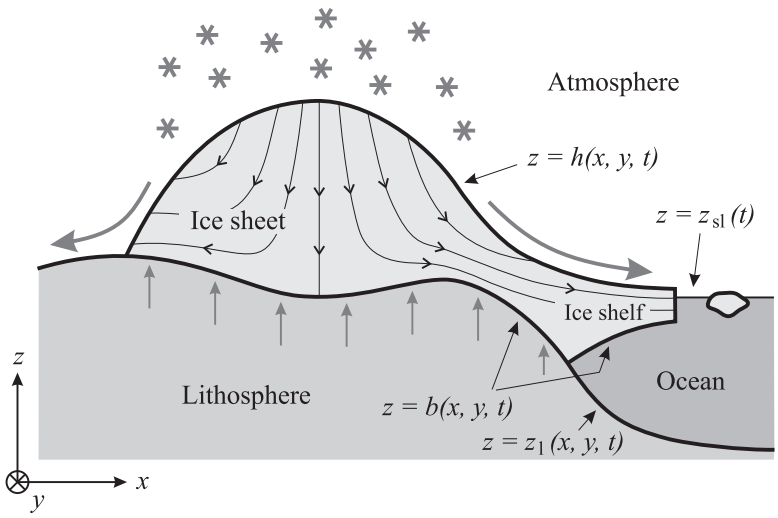

Figure 4.1: Ice sheet geometry (with attached ice shelf) and Cartesian coordinate system. x and y span the horizontal plane, z is positive upward. $z = h(x, y, t)$ denotes the free surface, $z = b(x, y, t)$ the ice base, $z = z_l(x, y, t)$ the lithosphere surface and $z = z_{sl}(t)$ the mean sea level. Interactions with the atmosphere, the lithosphere and the ocean are indicated. Vertical exaggeration factor $\sim$ 200-500.

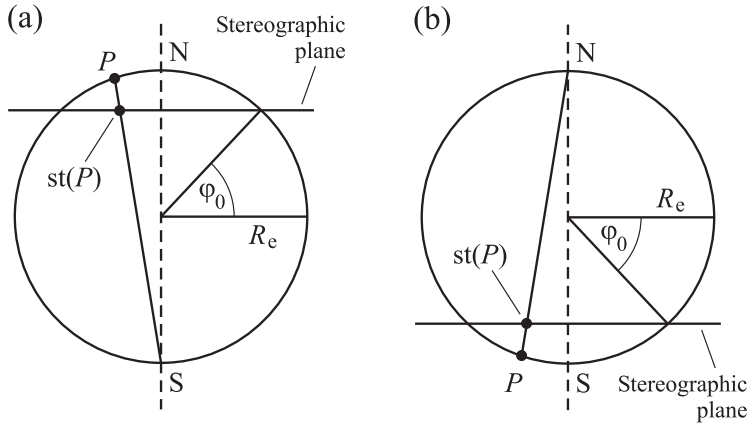

Figure 4.2: Polar stereographic projection for (a) the northern and (b) the southern hemisphere. The stereographic plane is parallel to the equatorial plane and defined by the standard parallel φ_0 (often chosen as 71°N or 71°S). A point P on the surface of the Earth is projected on the point st(P) by intersecting the line $\overline{PS}$ (case a) or $\overline{PN}$ (case b) with the stereographic plane.

The volume force $\mathbf{f}$ acting on an ice sheet on the rotating Earth consists of the force of gravity, the centrifugal force and the Coriolis force (the latter two are inertial forces). Since

the centrifugal force depends only on position, it is usually combined with the actual force of gravity to form the effective force of gravity $\rho\mathbf{g}$, where $\rho = 910\,\mathrm{kg\,m^{-3}}$ is the density of ice, and $\mathbf{g}$ is the gravitational acceleration. On the surface of the Earth, the gravitational acceleration takes values between ~ 9.78 and $9.83\,\mathrm{m\,s^{-2}}$ depending on latitude. Since this variability is negligible for our purposes, we adopt the constant standard value $g = |\mathbf{g}| = 9.81\,\mathrm{m\,s^{-2}}$ instead. The vector $\mathbf{g}$ is directed downward, so that $\mathbf{g} = -g\,\mathbf{e}_z$. The Coriolis force depends on the flow velocity $\mathbf{v}$ and the angular velocity $\boldsymbol{\Omega}$ of the Earth. The vector $\boldsymbol{\Omega}$ points northward parallel to the rotational axis of the Earth, and its value is $\Omega = |\boldsymbol{\Omega}| = 2\pi/(23.9345\,\mathrm{h}) = 7.2921 \times 10^{-5}\,\mathrm{s^{-1}}$. Hence, the volume force reads

$$\mathbf{f} = \rho\mathbf{g} - 2\rho\boldsymbol{\Omega} \times \mathbf{v}\,. \tag{4.3}$$

By inserting Eqs. (4.2) and (4.3) in the momentum balance (2.64) we obtain the equation of motion

$$\begin{aligned} \rho\frac{\mathrm{d}\mathbf{v}}{\mathrm{d}t} &= -\mathrm{grad}\,p + \eta\,\Delta\mathbf{v} + \Big(\mathrm{grad}\,\mathbf{v} + (\mathrm{grad}\,\mathbf{v})^{\mathrm{T}}\Big)\cdot\mathrm{grad}\,\eta \\ &\quad + \rho\mathbf{g} - 2\rho\boldsymbol{\Omega}\times\mathbf{v}\,. \end{aligned} \tag{4.4}$$

In this equation, let us compare the acceleration term on the left-hand side with the pressure-gradient term on the right-hand side. To this end, we introduce *typical values* for the horizontal and vertical extent of an ice sheet, the horizontal and vertical flow velocities, the pressure and the time as follows,

$$\begin{aligned} \text{typical horizontal extent} \quad [L] &= 1000\,\mathrm{km}\,, \\ \text{typical vertical extent} \quad [H] &= 1\,\mathrm{km}\,, \\ \text{typical horizontal velocity} \quad [U] &= 100\,\mathrm{m\,a^{-1}}\,, \\ \text{typical vertical velocity} \quad [W] &= 0.1\,\mathrm{m\,a^{-1}}\,, \\ \text{typical pressure} \quad [P] &= \rho g[H] \approx 10\,\mathrm{MPa}\,, \\ \text{typical time-scale} \quad [t] &= [L]/[U] = [H]/[W] = 10^4\,\mathrm{a}\,. \end{aligned} \tag{4.5}$$

Further, the *aspect ratio* ε is defined as the ratio of vertical to horizontal extents and velocities, respectively:

$$\varepsilon = \frac{[H]}{[L]} = \frac{[W]}{[U]} = 10^{-3}\,. \tag{4.6}$$

For the horizontal direction, the ratio of acceleration and pressure gradient, called the *Froude number* Fr, is then

$$Fr = \frac{\rho[U]/[t]}{[P]/[L]} = \frac{\rho[U]^2/[L]}{\rho g[H]/[L]} = \frac{[U]^2}{g[H]} \approx 10^{-15} \tag{4.7}$$

(note that $1\,\mathrm{a} = 31556926\,\mathrm{s} \approx \sqrt{10^{15}}\,\mathrm{s}$), and for the vertical direction we obtain the ratio

$$\frac{\rho[W]/[t]}{[P]/[H]} = \frac{\rho[W]^2/[H]}{\rho g[H]/[H]} = \frac{[W]^2}{g[H]} = \varepsilon^2 Fr \approx 10^{-21}\,. \tag{4.8}$$

Consequently, for the flow of ice sheets, the acceleration term in the equation of motion (4.4) is negligible.

In a similar way, we estimate the ratio between the Coriolis and pressure-gradient terms in Eq. (4.4). Since the cross product in the Coriolis term mixes horizontal and vertical contributions, we apply the common scales $2\rho\Omega[U]$ and $[P]/[L]$, respectively, for both the horizontal and vertical direction. By introducing the *Rossby number* Ro as

$$Ro = \frac{[U]}{2\Omega[L]} \approx 2 \times 10^{-8}\,, \tag{4.9}$$

the Coriolis-force-to-pressure-gradient ratio yields

$$\frac{2\rho\Omega[U]}{[P]/[L]} = \frac{2\Omega[U][L]}{g[H]} = \frac{[U]^2}{g[H]}\,\frac{2\Omega[L]}{[U]} = \frac{Fr}{Ro} \approx 5 \times 10^{-8}\,, \tag{4.10}$$

which is seven orders of magnitude larger than the Froude number, but still very small. Hence, the Coriolis term in the equation of motion (4.4) is also negligible, and it can be simplified to

$$-\operatorname{grad} p + \eta\,\Delta\mathbf{v} + \left(\operatorname{grad}\mathbf{v} + (\operatorname{grad}\mathbf{v})^{\mathrm{T}}\right)\cdot\operatorname{grad}\eta + \rho\mathbf{g} = \mathbf{0}\,. \tag{4.11}$$

This is the *Stokes equation*, and the resulting type of flow is called *Stokes flow*.

Since the Stokes equation is a differential equation for the velocity field, it is favourable to employ the form of the viscosity η which depends via the effective strain rate d_{e} on the velocity gradient. Therefore, $\eta = \eta(T', d_{\mathrm{e}})$, and it is determined for Glen's flow law by Eq. (3.22).

Owing to the temperature dependence of the viscosity, a thermo-mechanically coupled problem applies, and its complete formulation requires an evolution equation for the temperature field. As it was demonstrated in Sect. 2.4.2, this equation can be derived by inserting the constitutive equations for the stress deviator (3.21), the heat flux (3.25) and the internal energy (3.27) in the internal-energy balance (2.80). We obtain

$$\frac{\mathrm{d}u}{\mathrm{d}t} = c\frac{\mathrm{d}T}{\mathrm{d}t}\,, \qquad \operatorname{div}\mathbf{q} = -\operatorname{div}(\kappa\operatorname{grad}T) \tag{4.12}$$

and

$$\operatorname{tr}(\mathsf{t}\cdot\mathsf{D}) = \operatorname{tr}\left[(-p\,\mathsf{I} + 2\eta\mathsf{D})\cdot\mathsf{D}\right] = 2\eta\operatorname{tr}\mathsf{D}^2 = 4\eta\,d_{\mathrm{e}}^2 \tag{4.13}$$

[see (3.18)]. Further, except for the very uppermost few centimetres of ice exposed to sunlight, the radiation r is negligible in an ice sheet, so that we obtain the temperature evolution equation in the form

$$\rho c\frac{\mathrm{d}T}{\mathrm{d}t} = \operatorname{div}(\kappa\operatorname{grad}T) + 4\eta\,d_{\mathrm{e}}^2\,. \tag{4.14}$$

Since the ice temperature must not exceed the pressure melting point, the solution of (4.14) is subject to the secondary condition $T \le T_{\mathrm{m}}$. With the continuity equation (4.1), the equation of motion (4.11), the expression (3.22) for the viscosity and the temperature evolution equation (4.14), we have found a closed system of six equations for the six unknown fields v_x, v_y, v_z, η, p and T of the thermo-mechanical Stokes flow problem.

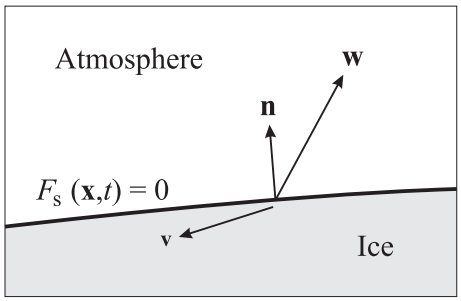

Figure 4.3: Geometry of the free surface $F_s(\mathbf{x}, t) = 0$. $\mathbf{n}$ is the unit normal vector, $\mathbf{v}$ the ice velocity and $\mathbf{w}$ the velocity of the free surface.

4.1.2 Boundary Conditions

In order to provide a solvable problem, the above system of equations needs to be completed by appropriate *boundary conditions* at the free surface and the ice base (see Fig. 4.1). The possible presence of attached ice shelves will be ignored for now.

Free Surface

Like any boundary, the free surface of an ice sheet can be regarded as a singular surface in the sense of Sect. 2.3.3. If we denote it in implicit form by the equation

$$F_s(\mathbf{x}, t) = z - h(x, y, t) = 0\,, \tag{4.15}$$

then it can be interpreted as a zero-equipotential surface of the function $F_s(\mathbf{x}, t)$, where the unit normal vector is the normalised gradient

$$\mathbf{n} = \frac{\operatorname{grad} F_s}{|\operatorname{grad} F_s|} = \frac{1}{N_s} \begin{pmatrix} -\dfrac{\partial h}{\partial x} \\ -\dfrac{\partial h}{\partial y} \\ 1 \end{pmatrix}, \tag{4.16}$$

which points into the atmosphere (Fig. 4.3). Note that the abbreviation N_s stands for the gradient norm,

$$N_s = |\operatorname{grad} F_s| = \left(1 + \left(\frac{\partial h}{\partial x}\right)^2 + \left(\frac{\partial h}{\partial y}\right)^2\right)^{1/2}. \tag{4.17}$$

As a direct consequence of Eq. (4.15), the time derivative of F_s *following the motion of the free surface* with velocity $\mathbf{w}$ must vanish,

$$\frac{\mathrm{d}_w F_s}{\mathrm{d}t} = \frac{\partial F_s}{\partial t} + (\operatorname{grad} F_s) \cdot \mathbf{w} = 0 \tag{4.18}$$

[compare Eq. (2.15)]. Let $\mathbf{v}$ be the ice surface velocity, then we can introduce the ice volume flux through the free surface,

$$a_{\mathrm{s}}^{\perp} = (\mathbf{w} - \mathbf{v}) \cdot \mathbf{n}\,, \tag{4.19}$$

which is also known as the *accumulation-ablation function* or *surface mass balance* (perpendicular to the free surface). The sign is chosen such that a supply (accumulation) is counted as positive and a loss (ablation) as negative. With this definition and (4.16), Eq. (4.18) can be rewritten as

$$\frac{\partial F_{\mathrm{s}}}{\partial t} + (\operatorname{grad} F_{\mathrm{s}}) \cdot \mathbf{v} = -N_{\mathrm{s}} a_{\mathrm{s}}^{\perp}\,, \tag{4.20}$$

or, by inserting $F_{\mathrm{s}} = z - h$ [see (4.15)],

$$\frac{\partial h}{\partial t} + v_x \frac{\partial h}{\partial x} + v_y \frac{\partial h}{\partial y} - v_z = N_{\mathrm{s}} a_{\mathrm{s}}^{\perp}\,. \tag{4.21}$$

Since this condition has been derived by geometrical considerations only, it is called the *kinematic boundary condition*. Provided that the accumulation-ablation function $a_{\mathrm{s}}^{\perp}$ is known, it evidently governs the evolution of the free surface.

If we identify the positive side of the free surface with the atmosphere and the negative side with the ice, then the momentum jump condition (2.65) (note that the free surface is a non-material surface if $a_{\mathrm{s}}^{\perp} \neq 0$) yields

$$\begin{aligned} &\mathsf{t}_{\mathrm{atm}} \cdot \mathbf{n} - \mathsf{t} \cdot \mathbf{n} - \rho((\mathbf{v} - \mathbf{w}) \cdot \mathbf{n}) \, [\![\mathbf{v}]\!] \\ &= \mathsf{t}_{\mathrm{atm}} \cdot \mathbf{n} - \mathsf{t} \cdot \mathbf{n} + \rho a_{\mathrm{s}}^{\perp} \, [\![\mathbf{v}]\!] = \mathbf{0} \end{aligned} \tag{4.22}$$

[in the first line, the term $\rho((\mathbf{v}-\mathbf{w})\cdot\mathbf{n})$ can be factored out of the jump brackets because of the mass balance (2.53)]. The advective term $\rho a_{\mathrm{s}}^{\perp} \, [\![\mathbf{v}]\!]$ is very small and thus negligible due to the small ice flow velocities, and the atmospheric stress $\mathsf{t}_{\mathrm{atm}} \cdot \mathbf{n}$ (atmospheric pressure plus wind stress) is also small compared to the typical stresses in an ice sheet. Thus, we can neglect both terms, and obtain the *stress-free condition*

$$\mathsf{t} \cdot \mathbf{n} = \mathbf{0}\,. \tag{4.23}$$

This is the *dynamic boundary condition* for the free surface.

For the temperature evolution equation (4.14), it is further required to provide a *thermodynamic boundary condition*. This can be simply done by prescribing the surface temperature T_{s},

$$T = T_{\mathrm{s}}\,. \tag{4.24}$$

Measurements have shown that T_{s} can be well approximated by the mean-annual surface air temperature, as long as the latter is $\leq 0°\mathrm{C}$.

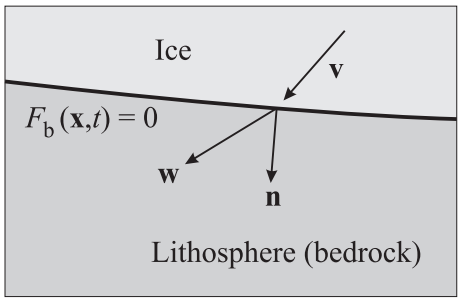

Figure 4.4: Geometry of the ice base $F_\mathrm{b}(\mathbf{x}, t) = 0$. $\mathbf{n}$ is the unit normal vector, $\mathbf{v}$ the ice velocity and $\mathbf{w}$ the velocity of the ice base.

Ice Base

In a similar manner to the free surface, a *kinematic boundary condition* for the ice base can be derived. Let

$$F_\mathrm{b}(\mathbf{x}, t) = b(x, y, t) - z = 0 \tag{4.25}$$

be its implicit representation, then the unit normal vector is

$$\mathbf{n} = \frac{\operatorname{grad} F_\mathrm{b}}{|\operatorname{grad} F_\mathrm{b}|} = \frac{1}{N_\mathrm{b}} \begin{pmatrix} \dfrac{\partial b}{\partial x} \\ \dfrac{\partial b}{\partial y} \\ -1 \end{pmatrix}, \tag{4.26}$$

which points into the bedrock (Fig. 4.4). The abbreviation N_b denotes the gradient norm,

$$N_\mathrm{b} = |\operatorname{grad} F_\mathrm{b}| = \left(1 + \left(\frac{\partial b}{\partial x}\right)^2 + \left(\frac{\partial b}{\partial y}\right)^2\right)^{1/2}. \tag{4.27}$$

Analogous to Eq. (4.18), the time derivative of F_b following the motion of the ice base vanishes,

$$\frac{\mathrm{d}_w F_\mathrm{b}}{\mathrm{d}t} = \frac{\partial F_\mathrm{b}}{\partial t} + (\operatorname{grad} F_\mathrm{b}) \cdot \mathbf{w} = 0\,, \tag{4.28}$$

where $\mathbf{w}$ is the velocity of the ice base. With the ice volume flux through the base,

$$a_\mathrm{b}^\perp = (\mathbf{v} - \mathbf{w}) \cdot \mathbf{n}\,, \tag{4.29}$$

where the sign has been chosen such that a mass loss due to basal melting (and subsequent penetration of the meltwater into the ground) is counted as positive, and which is therefore called the *basal melting rate* (perpendicular to the ice base), we obtain

$$\frac{\partial F_\mathrm{b}}{\partial t} + (\operatorname{grad} F_\mathrm{b}) \cdot \mathbf{v} = N_\mathrm{b} a_\mathrm{b}^\perp\,, \tag{4.30}$$

and, by inserting $F_\mathrm{b} = b - z$ [Eq. (4.25)],

$$\frac{\partial b}{\partial t} + v_x \frac{\partial b}{\partial x} + v_y \frac{\partial b}{\partial y} - v_z = N_\mathrm{b} a_\mathrm{b}^\perp \,. \tag{4.31}$$

We identify the positive side of the ice base with the lithosphere and the negative side with the ice. Then, corresponding to Eq. (4.22), the momentum jump condition reads

$$\mathsf{t}_\mathrm{lith} \cdot \mathbf{n} - \mathsf{t} \cdot \mathbf{n} - \rho a_\mathrm{b}^\perp \, [\![\mathbf{v}]\!] = \mathbf{0} \,. \tag{4.32}$$

Again, the advective term $\rho a_\mathrm{b}^\perp \, [\![\mathbf{v}]\!]$ is very small and therefore negligible, so that

$$\mathsf{t} \cdot \mathbf{n} = \mathsf{t}_\mathrm{lith} \cdot \mathbf{n} \,. \tag{4.33}$$

This is to say that the stress vector is continuous across the interface. However, since we do not have any information about the stress conditions in the bedrock, this finding does not provide a boundary condition for the basal stress in the ice. Instead, an empirical *sliding law* will serve as the required dynamic boundary condition. It is reasonable to assume that the ice is frozen to the ground if the basal temperature T_b is below the pressure melting point T_m, so that *no-slip conditions* prevail. By contrast, if the basal temperature is at the pressure melting point, basal sliding can be expected, and its amount can be related to the basal drag $\boldsymbol{\tau}_\mathrm{b}$ and the basal normal stress N_b in the form of a power law (*Weertman-type sliding law*). To this end, we split up the basal stress vector $\mathbf{t}_\mathbf{n}|_{z=b} = \mathsf{t}|_{z=b} \cdot \mathbf{n}$ into its normal component, $\mathbf{N}_\mathrm{b} = -N_\mathrm{b}\mathbf{n}$ (the minus sign causes N_b to be positive for compression, which is the expected situation), and its shear component, $\boldsymbol{\tau}_\mathrm{b} = \tau_\mathrm{b}\mathbf{e}_\mathrm{t}$,

$$\mathbf{t}_\mathbf{n}|_{z=b} = \mathbf{N}_\mathrm{b} + \boldsymbol{\tau}_\mathrm{b} = -N_\mathrm{b}\mathbf{n} + \tau_\mathrm{b}\mathbf{e}_\mathrm{t} \,, \tag{4.34}$$

where $\mathbf{e}_\mathrm{t}$ denotes the direction of the basal shear stress in the plane tangential to the ice base ($\mathbf{e}_\mathrm{t} \perp \mathbf{n}$). The basal sliding velocity $\mathbf{v}_\mathrm{b}$ is then expressed as

$$\mathbf{v}_\mathrm{b} = \begin{cases} \mathbf{0} \,, & \text{if } \; T_\mathrm{b} < T_\mathrm{m} \,, \\ -C_\mathrm{b} \dfrac{\tau_\mathrm{b}^p}{N_\mathrm{b}^q} \, \mathbf{e}_\mathrm{t} \,, & \text{if } \; T_\mathrm{b} = T_\mathrm{m} \,, \end{cases} \tag{4.35}$$

where p and q are the basal sliding exponents. As for the stress exponent n in the creep function (3.12) of Glen's flow law, the best choice for their values are a matter of debate, but commonly used values are $(p, q) = (3, 1)$ or $(3, 2)$ for sliding on hard rock, and $(p, q) = (1, 0)$ for sliding on soft, deformable sediment.

As for the *thermodynamic boundary condition*, sufficient information on the spatio-temporal distribution of the basal temperature is not available, so that it cannot be prescribed directly. Instead, we will have to formulate the energy jump condition (2.82) for the ice base. We obtain

$$\mathbf{q}_\mathrm{lith} \cdot \mathbf{n} - \mathbf{q} \cdot \mathbf{n} - [\![\mathbf{v}]\!] \cdot \mathsf{t} \cdot \mathbf{n} + \rho((\mathbf{v} - \mathbf{w}) \cdot \mathbf{n}) \left[\!\left[u + \frac{v^2}{2} \right]\!\right] = 0 \,. \tag{4.36}$$

Note that the term $\rho((\mathbf{v}-\mathbf{w})\cdot\mathbf{n})$ has been factored out of the jump brackets because of the mass balance (2.53), and the stress vector $\mathbf{t}\cdot\mathbf{n}$ has been factored out due to (4.33). The term $-\mathbf{q}_{\mathrm{lith}}\cdot\mathbf{n}$ can be identified with the *geothermal heat flux* $q^{\perp}_{\mathrm{geo}}$, that is, the heat flow which enters the ice body from below due to the warmer Earth's interior. Further, we insert Eqs. (3.25) and (4.29), and neglect the very small kinetic energy $v^2/2$ in comparison with the internal energy u, so that

$$\kappa\,(\operatorname{grad} T\cdot\mathbf{n}) - q^{\perp}_{\mathrm{geo}} - [\![\mathbf{v}]\!]\cdot\mathbf{t}\cdot\mathbf{n} + \rho a^{\perp}_{\mathrm{b}}\,[\![u]\!] = 0\,. \tag{4.37}$$

Two cases are to be distinguished. For a *cold base*, that is, a basal temperature below the pressure melting point, there cannot be any basal melting ($a^{\perp}_{\mathrm{b}}=0$), and no-slip conditions prevail [see $(4.35)_1$], so that $[\![\mathbf{v}]\!]=\mathbf{0}$. Thus, Eq. (4.37) simplifies to

$$\kappa\,(\operatorname{grad} T\cdot\mathbf{n}) = q^{\perp}_{\mathrm{geo}}\,, \tag{4.38}$$

which is a Neumann-type boundary condition for the basal temperature. By contrast, in case of a *temperate base* (basal temperature at the pressure melting point), the basal temperature itself is known, namely

$$T = T_{\mathrm{m}} \tag{4.39}$$

(Dirichlet-type condition). As a consequence, the energy jump condition (4.37) is no longer needed as a boundary condition for the temperature field, but it can be used to compute the unknown basal melting rate $a^{\perp}_{\mathrm{b}}$. Since there will be meltwater on the positive (lithosphere) side and ice on the negative (ice) side of the base, the jump of the internal energy $[\![u]\!]$ is equal to the *latent heat* L of ice melt, that is, $[\![u]\!]=L$. Furthermore, the velocity jump is given by the sliding velocity $(4.35)_2$, so that $[\![\mathbf{v}]\!]=-\mathbf{v}_{\mathrm{b}}$. With these settings, the energy jump condition (4.37), solved for $a^{\perp}_{\mathrm{b}}$, yields

$$a^{\perp}_{\mathrm{b}} = \frac{q^{\perp}_{\mathrm{geo}} - \kappa\,(\operatorname{grad} T\cdot\mathbf{n}) - \mathbf{v}_{\mathrm{b}}\cdot\mathbf{t}\cdot\mathbf{n}}{\rho L}\,. \tag{4.40}$$

Evidently, the situation is different from that of the free surface, where the accumulation-ablation function $a^{\perp}_{\mathrm{s}}$ must be prescribed as climatic input (along with the surface temperature T_{s}), whereas the basal melting rate $a^{\perp}_{\mathrm{b}}$ can be computed. Instead, at the ice base the geothermal heat flux $q^{\perp}_{\mathrm{geo}}$ must be prescribed as an input quantity.

4.1.3 Ice Thickness Equation

By combining the continuity equation (4.1) with the kinematic boundary conditions (4.21) and (4.31), we can now derive an evolution equation for the ice thickness $H(x,y,t) = h(x,y,t) - b(x,y,t)$. To this end, we write (4.1) in component form,

$$\frac{\partial v_x}{\partial x} + \frac{\partial v_y}{\partial y} + \frac{\partial v_z}{\partial z} = 0\,, \tag{4.41}$$

and integrate it from the ice base to the free surface:

$$\int_b^h \frac{\partial v_x}{\partial x}\,\mathrm{d}z + \int_b^h \frac{\partial v_y}{\partial y}\,\mathrm{d}z + \int_b^h \frac{\partial v_z}{\partial z}\,\mathrm{d}z = 0\,. \tag{4.42}$$

The first two terms can be modified using Leibniz's rule,

$$\frac{\partial}{\partial x}\int_b^h v_x\,\mathrm{d}z = \int_b^h \frac{\partial v_x}{\partial x}\,\mathrm{d}z + v_x|_{z=h}\,\frac{\partial h}{\partial x} - v_x|_{z=b}\,\frac{\partial b}{\partial x} \tag{4.43}$$

(and accordingly for the y-derivative), and the third term is simply

$$\int_b^h \frac{\partial v_z}{\partial z}\,\mathrm{d}z = v_z|_{z=h} - v_z|_{z=b}\,, \tag{4.44}$$

so that

$$\begin{aligned}\frac{\partial}{\partial x}\int_b^h v_x\,\mathrm{d}z + \frac{\partial}{\partial y}\int_b^h v_y\,\mathrm{d}z - v_x|_{z=h}\,\frac{\partial h}{\partial x} - v_y|_{z=h}\,\frac{\partial h}{\partial y} + v_z|_{z=h} \\ + v_x|_{z=b}\,\frac{\partial b}{\partial x} + v_y|_{z=b}\,\frac{\partial b}{\partial y} - v_z|_{z=b} = 0\,.\end{aligned} \tag{4.45}$$

With the kinematic conditions (4.21) and (4.31), this yields

$$\frac{\partial}{\partial x}\int_b^h v_x\,\mathrm{d}z + \frac{\partial}{\partial y}\int_b^h v_y\,\mathrm{d}z + \frac{\partial h}{\partial t} - N_\mathrm{s}a_\mathrm{s}^\perp - \frac{\partial b}{\partial t} + N_\mathrm{b}a_\mathrm{b}^\perp = 0\,. \tag{4.46}$$

By introducing the *volume flux* $\mathbf{Q}$ as the vertically integrated horizontal velocity, that is,

$$\mathbf{Q} = \begin{pmatrix} Q_x \\ Q_y \end{pmatrix} = \begin{pmatrix} \int_b^h v_x\,\mathrm{d}z \\ \int_b^h v_y\,\mathrm{d}z \end{pmatrix}, \tag{4.47}$$

rearranging (4.46) and introducing the ice thickness $H = h - b$, we obtain

$$\frac{\partial H}{\partial t} = -\mathrm{div}\,\mathbf{Q} + N_\mathrm{s}a_\mathrm{s}^\perp - N_\mathrm{b}a_\mathrm{b}^\perp \tag{4.48}$$

(note that $\mathrm{div}\,\mathbf{Q} = \partial Q_x/\partial x + \partial Q_y/\partial y$). This result is known as the *ice thickness equation*.

Recall that the accumulation-ablation function (surface mass balance) $a_\mathrm{s}^\perp$ and the basal melting rate $a_\mathrm{b}^\perp$ are fluxes perpendicular to the free surface and the ice base, respectively. However, since the term $\partial H/\partial t$ in Eq. (4.48) refers to the vertical direction, it is desirable to introduce new quantities a_s and a_b, which are also taken in the vertical direction.

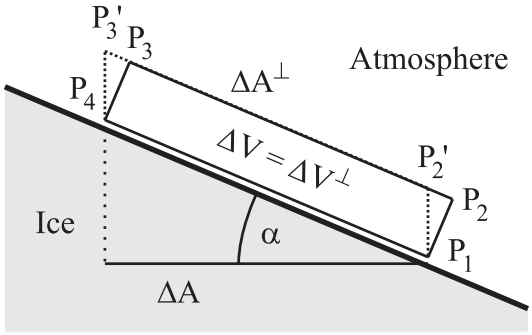

Figure 4.5: On the accumulation-ablation functions in the vertical direction (a_s) and perpendicular to the free surface ($a_\mathrm{s}^\perp$). The volumes $\Delta V^\perp = P_1P_2P_3P_4$ and $\Delta V = P_1P_2'P_3'P_4$ are equal. The areas $\Delta A^\perp = P_1P_4 = P_2P_3$ and ΔA (projection of $\Delta A^\perp$ into the horizontal plane) are related by $\Delta A = \Delta A^\perp \cos\alpha$.

Let $\Delta V^\perp$ be the ice volume which is accumulated on the area $\Delta A^\perp$ on the surface of the ice sheet during the time Δt (Fig. 4.5). The accumulation-ablation function perpendicular to the free surface is then

$$a_\mathrm{s}^\perp = \lim_{\Delta t \to 0} \frac{\Delta V^\perp}{\Delta A^\perp \, \Delta t} \tag{4.49}$$

(where $\Delta V^\perp$ is positive in case of positive $a_\mathrm{s}^\perp$ and negative in case of negative $a_\mathrm{s}^\perp$). Similarly, the accumulation-ablation function in the vertical direction is

$$a_\mathrm{s} = \lim_{\Delta t \to 0} \frac{\Delta V}{\Delta A \, \Delta t} \,. \tag{4.50}$$

Since $\Delta V = \Delta V^\perp$ and $\Delta A = \Delta A^\perp \cos\alpha$ (where α is the surface inclination angle, see Fig. 4.5), the two accumulation-ablation functions are related by

$$a_\mathrm{s} = \frac{a_\mathrm{s}^\perp}{\cos\alpha} \,. \tag{4.51}$$

Without loss of generality, let us assume for the moment that the coordinates x and y are oriented such that x is parallel to the line of steepest descent, so that $\partial h/\partial x = \tan\alpha$ and $\partial h/\partial y = 0$. Then, due to Eq. (4.17),

$$\begin{aligned} N_\mathrm{s} &= \left(1 + \left(\frac{\partial h}{\partial x}\right)^2\right)^{1/2} = \left(1 + \tan^2\alpha\right)^{1/2} = \left(\frac{\cos^2\alpha + \sin^2\alpha}{\cos^2\alpha}\right)^{1/2} \\ &= \frac{1}{\cos\alpha} \,. \end{aligned} \tag{4.52}$$

By inserting (4.52) in (4.51), we find

$$a_\mathrm{s} = N_\mathrm{s} \, a_\mathrm{s}^\perp \,. \tag{4.53}$$

With the same arguments, an analogous relation can be established for the basal melting rates,

$$a_\mathrm{b} = N_\mathrm{b}\, a_\mathrm{b}^\perp \,. \tag{4.54}$$

We can now insert Eqs. (4.53) and (4.54) in the ice thickness equation (4.48) in order to obtain the simplified form

$$\frac{\partial H}{\partial t} = -\mathrm{div}\,\mathbf{Q} + a_\mathrm{s} - a_\mathrm{b} \,. \tag{4.55}$$

The ice thickness equation is usually presented in this form. It is the central evolution equation in ice sheet dynamics.

4.2 Hydrostatic Approximation

In order to derive a simplified, approximated system of equations for the large-scale dynamics of ice sheets, we go back to the momentum balance (2.64), and write it in component form. By neglecting again the acceleration and Coriolis terms [see (4.7)–(4.10)] and setting $\mathbf{f} = \rho\mathbf{g} = -\rho g\,\mathbf{e}_z$, we obtain

$$\begin{aligned} \frac{\partial t_{xx}}{\partial x} + \frac{\partial t_{xy}}{\partial y} + \frac{\partial t_{xz}}{\partial z} &= 0 \,, \\ \frac{\partial t_{xy}}{\partial x} + \frac{\partial t_{yy}}{\partial y} + \frac{\partial t_{yz}}{\partial z} &= 0 \,, \\ \frac{\partial t_{xz}}{\partial x} + \frac{\partial t_{yz}}{\partial y} + \frac{\partial t_{zz}}{\partial z} &= \rho g \,. \end{aligned} \tag{4.56}$$

In all parts of an ice sheet, the shear stresses t_{xz} and t_{yz} ($\lesssim 100\,\mathrm{kPa}$) are small compared to the vertical normal stress t_{zz}, which is approximately equal to the pressure p, so that $[t_{zz}] \approx [P] = \rho g[H] \approx 10\,\mathrm{MPa}$ [see (4.5)]. Consequently, the vertical momentum balance $(4.56)_3$ can be reduced to a balance between the vertical gradient of t_{zz} and the gravity force,

$$\frac{\partial t_{zz}}{\partial z} = \rho g \,. \tag{4.57}$$

The same approximation in the vertical component of the stress-free condition at the free surface (4.23) yields

$$t_{zz}|_{z=h} = 0 \,, \tag{4.58}$$

so that Eq. (4.57) can readily be integrated,

$$t_{zz} = -\rho g(h - z) \,. \tag{4.59}$$

Evidently, the vertical normal stress t_{zz} is hydrostatic. With this result, the pressure p reads

$$\begin{aligned} p &= p - t_{xx}^\mathrm{D} - t_{yy}^\mathrm{D} - t_{zz}^\mathrm{D} = -t_{xx}^\mathrm{D} - t_{yy}^\mathrm{D} - t_{zz} \\ &= \rho g(h - z) - t_{xx}^\mathrm{D} - t_{yy}^\mathrm{D} \,. \end{aligned} \tag{4.60}$$

Thus, the horizontal normal stresses t_{xx}, t_{yy} can be expressed as

$$\begin{aligned} t_{xx} = -p + t^{\mathrm{D}}_{xx} &= 2t^{\mathrm{D}}_{xx} + t^{\mathrm{D}}_{yy} - \rho g(h-z)\,, \\ t_{yy} = -p + t^{\mathrm{D}}_{yy} &= 2t^{\mathrm{D}}_{yy} + t^{\mathrm{D}}_{xx} - \rho g(h-z)\,. \end{aligned} \tag{4.61}$$

Inserting these in the horizontal (x, y) components of the momentum balance $(4.56)_{1,2}$ yields

$$\begin{aligned} 2\frac{\partial t^{\mathrm{D}}_{xx}}{\partial x} + \frac{\partial t^{\mathrm{D}}_{yy}}{\partial x} + \frac{\partial t_{xy}}{\partial y} + \frac{\partial t_{xz}}{\partial z} &= \rho g \frac{\partial h}{\partial x}\,, \\ 2\frac{\partial t^{\mathrm{D}}_{yy}}{\partial y} + \frac{\partial t^{\mathrm{D}}_{xx}}{\partial y} + \frac{\partial t_{xy}}{\partial x} + \frac{\partial t_{yz}}{\partial z} &= \rho g \frac{\partial h}{\partial y}\,, \end{aligned} \tag{4.62}$$

and the viscous rheology of ice [Eqs. (3.7), (3.21)] in Cartesian coordinates is

$$\begin{aligned} t^{\mathrm{D}}_{xx} &= 2\eta\,\frac{\partial v_x}{\partial x}\,, \\ t^{\mathrm{D}}_{yy} &= 2\eta\,\frac{\partial v_y}{\partial y}\,, \\ t^{\mathrm{D}}_{zz} &= 2\eta\,\frac{\partial v_z}{\partial z}\,, \\ t_{xz} &= \eta\left(\frac{\partial v_x}{\partial z} + \frac{\partial v_z}{\partial x}\right), \\ t_{yz} &= \eta\left(\frac{\partial v_y}{\partial z} + \frac{\partial v_z}{\partial y}\right), \\ t_{xy} &= \eta\left(\frac{\partial v_x}{\partial y} + \frac{\partial v_y}{\partial x}\right). \end{aligned} \tag{4.63}$$

Since the trace of the deviatoric stress tensor vanishes ($t^{\mathrm{D}}_{xx} + t^{\mathrm{D}}_{yy} + t^{\mathrm{D}}_{zz} = 0$), only two out of the first three equations of (4.63) are independent. Inserting $(4.63)_{1,2,4,5,6}$ in (4.62) yields

$$\begin{aligned} &4\frac{\partial}{\partial x}\left(\eta\frac{\partial v_x}{\partial x}\right) + 2\frac{\partial}{\partial x}\left(\eta\frac{\partial v_y}{\partial y}\right) + \frac{\partial}{\partial y}\left(\eta\Big(\frac{\partial v_x}{\partial y} + \frac{\partial v_y}{\partial x}\Big)\right) \\ &\qquad + \frac{\partial}{\partial z}\left(\eta\Big(\frac{\partial v_x}{\partial z} + \frac{\partial v_z}{\partial x}\Big)\right) = \rho g\frac{\partial h}{\partial x}\,, \\ &4\frac{\partial}{\partial y}\left(\eta\frac{\partial v_y}{\partial y}\right) + 2\frac{\partial}{\partial y}\left(\eta\frac{\partial v_x}{\partial x}\right) + \frac{\partial}{\partial x}\left(\eta\Big(\frac{\partial v_x}{\partial y} + \frac{\partial v_y}{\partial x}\Big)\right) \\ &\qquad + \frac{\partial}{\partial z}\left(\eta\Big(\frac{\partial v_y}{\partial z} + \frac{\partial v_z}{\partial y}\Big)\right) = \rho g\frac{\partial h}{\partial y}\,. \end{aligned} \tag{4.64}$$

As for the full Stokes flow problem discussed above, we complement these differential equations for the velocity field by the functional form $\eta(T', d_{\mathrm{e}})$ of the viscosity, which is

given for Glen's flow law by Eq. (3.22). The component form of the effective strain rate d_e reads

$$\begin{aligned} d_\mathrm{e} &= \sqrt{\tfrac{1}{2}\,\mathrm{tr}\,\mathsf{D}^2} = \sqrt{\tfrac{1}{2}\,D_{ij}D_{ij}} \\ &= \sqrt{\tfrac{1}{2}\,(D_{11}^2 + D_{22}^2 + D_{33}^2 + 2D_{12}^2 + 2D_{13}^2 + 2D_{23}^2)}\,, \end{aligned} \tag{4.65}$$

and, due to the continuity equation (4.1), we have $\mathrm{div}\,\mathbf{v} = \mathrm{tr}\,\mathsf{D} = D_{11} + D_{22} + D_{33} = 0$, so that

$$\begin{aligned} d_\mathrm{e} &= \sqrt{\tfrac{1}{2}\,[D_{11}^2 + D_{22}^2 + (-D_{11} - D_{22})^2 + 2D_{12}^2 + 2D_{13}^2 + 2D_{23}^2]} \\ &= \sqrt{D_{11}^2 + D_{22}^2 + D_{11}D_{22} + D_{12}^2 + D_{13}^2 + D_{23}^2} \\ &= \left\{ \left(\frac{\partial v_x}{\partial x}\right)^2 + \left(\frac{\partial v_y}{\partial y}\right)^2 + \frac{\partial v_x}{\partial x}\,\frac{\partial v_y}{\partial y} + \frac{1}{4}\left(\frac{\partial v_x}{\partial y} + \frac{\partial v_y}{\partial x}\right)^2 \right. \\ &\qquad \left. + \frac{1}{4}\left(\frac{\partial v_x}{\partial z} + \frac{\partial v_z}{\partial x}\right)^2 + \frac{1}{4}\left(\frac{\partial v_y}{\partial z} + \frac{\partial v_z}{\partial y}\right)^2 \right\}^{1/2} . \end{aligned} \tag{4.66}$$

Equations (4.64) and (3.22) together with the continuity equation (4.41) and the temperature evolution equation (4.14), which is

$$\begin{aligned} &\rho c\Big(\frac{\partial T}{\partial t} + v_x\frac{\partial T}{\partial x} + v_y\frac{\partial T}{\partial y} + v_z\frac{\partial T}{\partial z}\Big) \\ &\qquad = \frac{\partial}{\partial x}\Big(\kappa\frac{\partial T}{\partial x}\Big) + \frac{\partial}{\partial y}\Big(\kappa\frac{\partial T}{\partial y}\Big) + \frac{\partial}{\partial z}\Big(\kappa\frac{\partial T}{\partial z}\Big) + 4\eta\, d_\mathrm{e}^2\,, \end{aligned} \tag{4.67}$$

are five equations for the five unknown fields v_x, v_y, v_z, η and T. This set of field equations is called the *hydrostatic approximation*. Compared to the full Stokes flow problem formulated in Sect. 4.1.1, the pressure has been eliminated, which is a substantial simplification of the problem. The field equations are completed by the kinematic boundary condition (4.21), the stress-free condition (4.23) and the temperature condition (4.24) at the free surface, the kinematic condition (4.31), the sliding law (4.35) and the thermodynamic conditions (4.38), (4.39), (4.40) at the ice base, and the ice thickness equation (4.55).

4.3 First Order Approximation

With the typical values (4.5) and the aspect ratio (4.6), we find for the ratio of components of the velocity gradient

$$\frac{\partial v_z}{\partial x}\Big/\frac{\partial v_x}{\partial z}\,,\quad \frac{\partial v_z}{\partial y}\Big/\frac{\partial v_y}{\partial z} \;\sim\; \frac{[W]}{[L]}\Big/\frac{[U]}{[H]} = \frac{[W]}{[U]}\,\frac{[H]}{[L]} = \varepsilon^2 \sim 10^{-6}\,, \tag{4.68}$$

so that horizontal derivatives of the vertical velocity are negligible compared to vertical derivatives of the horizontal velocity. This allows us to neglect the terms containing horizontal derivatives of the vertical velocity in the viscous rheology $(4.63)_{1,2,4,5,6}$, which yields

$$\begin{aligned} t^{\mathrm{D}}_{xx} &= 2\eta\,\frac{\partial v_x}{\partial x}\,, \\ t^{\mathrm{D}}_{yy} &= 2\eta\,\frac{\partial v_y}{\partial y}\,, \\ t_{xz} &= \eta\,\frac{\partial v_x}{\partial z}\,, \\ t_{yz} &= \eta\,\frac{\partial v_y}{\partial z}\,, \\ t_{xy} &= \eta\left(\frac{\partial v_x}{\partial y}+\frac{\partial v_y}{\partial x}\right). \end{aligned} \tag{4.69}$$

Consequently, the momentum balance (4.64) simplifies to

$$\begin{aligned} &4\frac{\partial}{\partial x}\left(\eta\frac{\partial v_x}{\partial x}\right)+2\frac{\partial}{\partial x}\left(\eta\frac{\partial v_y}{\partial y}\right)+\frac{\partial}{\partial y}\left(\eta\big(\frac{\partial v_x}{\partial y}+\frac{\partial v_y}{\partial x}\big)\right) \\ &\qquad\qquad +\frac{\partial}{\partial z}\left(\eta\,\frac{\partial v_x}{\partial z}\right)=\rho g\frac{\partial h}{\partial x}\,, \\ &4\frac{\partial}{\partial y}\left(\eta\frac{\partial v_y}{\partial y}\right)+2\frac{\partial}{\partial y}\left(\eta\frac{\partial v_x}{\partial x}\right)+\frac{\partial}{\partial x}\left(\eta\big(\frac{\partial v_x}{\partial y}+\frac{\partial v_y}{\partial x}\big)\right) \\ &\qquad\qquad +\frac{\partial}{\partial z}\left(\eta\,\frac{\partial v_y}{\partial z}\right)=\rho g\frac{\partial h}{\partial y}\,. \end{aligned} \tag{4.70}$$

Again, the viscosity is taken as $\eta(T', d_{\mathrm{e}})$ and given by Eq. (3.22), with

$$\begin{aligned} d_{\mathrm{e}} &= \left\{\left(\frac{\partial v_x}{\partial x}\right)^2+\left(\frac{\partial v_y}{\partial y}\right)^2+\frac{\partial v_x}{\partial x}\,\frac{\partial v_y}{\partial y}\right. \\ &\quad \left.+\frac{1}{4}\left(\frac{\partial v_x}{\partial y}+\frac{\partial v_y}{\partial x}\right)^2+\frac{1}{4}\left(\frac{\partial v_x}{\partial z}\right)^2+\frac{1}{4}\left(\frac{\partial v_y}{\partial z}\right)^2\right\}^{1/2} \\ &= \left\{\left(\frac{\partial v_x}{\partial x}\right)^2+\left(\frac{\partial v_y}{\partial y}\right)^2+\frac{\partial v_x}{\partial x}\,\frac{\partial v_y}{\partial y}+\frac{1}{2}\frac{\partial v_x}{\partial y}\,\frac{\partial v_y}{\partial x}\right. \\ &\quad \left.+\frac{1}{4}\left(\frac{\partial v_x}{\partial y}\right)^2+\frac{1}{4}\left(\frac{\partial v_y}{\partial x}\right)^2+\frac{1}{4}\left(\frac{\partial v_x}{\partial z}\right)^2+\frac{1}{4}\left(\frac{\partial v_y}{\partial z}\right)^2\right\}^{1/2}. \end{aligned} \tag{4.71}$$

In this simplified hydrostatic approximation, generally called the *first order approximation*, Eqs. (4.70) and (4.71) [and therefore the viscosity $\eta(T', d_{\mathrm{e}})$] contain only the horizontal

components of the velocity, v_x and v_y. Thus, the solution of these equations is fully decoupled from the determination of the vertical velocity v_z via the continuity equation (4.41), in contrast to the hydrostatic approximation and the full Stokes flow problem. Once the horizontal velocity has been computed, the vertical velocity can be obtained by integrating Eq. (4.41) from $z = b$ to z,

$$v_z = v_z|_{z=b} - \int_b^z \left(\frac{\partial v_x}{\partial x} + \frac{\partial v_y}{\partial y} \right) \mathrm{d}\bar{z} \,. \tag{4.72}$$

The vertical velocity at the ice base $v_z|_{z=b}$ is obtained from the kinematic condition (4.31).

4.4 Shallow Ice Approximation

Everywhere in an ice sheet, except the immediate vicinity of ice domes (up to and within $\sim 10\,\mathrm{km}$ in the horizontal direction) and ice margins, the flow regime is essentially simple, bed-parallel shear, and the slopes of the free surface and the ice base are small (Fig. 4.6). Under these conditions, the relevant components of the stress deviator t^{D} are the shear stresses in the horizontal plane, t_{xz} and t_{yz}, which are supported by the basal drag. The normal stress deviators t^{D}_{xx}, t^{D}_{yy} and t^{D}_{zz} as well as the shear stress in the vertical planes, t_{xy}, are consequently negligible.

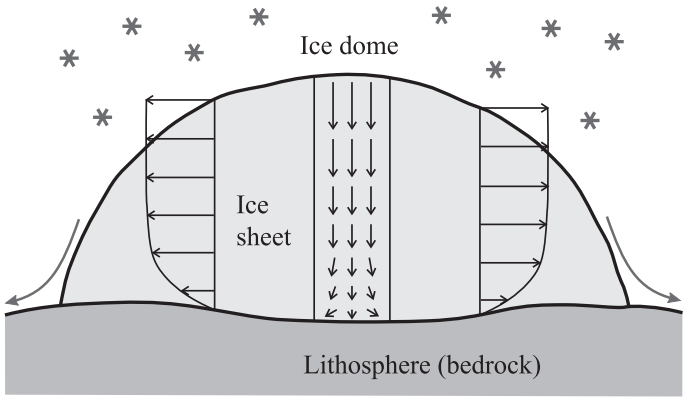

Figure 4.6: Flow regimes in an ice sheet. In most regions, simple, bed-parallel shear flow prevails. By contrast, in the vicinity of an ice dome, the flow direction is essentially downward, which leads to vertical compression and horizontal extension. Close to the ice margin, the slope of the free surface can be large. Vertical exaggeration factor $\sim$ 200-500.

This allows further simplifications of the hydrostatic approximation to be made, which go beyond the first order approximation, and are known as the *shallow ice approximation* (SIA) (Hutter 1983, Morland 1984). All normal stresses are equal to the negative pressure,

$$t_{xx} = t_{yy} = t_{zz} = -p \,, \tag{4.73}$$

so that the vertical momentum balance (4.57) reads

$$\frac{\partial p}{\partial z} = -\rho g\,, \tag{4.74}$$

and its integrated form [see (4.59)] gives the hydrostatic pressure distribution

$$p = p_{\mathrm{hyd}} = \rho g(h - z)\,. \tag{4.75}$$

The horizontal components of the momentum balance, $(4.56)_{1,2}$ or $(4.62)_{1,2}$, simplify to

$$\begin{aligned} \frac{\partial t_{xz}}{\partial z} &= \frac{\partial p}{\partial x} = \rho g \frac{\partial h}{\partial x}\,, \\ \frac{\partial t_{yz}}{\partial z} &= \frac{\partial p}{\partial y} = \rho g \frac{\partial h}{\partial y}\,. \end{aligned} \tag{4.76}$$

Due to the small surface slope, the derivatives $\partial h/\partial x$ and $\partial h/\partial y$ are small, typically of the order of the aspect ratio ε:

$$\frac{\partial h}{\partial x},\ \frac{\partial h}{\partial y} \sim \frac{[H]}{[L]} = \varepsilon \tag{4.77}$$

[see Eqs. (4.5) and (4.6)]. Thus, the unit normal vector of the free surface (4.16) is approximately vertical,

$$\mathbf{n} = \begin{pmatrix} 0 \\ 0 \\ 1 \end{pmatrix} = \mathbf{e}_z\,, \tag{4.78}$$

and the stress-free condition (4.23) reduces to

$$p|_{z=h} = 0\,, \quad t_{xz}|_{z=h} = 0\,, \quad t_{yz}|_{z=h} = 0\,. \tag{4.79}$$

With this finding, Eq. (4.76), the right-hand side of which does not depend on z, can readily be integrated and yields

$$\begin{aligned} t_{xz} &= -\rho g(h - z)\frac{\partial h}{\partial x}\,, \\ t_{yz} &= -\rho g(h - z)\frac{\partial h}{\partial y}\,. \end{aligned} \tag{4.80}$$

Equations (4.75) and (4.80) tell us that in the SIA the stress field, the only non-negligible components of which are p, t_{xz} and t_{yz}, is fully determined if the geometry of the ice sheet is known. The effective stress σ_{e} [see $(3.8)_2$ and (3.9)] is then

$$\begin{aligned} \sigma_{\mathrm{e}} &= \sqrt{t_{xz}^2 + t_{yz}^2} \\ &= \rho g(h - z)\left(\left(\frac{\partial h}{\partial x}\right)^2 + \left(\frac{\partial h}{\partial y}\right)^2\right)^{1/2} = \rho g(h - z)\,|\mathrm{grad}\, h|\,. \end{aligned} \tag{4.81}$$

The above results are therefore inserted in the x-z and y-z components of Glen's flow law in the form (3.16):

$$\begin{aligned}
\frac{1}{2}\left(\frac{\partial v_x}{\partial z}+\frac{\partial v_z}{\partial x}\right) &= A(T')\,\sigma_{\mathrm{e}}^{n-1}\,t_{xz} \\
&= -A(T')\,[\rho g(h-z)]^n|\mathrm{grad}\,h|^{n-1}\frac{\partial h}{\partial x}\,, \\
\frac{1}{2}\left(\frac{\partial v_y}{\partial z}+\frac{\partial v_z}{\partial y}\right) &= A(T')\,\sigma_{\mathrm{e}}^{n-1}\,t_{yz} \\
&= -A(T')\,[\rho g(h-z)]^n|\mathrm{grad}\,h|^{n-1}\frac{\partial h}{\partial y}\,.
\end{aligned} \tag{4.82}$$

Based on the order of magnitudes of the spatial derivatives of velocity components, Eq. (4.68), the horizontal derivatives of the vertical velocity are negligible. This yields

$$\begin{aligned}
\frac{\partial v_x}{\partial z} &= -2A(T')\,[\rho g(h-z)]^n|\mathrm{grad}\,h|^{n-1}\frac{\partial h}{\partial x}\,, \\
\frac{\partial v_y}{\partial z} &= -2A(T')\,[\rho g(h-z)]^n|\mathrm{grad}\,h|^{n-1}\frac{\partial h}{\partial y}\,,
\end{aligned} \tag{4.83}$$

which can be integrated from the ice base $z=b$ to an arbitrary position z in the ice sheet in order to compute the horizontal velocities,

$$\begin{aligned}
v_x &= v_{\mathrm{b}x} - 2(\rho g)^n|\mathrm{grad}\,h|^{n-1}\frac{\partial h}{\partial x}\int_b^z A(T')\,(h-\bar{z})^n\,\mathrm{d}\bar{z}\,, \\
v_y &= v_{\mathrm{b}y} - 2(\rho g)^n|\mathrm{grad}\,h|^{n-1}\frac{\partial h}{\partial y}\int_b^z A(T')\,(h-\bar{z})^n\,\mathrm{d}\bar{z}\,,
\end{aligned} \tag{4.84}$$

where $v_{\mathrm{b}x}$ and $v_{\mathrm{b}y}$ are the respective velocities at the ice base. Since the bed slopes are of the same order of magnitude as the surface slopes [see (4.77)],

$$\frac{\partial b}{\partial x},\ \frac{\partial b}{\partial y}\ \sim\ \frac{[H]}{[L]}=\varepsilon\,, \tag{4.85}$$

and the unit normal vector of the ice base (4.26) is approximately vertical,

$$\mathbf{n}=\begin{pmatrix}0\\0\\-1\end{pmatrix}=-\mathbf{e}_z\,, \tag{4.86}$$

the tangential plane to the ice base is approximately equal to the horizontal plane. Therefore, $v_{\mathrm{b}x}$ and $v_{\mathrm{b}y}$ are the two components of the basal sliding velocity $\mathbf{v}_{\mathrm{b}}$ given by the Weertman-type sliding law (4.35). The basal drag $\boldsymbol{\tau}_{\mathrm{b}}=\tau_{\mathrm{b}}\mathbf{e}_{\mathrm{t}}$ consists of the x- and y-components of the stress vector $\mathbf{t}_{\mathbf{n}}|_{z=b}=\mathsf{t}|_{z=b}\cdot\mathbf{n}=-\mathsf{t}|_{z=b}\cdot\mathbf{e}_z$, that is,

$$\boldsymbol{\tau}_{\mathrm{b}}=-\begin{pmatrix}t_{xz}|_{z=b}\\t_{yz}|_{z=b}\end{pmatrix}=\rho gH\begin{pmatrix}\dfrac{\partial h}{\partial x}\\[2ex]\dfrac{\partial h}{\partial y}\end{pmatrix}. \tag{4.87}$$

Thus,

$$\tau_\mathrm{b} = \left| - \begin{pmatrix} t_{xz}|_{z=b} \\ t_{yz}|_{z=b} \end{pmatrix} \right| = \sqrt{t_{xz}^2|_{z=b} + t_{yz}^2|_{z=b}} = \rho g H \, |\mathrm{grad}\, h| \tag{4.88}$$

and

$$\mathbf{e}_\mathrm{t} = -\frac{1}{\tau_\mathrm{b}} \begin{pmatrix} t_{xz}|_{z=b} \\ t_{yz}|_{z=b} \end{pmatrix} = \frac{1}{|\mathrm{grad}\, h|} \begin{pmatrix} \dfrac{\partial h}{\partial x} \\ \dfrac{\partial h}{\partial y} \end{pmatrix} . \tag{4.89}$$

The basal normal stress $\mathbf{N}_\mathrm{b} = -N_\mathrm{b}\mathbf{n} = N_\mathrm{b}\mathbf{e}_z$ is equal to the z-component of the stress vector,

$$\mathbf{N}_\mathrm{b} = -t_{zz}|_{z=b}\, \mathbf{e}_z \quad \Rightarrow \quad N_\mathrm{b} = -t_{zz}|_{z=b} = \rho g H \, . \tag{4.90}$$

Thus we obtain

$$\begin{aligned} v_{\mathrm{b}x} &= \begin{cases} 0 \, , & \text{if } \; T_\mathrm{b} < T_\mathrm{m} \, , \\ -C_\mathrm{b} (\rho g H)^{p-q} |\mathrm{grad}\, h|^{p-1} \dfrac{\partial h}{\partial x} \, , & \text{if } \; T_\mathrm{b} = T_\mathrm{m} \, , \end{cases} \\ v_{\mathrm{b}y} &= \begin{cases} 0 \, , & \text{if } \; T_\mathrm{b} < T_\mathrm{m} \, , \\ -C_\mathrm{b} (\rho g H)^{p-q} |\mathrm{grad}\, h|^{p-1} \dfrac{\partial h}{\partial y} \, , & \text{if } \; T_\mathrm{b} = T_\mathrm{m} \, . \end{cases} \end{aligned} \tag{4.91}$$

By introducing the horizontal velocity vector

$$\mathbf{v}_\mathrm{h} = \begin{pmatrix} v_x \\ v_y \end{pmatrix} \tag{4.92}$$

and the scalar function

$$C = \begin{cases} 2(\rho g)^n |\mathrm{grad}\, h|^{n-1} \displaystyle\int_b^z A(T') \, (h - \bar{z})^n \, \mathrm{d}\bar{z} \, , & \text{if } \; T_\mathrm{b} < T_\mathrm{m} \, , \\ C_\mathrm{b} (\rho g H)^{p-q} |\mathrm{grad}\, h|^{p-1} & \\ \quad + 2(\rho g)^n |\mathrm{grad}\, h|^{n-1} \displaystyle\int_b^z A(T') \, (h - \bar{z})^n \, \mathrm{d}\bar{z} \, , & \text{if } \; T_\mathrm{b} = T_\mathrm{m} \, , \end{cases} \tag{4.93}$$

we can express the horizontal velocity (4.84) as

$$\begin{pmatrix} v_x \\ v_y \end{pmatrix} = -C \begin{pmatrix} \dfrac{\partial h}{\partial x} \\ \dfrac{\partial h}{\partial y} \end{pmatrix} , \quad \text{or} \quad \mathbf{v}_\mathrm{h} = -C \, \mathrm{grad}\, h \, . \tag{4.94}$$

That is, in the shallow ice approximation, the direction of the horizontal velocity is anti-parallel to the gradient of the free surface. In other words, the ice always flows down the steepest surface slope, irrespective of the bedrock topography (see Fig. 4.7). This holds

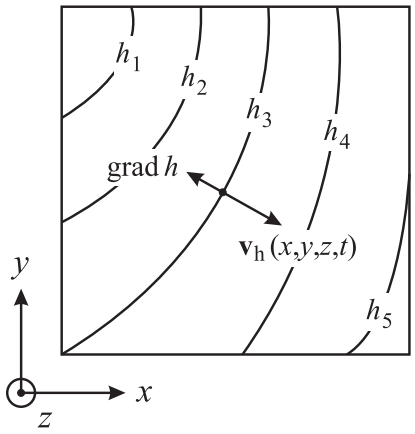

Figure 4.7: Surface topography and horizontal velocity in the shallow ice approximation. The horizontal velocity $\mathbf{v}_\mathrm{h}$ is anti-parallel to the direction of the surface gradient $\operatorname{grad} h$. Surface-topography contours: $h_1 > h_2 > h_3 > h_4 > h_5$.

for any particle of the ice sheet, even the near-basal ice. However, note that this result is only valid as long as the bed slopes are sufficiently small, as described by Eq. (4.85).

As for the first order approximation, the vertical velocity can now be computed by integrating the continuity equation (4.41) from $z = b$ to z,

$$v_z = v_z|_{z=b} - \int_b^z \left(\frac{\partial v_x}{\partial x} + \frac{\partial v_y}{\partial y} \right) \mathrm{d}\bar{z}\,. \tag{4.95}$$

In this equation, v_x and v_y are given by (4.94), and the vertical velocity at the ice base $v_z|_{z=b}$ is determined by the kinematic condition (4.31).

In order to formulate the ice thickness equation in the shallow ice approximation, we compute the volume flux $\mathbf{Q}$ [see Eq. (4.47)] with the horizontal velocities (4.94). This yields

$$\begin{pmatrix} Q_x \\ Q_y \end{pmatrix} = -D \begin{pmatrix} \dfrac{\partial h}{\partial x} \\ \dfrac{\partial h}{\partial y} \end{pmatrix}, \quad \text{with} \quad D = \int_b^h C\,\mathrm{d}z\,. \tag{4.96}$$

The function C depends on z only via the integral term in (4.93), for which we find by

integration by parts

$$\begin{aligned}
&\int_b^h \int_b^z A(T')\,(h-\bar{z})^n\,\mathrm{d}\bar{z}\,\mathrm{d}z = \int_b^h 1 \int_b^z A(T')\,(h-\bar{z})^n\,\mathrm{d}\bar{z}\,\mathrm{d}z \\
&= \Big[z\int_b^z A(T')\,(h-\bar{z})^n\,\mathrm{d}\bar{z}\Big]_b^h - \int_b^h zA(T')\,(h-z)^n\,\mathrm{d}z \\
&= h\int_b^h A(T')\,(h-\bar{z})^n\,\mathrm{d}\bar{z} - \int_b^h zA(T')\,(h-z)^n\,\mathrm{d}z \\
&= \int_b^h A(T')\,(h-z)^{n+1}\,\mathrm{d}z\,. \qquad (4.97)
\end{aligned}$$

Thus, the function D is

$$D = \begin{cases} 2(\rho g)^n |\mathrm{grad}\, h|^{n-1} \displaystyle\int_b^h A(T')\,(h-z)^{n+1}\,\mathrm{d}z\,, & \text{if } T_\mathrm{b} < T_\mathrm{m}\,, \\ C_\mathrm{b} H (\rho g H)^{p-q} |\mathrm{grad}\, h|^{p-1} & \\ \quad + 2(\rho g)^n |\mathrm{grad}\, h|^{n-1} \displaystyle\int_b^h A(T')\,(h-z)^{n+1}\,\mathrm{d}z\,, & \text{if } T_\mathrm{b} = T_\mathrm{m}\,. \end{cases} \qquad (4.98)$$

By inserting the volume flux (4.96) with the function (4.98) into the ice thickness equation (4.55), we obtain

$$\frac{\partial H}{\partial t} = \frac{\partial}{\partial x}\Big(D\frac{\partial h}{\partial x}\Big) + \frac{\partial}{\partial y}\Big(D\frac{\partial h}{\partial y}\Big) + a_\mathrm{s} - a_\mathrm{b}\,, \qquad (4.99)$$

or, alternatively, expressed as an evolution equation for the surface topography h,

$$\frac{\partial h}{\partial t} = \frac{\partial}{\partial x}\Big(D\frac{\partial h}{\partial x}\Big) + \frac{\partial}{\partial y}\Big(D\frac{\partial h}{\partial y}\Big) + a_\mathrm{s} - a_\mathrm{b} + \frac{\partial b}{\partial t}\,. \qquad (4.100)$$

Note also that, due to Eqs. (4.77) and (4.85), we have $N_\mathrm{s} \approx 1$ and $N_\mathrm{b} \approx 1$, so that the accumulation-ablation functions and basal melting rates in the vertical direction and perpendicular to the respective interfaces are approximately equal,

$$a_\mathrm{s} \approx a_\mathrm{s}^\perp\,, \quad a_\mathrm{b} \approx a_\mathrm{b}^\perp\,. \qquad (4.101)$$

Mathematically, Eq. (4.100) is a non-linear diffusion equation (the function D depends itself on h) with additional source terms. As described at the end of Sect. 4.1.2, the accumulation-ablation function a_s is a climatic input quantity, and the basal melting rate a_b is determined by Eq. (4.40). The unknown variation $\partial b/\partial t$ of the ice-base/bedrock topography can be obtained from a model of glacial isostasy, which will be treated later (see Chap. 7).

As for the temperature evolution equation (4.67), we complement the typical values (4.5) by the typical temperature variation magnitude

$$[\Delta T] = 20\,\mathrm{K}\,. \qquad (4.102)$$

Then, we find for the ratio of horizontal and vertical heat conduction

$$\frac{\partial}{\partial x}\Big(\kappa\frac{\partial T}{\partial x}\Big)\Big/\frac{\partial}{\partial z}\Big(\kappa\frac{\partial T}{\partial z}\Big)\,,\quad \frac{\partial}{\partial y}\Big(\kappa\frac{\partial T}{\partial y}\Big)\Big/\frac{\partial}{\partial z}\Big(\kappa\frac{\partial T}{\partial z}\Big)$$
$$\sim\ \kappa\frac{[\Delta T]}{[L]^2}\Big/\kappa\frac{[\Delta T]}{[H]^2}=\frac{[H]^2}{[L]^2}=\varepsilon^2\sim 10^{-6}\,, \tag{4.103}$$

so that horizontal heat conduction is negligible. Furthermore, in the dissipation term we express the effective strain rate d_e in terms of the effective stress σ_e by using $(3.19)_1$. This yields

$$\rho c\Big(\frac{\partial T}{\partial t}+v_x\frac{\partial T}{\partial x}+v_y\frac{\partial T}{\partial y}+v_z\frac{\partial T}{\partial z}\Big)=\frac{\partial}{\partial z}\Big(\kappa\frac{\partial T}{\partial z}\Big)+4\eta\,A^2(T')\,\sigma_\mathrm{e}^{2n}\,, \tag{4.104}$$

and, by inserting (3.10) and (3.12), we obtain

$$\rho c\Big(\frac{\partial T}{\partial t}+v_x\frac{\partial T}{\partial x}+v_y\frac{\partial T}{\partial y}+v_z\frac{\partial T}{\partial z}\Big)=\frac{\partial}{\partial z}\Big(\kappa\frac{\partial T}{\partial z}\Big)+2A(T')\,\sigma_\mathrm{e}^{n+1}\,, \tag{4.105}$$

where σ_e is given by Eq. (4.81). The boundary conditions for this equation are the prescribed surface temperature (4.24), the temperature gradient (4.38) for a cold base and the melting temperature (4.39) for a temperate base.

The shallow ice approximation simplifies the problem of large-scale ice sheet flow drastically. The stress field is given by the simple, analytic expressions (4.75), (4.80) and (4.81), and the velocity field depends only on the *local* ice sheet geometry and temperature via (4.94) and (4.95), whereas in the full Stokes flow problem, the hydrostatic approximation and the first order approximation systems of non-linear differential equations [Eqs. (4.11), (4.64) and (4.70), respectively] must be solved. The remaining "hard work" is the solution of the surface evolution equation (4.100) and of the temperature evolution equation (4.105).

4.5 Driving Stress

Equation (4.80) represents the bed-parallel shear stress in the shallow ice approximation. Evaluating this equation at the bed ($z=b$) yields the vector

$$\boldsymbol{\tau}_\mathrm{d}=-\rho g H\begin{pmatrix}\dfrac{\partial h}{\partial x}\\[2ex]\dfrac{\partial h}{\partial y}\end{pmatrix}\,, \tag{4.106}$$

which is often called the *driving stress*.

By construction, the driving stress corresponds to the basal shear stress in the shallow ice approximation. However, its definition is not limited to the shallow ice approximation, and

it can be interpreted in general as the action which drives the flow of the ice sheet. In the shallow ice approximation, the driving stress $\boldsymbol{\tau}_\mathrm{d}$ is equal to the negative of the basal drag $\boldsymbol{\tau}_\mathrm{b}$ [see Eq. (4.87)], which means that the driving forces and the resistive forces are balanced locally at the bed of the ice sheet. In the full Stokes problem, the hydrostatic approximation and the first order approximation such a local balance does not hold; however, the driving stress and the basal drag still balance *on average* for the entire domain of the ice sheet (van der Veen 1999). Local imbalances are compensated by the deviatoric normal stresses t^D_{xx} and t^D_{yy} as well as the shear stress in the vertical plane t_{xy}.

4.6 Analytical Solutions

4.6.1 Simplified Problem

For very simple, idealised cases, the equations of the shallow ice approximation derived above can be solved analytically. Let us consider the following situation:

- Plane strain approximation: two-dimensional flow in the x-z plane, any lateral effects neglected (see Sect. 2.4.2).
- Steady-state conditions: $\partial(\cdot)/\partial t = 0$ for all field quantities.
- Flat, rigid bed: $b(x) = 0$.
- Ice sheet extent between $x = -L$ and $x = L$, symmetric around the ice divide at $x = 0$.
- No basal melting ($a_\mathrm{b} = 0$), no basal sliding ($C_\mathrm{b} = 0$).
- Constant rate factor: $A(T') = A = \text{const}$.

The last assumption decouples the mechanical from the thermodynamical problem, and therefore we do not have to deal with the temperature evolution equation (4.105).

With the assumptions made above, the ice thickness equation (4.55) becomes

$$\operatorname{div} \mathbf{Q} = a_\mathrm{s} \,, \tag{4.107}$$

where, according to Eqs. (4.47) and (4.98),

$$\begin{aligned}
\mathbf{Q} &= -2A(\rho g)^n \left|\operatorname{grad} h\right|^{n-1} \operatorname{grad} h \int_b^h (h-z)^{n+1} \,\mathrm{d}z \\
&= -2A(\rho g)^n \left|\operatorname{grad} h\right|^{n-1} \operatorname{grad} h \left[-\frac{(h-z)^{n+2}}{n+2}\right]_b^h \\
&= -\frac{2A(\rho g)^n}{n+2} H^{n+2} \left|\operatorname{grad} h\right|^{n-1} \operatorname{grad} h \\
&= -A_0 H^{n+2} \left|\operatorname{grad} h\right|^{n-1} \operatorname{grad} h \,.
\end{aligned} \tag{4.108}$$

In the last step, the abbreviation

$$A_0 = \frac{2A(\rho g)^n}{n+2} \tag{4.109}$$

has been introduced.

Due to the flat bed, the ice thickness H is equal to the surface topography h, and due to the plane strain approximation, the volume flux $\mathbf{Q} = Q\,\mathbf{e}_x$ and the surface gradient $\operatorname{grad} h = (\mathrm{d}h/\mathrm{d}x)\,\mathbf{e}_x$. Hence,

$$Q = -A_0\, h^{n+2} \left|\frac{\mathrm{d}h}{\mathrm{d}x}\right|^{n-1} \frac{\mathrm{d}h}{\mathrm{d}x}\,, \tag{4.110}$$

and

$$\frac{\mathrm{d}Q}{\mathrm{d}x} = -\frac{\mathrm{d}}{\mathrm{d}x}\left(A_0\, h^{n+2} \left|\frac{\mathrm{d}h}{\mathrm{d}x}\right|^{n-1} \frac{\mathrm{d}h}{\mathrm{d}x}\right) = a_\mathrm{s}\,. \tag{4.111}$$

In order to find analytical solutions of the steady-state ice thickness equation (4.111), we recognise that it is a separable ordinary differential equation, provided that the surface mass balance a_s is a function of x only. The assumption of symmetry with respect to $x = 0$ implies $Q(0) = 0$ and $(\mathrm{d}h/\mathrm{d}x)_{x=0} = 0$. Thus, a first integral of Eq. (4.111) yields

$$A_0\, h^{n+2} \left|\frac{\mathrm{d}h}{\mathrm{d}x}\right|^{n-1} \frac{\mathrm{d}h}{\mathrm{d}x} = -\int_0^x a_\mathrm{s}(x')\,\mathrm{d}x' = -Q(x)\,. \tag{4.112}$$

For the half-domain $0 < x < L$, the surface topography h decreases monotonically from the ice divide at $x = 0$ to the margin at $x = L$, so that $Q > 0$ and $\mathrm{d}h/\mathrm{d}x < 0$. This allows to take the nth root of Eq. (4.112),

$$h^{(n+2)/n}\,\frac{\mathrm{d}h}{\mathrm{d}x} = -\left(\frac{Q(x)}{A_0}\right)^{1/n}\,, \tag{4.113}$$

and, by separation of variables, compute the second integral

$$h(x)^{(2n+2)/n} = h_0^{(2n+2)/n} - \frac{2n+2}{n}\int_0^x \left(\frac{Q(x')}{A_0}\right)^{1/n} \mathrm{d}x'\,, \tag{4.114}$$

where h_0 is the surface elevation at the ice divide. The ice thickness equation (4.111) has thus been reduced to a quadrature, which can be solved analytically depending on the mass balance function $a_\mathrm{s}(x)$.

4.6.2 Vialov Profile

In order to simplify the problem further, we assume that the surface mass balance a_s is a positive constant over the entire domain. From Eq. (4.112), we obtain the volume flux

$$Q(x) = a_\mathrm{s} x\,, \tag{4.115}$$

so that Eq. (4.114) reads

$$h(x)^{(2n+2)/n} = h_0^{(2n+2)/n} - 2\left(\frac{a_\mathrm{s}}{A_0}\right)^{1/n} x^{(n+1)/n}\,. \tag{4.116}$$

With the boundary condition $h(L) = 0$, we obtain for the surface elevation at the ice divide

$$h_0 = 2^{n/(2n+2)}\left(\frac{a_\mathrm{s}}{A_0}\right)^{1/(2n+2)} L^{1/2}\,. \tag{4.117}$$

Inserting this result into Eq. (4.116) yields

$$\begin{aligned} h^{(2n+2)/n} &= 2\left(\frac{a_\mathrm{s}}{A_0}\right)^{1/n}\left(L^{(n+1)/n} - x^{(n+1)/n}\right) \\ &= 2\left(\frac{a_\mathrm{s}}{A_0}\right)^{1/n} L^{(n+1)/n}\left[1 - \left(\frac{x}{L}\right)^{(n+1)/n}\right], \end{aligned} \tag{4.118}$$

which can be written in simpler form as

$$h = h_0\left[1 - \left(\frac{x}{L}\right)^{(n+1)/n}\right]^{n/(2n+2)}. \tag{4.119}$$

This solution is called the *Vialov profile* (Vialov 1958). Note that for negative values of x, that is, for the half-domain $-L < x < 0$, the variable x must be replaced by $|x|$ in order to maintain the symmetry of the profile.

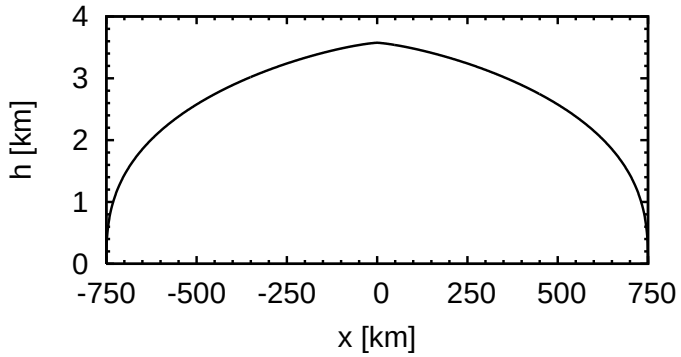

Figure 4.8: Vialov profile (4.119) for $L = 750\,\mathrm{km}$, $n = 3$, $a_\mathrm{s} = 0.3\,\mathrm{m\,a^{-1}}$, $A = 10^{-16}\,\mathrm{a^{-1}\,Pa^{-3}}$, $\rho = 910\,\mathrm{kg\,m^{-3}}$ and $g = 9.81\,\mathrm{m\,s^{-2}}$.

An example is shown in Fig. 4.8. The parameters are those of the EISMINT model intercomparison exercise described by Huybrechts et al. (1996), which resemble the conditions of the Greenland Ice Sheet. For a half-span of $L = 750\,\mathrm{km}$, the maximum elevation resulting from (4.117) is $h_0 = 3575.1\,\mathrm{m}$. It is interesting to note that the profile appears

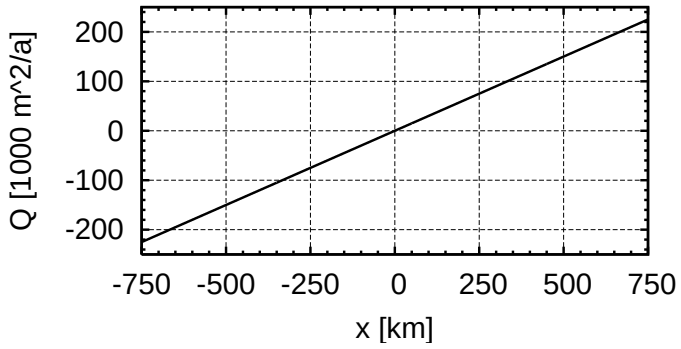

Figure 4.9: Volume flux for the Vialov profile shown in Fig. 4.8.

pointed at the divide. This is the case since at $x = 0$ the curvature (second derivative) of the function $h(x)$ defined by (4.119) is infinite, a problem which is related to the fact that the shallow ice approximation is not valid there. Further, the slope (first derivative) of the profile is infinite at the margins $x = \pm L$, which violates the assumption of small surface slopes.

The volume flux Q follows from Eq. (4.115). For the above EISMINT parameters, it is shown in Fig. 4.9. The volume flux vanishes at the ice divide, and it increases linearly away from the divide with a gradient of $\mathrm{d}Q/\mathrm{d}x = a_\mathrm{s} = 0.3\,\mathrm{m}^2\,\mathrm{a}^{-1}/\mathrm{m}$ in order to balance the ice accumulation. At the margin, the volume flux reaches a value of $Q(L) = 2.25 \times 10^5\,\mathrm{m}^2\,\mathrm{a}^{-1}$, which can be interpreted as the *calving rate* into a surrounding ocean.

An unrealistic feature of the Vialov profile is the behaviour of the shear stress near the margin. According to Eq. (4.106), the basal shear stress in the shallow ice approximation (driving stress) is proportional to the product of the ice thickness and the inclination of the ice surface, which yields for the Vialov profile (4.119)

$$\tau_\mathrm{d} = -\rho g h \frac{\mathrm{d}h}{\mathrm{d}x} = \frac{\rho g h_0^2}{2L} \left[1 - \left(\frac{x}{L}\right)^{(n+1)/n}\right]^{-1/(n+1)} \left(\frac{x}{L}\right)^{1/n} . \tag{4.120}$$

In the limit of $x \to L$ this expression diverges, thus the basal shear stress is unbounded at the ice margin.

Analytical solutions of Eq. (4.114) for variable mass balance functions $a_\mathrm{s}(x)$ based on Bueler (2003) and Bueler et al. (2005) are discussed in the textbook by Greve and Blatter (2009).

5 Large-Scale Dynamics of Ice Shelves

5.1 Full Stokes Flow Problem

5.1.1 Field Equations, Boundary Conditions at the Free Surface

Ice shelves are floating ice masses, which are connected to and nourished by a grounded ice sheet (see Fig. 4.1). Most ice shelves, like the three major ice shelves of Antarctica (Ross Ice Shelf, Filchner-Rønne Ice Shelf, Amery Ice Shelf), are confined by large embayments. Smaller ice shelves can also be unconfined. In the latter case, stabilisation typically results from the contact with small islands or grounding on shoals.

Ice shelves are smaller and thinner than ice sheets and, on average, the ice flow is distinctly faster. Suitable typical values are

$$\begin{aligned}
\text{typical horizontal extent} \quad & [L] &&= 500\,\mathrm{km}\,, \\
\text{typical vertical extent} \quad & [H] &&= 500\,\mathrm{m}\,, \\
\text{typical horizontal velocity} \quad & [U] &&= 1000\,\mathrm{m\,a^{-1}}\,, \\
\text{typical vertical velocity} \quad & [W] &&= 1\,\mathrm{m\,a^{-1}}\,, \\
\text{typical pressure} \quad & [P] &&= \rho g[H] \approx 5\,\mathrm{MPa}\,, \\
\text{typical time-scale} \quad & [t] &&= [L]/[U] = [H]/[W] = 500\,\mathrm{a}\,, \\
\text{typical temperature variation} \quad & [\Delta T] &&= 20\,\mathrm{K}\,.
\end{aligned} \tag{5.1}$$

[compare Eqs. (4.5) and (4.102) for ice sheets]. Note the resulting time-scale $[t]$, which is twenty times smaller than that of ice sheets. The scales (5.1) give an aspect ratio of

$$\varepsilon = \frac{[H]}{[L]} = \frac{[W]}{[U]} = 10^{-3}\,, \tag{5.2}$$

a Froude number of

$$Fr = \frac{[U]^2}{g[H]} \approx 2 \times 10^{-13}\,, \tag{5.3}$$

a Rossby number of

$$Ro = \frac{[U]}{2\Omega[L]} \approx 4 \times 10^{-7}\,, \tag{5.4}$$

and a Coriolis-force-to-pressure-gradient ratio of

$$\frac{2\rho\Omega[U]}{[P]/[L]} = \frac{Fr}{Ro} \approx 5 \times 10^{-7}\,. \tag{5.5}$$

Evidently, the aspect ratio is the same as for ice sheets, whereas the Froude number and Coriolis-force-to-pressure-gradient ratio are larger by factors 200 and 10, respectively, but still very small. As a consequence, the flow of ice shelves is also governed by *Stokes flow*, and the equation of motion (4.11) remains valid. Also, the mass balance (4.1), the temperature evolution equation (4.14), the kinematic boundary condition (4.21), the stress-free condition (4.23) and the temperature boundary condition (4.24) for the free surface hold without any changes.

5.1.2 Boundary Conditions at the Ice Base

The situation is different at the ice base. First of all, it is an interface between ice and sea water and therefore situated *above* the lithosphere surface ($b \geq z_\mathrm{l}$, see Fig. 4.1). Both melting and freezing processes can occur, so that the quantity $a_\mathrm{b}^\perp$ defined in (4.29) can have either sign and must be interpreted as a *basal melting-freezing rate*. It is positive for melting and negative for freezing. Apart from this extended interpretation of $a_\mathrm{b}^\perp$, the kinematic boundary condition (4.31) remains valid. Consequently, the ice thickness equation (4.55), which has been derived by using the mass balance and the kinematic conditions at the free surface and the ice base, holds as well.

Analogous to Eq. (4.32), the momentum jump condition is

$$\mathsf{t}_\mathrm{sea} \cdot \mathbf{n} - \mathsf{t} \cdot \mathbf{n} - \rho a_\mathrm{b}^\perp \, [\![\mathbf{v}]\!] = \mathbf{0} \,, \tag{5.6}$$

where the lithospheric stress t_lith has been replaced by the stress at the sea side of the interface, t_sea. Whereas the lithospheric stress under an ice sheet is unknown, the stress conditions in the sea can be described by a hydrostatic pressure p_sea plus a shear stress $\boldsymbol{\tau}_\mathrm{sea}$ induced by the circulating sea water. The former corresponds to the weight of the water column from the water surface (mean sea level $z = z_\mathrm{sl}$) to the ice base ($z = b$),

$$p_\mathrm{sea} = \rho_\mathrm{sw} g (z_\mathrm{sl} - b) \,, \tag{5.7}$$

where $\rho_\mathrm{sw} = 1028 \,\mathrm{kg\,m^{-3}}$ is the density of sea water. The latter can be related to the flow velocity of the subglacial sea water, $\mathbf{v}_\mathrm{sea}$, by the empirical relation

$$\boldsymbol{\tau}_\mathrm{sea} = C_\mathrm{wi} \rho_\mathrm{sw} |\mathbf{v}_\mathrm{sea}|^2 \, \mathbf{e}_\mathrm{t} \,, \tag{5.8}$$

where C_wi is the dimensionless water-ice drag coefficient ($C_\mathrm{wi} \approx 2.5 \times 10^{-3}$, depending on the roughness of the basal ice), and $\mathbf{e}_\mathrm{t}$ is the direction of $\boldsymbol{\tau}_\mathrm{sea}$ in the tangential plane to the ice base ($\mathbf{e}_\mathrm{t} \perp \mathbf{n}$), assumed parallel to $\mathbf{v}_\mathrm{sea}$ (so that $\mathbf{e}_\mathrm{t} = \mathbf{v}_\mathrm{sea} / |\mathbf{v}_\mathrm{sea}|$). Thus,

$$\mathsf{t}_\mathrm{sea} \cdot \mathbf{n} = -p_\mathrm{sea} \, \mathbf{n} + \boldsymbol{\tau}_\mathrm{sea} = -\rho_\mathrm{sw} g (z_\mathrm{sl} - b) \, \mathbf{n} + C_\mathrm{wi} \rho_\mathrm{sw} |\mathbf{v}_\mathrm{sea}|^2 \, \mathbf{e}_\mathrm{t} \,. \tag{5.9}$$

Further, the advective term $\rho a_\mathrm{b}^\perp \, [\![\mathbf{v}]\!]$ in the momentum jump condition (5.6) is negligible. Therefore, we obtain the *stress condition*

$$\mathsf{t} \cdot \mathbf{n} = -\rho_\mathrm{sw} g (z_\mathrm{sl} - b) \, \mathbf{n} + C_\mathrm{wi} \rho_\mathrm{sw} |\mathbf{v}_\mathrm{sea}|^2 \, \mathbf{e}_\mathrm{t} \,. \tag{5.10}$$

This relation serves as a dynamic boundary condition at the base of an ice shelf. Consequently, the additional formulation of an empirical sliding law like (4.35) is not required.

The temperature of the ice at the ice base is equal to the temperature of the sea water immediately below,

$$T = T_{\mathrm{sea}}\,, \tag{5.11}$$

which will be at the freezing point under the prevailing pressure and salinity conditions (typically around $-2°\mathrm{C}$). The situation is therefore comparable to that of a temperate base of an ice sheet [see Eq. (4.39)]. In addition to (5.11), we can formulate an energy jump condition similar to (4.37),

$$\kappa\,(\operatorname{grad} T \cdot \mathbf{n}) - q^{\perp}_{\mathrm{sea}} - [\![\mathbf{v}]\!] \cdot \mathtt{t} \cdot \mathbf{n} + \rho a^{\perp}_{\mathrm{b}}\,[\![u]\!] = 0\,, \tag{5.12}$$

where $q^{\perp}_{\mathrm{sea}}$ is the heat flux entering the ice body from the sea water below. For the third term of (5.12), we find, using (5.8) and (5.10)

$$[\![\mathbf{v}]\!] \cdot \mathtt{t} \cdot \mathbf{n} = -\rho_{\mathrm{sw}} g (z_{\mathrm{sl}} - b)\,[\![\mathbf{v} \cdot \mathbf{n}]\!] + [\![\mathbf{v}]\!] \cdot \boldsymbol{\tau}_{\mathrm{sea}}\,. \tag{5.13}$$

Using the general mass jump condition (2.53) and the definition (4.29) of $a^{\perp}_{\mathrm{b}}$ yields

$$\begin{aligned} &\rho_{\mathrm{sw}}(\mathbf{v}_{\mathrm{sea}} - \mathbf{w}) \cdot \mathbf{n} = \rho(\mathbf{v} - \mathbf{w}) \cdot \mathbf{n} = \rho a^{\perp}_{\mathrm{b}} \\ &\Rightarrow\ (\mathbf{v}_{\mathrm{sea}} - \mathbf{w}) \cdot \mathbf{n} = \frac{\rho}{\rho_{\mathrm{sw}}} a^{\perp}_{\mathrm{b}}\,, \quad (\mathbf{v} - \mathbf{w}) \cdot \mathbf{n} = a^{\perp}_{\mathrm{b}}\,, \end{aligned} \tag{5.14}$$

so that the jump of the normal velocity in (5.13) is

$$[\![\mathbf{v} \cdot \mathbf{n}]\!] = (\mathbf{v}_{\mathrm{sea}} - \mathbf{w}) \cdot \mathbf{n} - (\mathbf{v} - \mathbf{w}) \cdot \mathbf{n} = \frac{\rho - \rho_{\mathrm{sw}}}{\rho_{\mathrm{sw}}}\, a^{\perp}_{\mathrm{b}}\,. \tag{5.15}$$

Further, we define the *frictional dissipation* of the boundary-layer current below the ice shelf as

$$\begin{aligned} \delta_{\mathrm{sea}} &= [\![\mathbf{v}]\!] \cdot \boldsymbol{\tau}_{\mathrm{sea}} \\ &\overset{(5.8)}{=} C_{\mathrm{wi}} \rho_{\mathrm{sw}} |\mathbf{v}_{\mathrm{sea}}|^2\, [\![\mathbf{v} \cdot \mathbf{e}_{\mathrm{t}}]\!] \\ &= C_{\mathrm{wi}} \rho_{\mathrm{sw}} |\mathbf{v}_{\mathrm{sea}}|^2\, (\mathbf{v}_{\mathrm{sea}} \cdot \mathbf{e}_{\mathrm{t}} - \mathbf{v} \cdot \mathbf{e}_{\mathrm{t}}) \\ &\approx C_{\mathrm{wi}} \rho_{\mathrm{sw}} |\mathbf{v}_{\mathrm{sea}}|^3\,. \end{aligned} \tag{5.16}$$

In the last step, the assumptions that the sea-water flow is essentially parallel to the ice base ($\mathbf{v}_{\mathrm{sea}} \approx |\mathbf{v}_{\mathrm{sea}}|\,\mathbf{e}_{\mathrm{t}}$) and much larger than the flow of the ice shelf ($\mathbf{v}_{\mathrm{sea}} \gg \mathbf{v}$) are made. Equation (5.13) then becomes

$$[\![\mathbf{v}]\!] \cdot \mathtt{t} \cdot \mathbf{n} = (\rho_{\mathrm{sw}} - \rho) g (z_{\mathrm{sl}} - b)\, a^{\perp}_{\mathrm{b}} + \delta_{\mathrm{sea}}\,. \tag{5.17}$$

For the fourth term of (5.12), we state that, as for an ice sheet with a temperate base, the jump of the internal energy is approximately equal to the latent heat of ice melt ($[\![u]\!] = L$). By inserting this and (5.17) in (5.12), we obtain

$$\kappa\,(\operatorname{grad} T \cdot \mathbf{n}) - (\rho_{\mathrm{sw}} - \rho) g (z_{\mathrm{sl}} - b)\, a^{\perp}_{\mathrm{b}} + \rho L a^{\perp}_{\mathrm{b}} = q^{\perp}_{\mathrm{sea}} + \delta_{\mathrm{sea}} \tag{5.18}$$

as the energy jump condition at the ice shelf base. Since the basal temperature is already determined by (5.11), Eq. (5.18) is not required as a boundary condition for the temperature field. However, provided that $q_{\mathrm{sea}}^{\perp}$ and δ_{sea} are known (for instance, from measurements), it determines the basal melting-freezing rate $a_{\mathrm{b}}^{\perp}$. Alternatively, if $a_{\mathrm{b}}^{\perp}$ is known, Eq. (5.18) can be used to compute the total heat input $q_{\mathrm{sea}}^{\perp} + \delta_{\mathrm{sea}}$ from the sea water below the ice shelf.

Concerning the effect of the basal shear stress $\boldsymbol{\tau}_{\mathrm{sea}}$, an estimate with $C_{\mathrm{wi}} = 2.5 \times 10^{-3}$, $\rho_{\mathrm{sw}} = 1028\,\mathrm{kg\,m^{-3}}$ and $|\mathbf{v}_{\mathrm{sea}}| = 0.1\,\mathrm{m\,s^{-1}}$ gives the values $|\boldsymbol{\tau}_{\mathrm{sea}}| \approx 0.025\,\mathrm{Pa}$ and $\delta_{\mathrm{sea}} \approx 2.5\,\mathrm{mW\,m^{-2}}$. Evidently, the shear stress itself is extremely small, and therefore its contribution to the stress condition (5.10) is negligible. By contrast, the frictional dissipation resulting from it is significant and should be taken into account in the energy jump condition (5.18).

5.1.3 Boundary Conditions at the Grounding Line and Calving Front

Boundary conditions are also required at the lateral margins, that is, the grounding line (in contact with the attached ice sheet) and the calving front (in contact with the surrounding ocean). At the grounding line, the inflow $\mathbf{v}_{\mathrm{gl}}$ and temperature T_{gl} from the ice sheet are usually prescribed directly. At the calving front, the temperature can also be prescribed directly as T_{cf}. The hydrostatic pressure distribution p_{sw} of the sea water provides a boundary condition for the stress vector $\mathsf{t}|_{\mathrm{cf}} \cdot \mathbf{n}$,

$$\mathsf{t}|_{\mathrm{cf}} \cdot \mathbf{n} = -p_{\mathrm{sw}}\mathbf{n}\,, \tag{5.19}$$

where $\mathbf{n}$ is the unit normal vector which points in a horizontal direction away from the calving front (assumed to be vertical). The sea water pressure is given by

$$p_{\mathrm{sw}} = \begin{cases} 0\,, & \text{for } z \geq z_{\mathrm{sl}}\,, \\ \rho_{\mathrm{sw}} g (z_{\mathrm{sl}} - z)\,, & \text{for } z \leq z_{\mathrm{sl}} \end{cases} \tag{5.20}$$

[compare Eq. (5.10) for the ice shelf base]. This relation is illustrated in Fig. 5.1.

For the positions of the grounding line and calving front, let us assume that they are described by implicit functions

$$F_{\mathrm{gl}}(x, y, t) = 0 \tag{5.21}$$

and

$$F_{\mathrm{cf}}(x, y, t) = 0\,, \tag{5.22}$$

respectively. Since both boundaries are vertical faces, these functions do not depend on the vertical coordinate z. The unit normal vectors are the normalised gradients,

$$\mathbf{n} = \frac{\operatorname{grad} F_{\mathrm{gl/cf}}}{|\operatorname{grad} F_{\mathrm{gl/cf}}|} = \frac{1}{N_{\mathrm{gl/cf}}} \begin{pmatrix} \dfrac{\partial F_{\mathrm{gl/cf}}}{\partial x} \\ \dfrac{\partial F_{\mathrm{gl/cf}}}{\partial y} \\ 0 \end{pmatrix}, \tag{5.23}$$

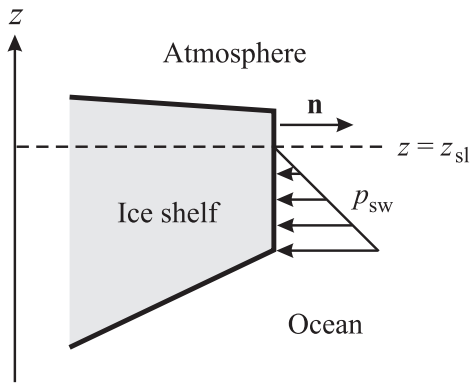

Figure 5.1: Stress condition at the calving front of an ice shelf.

with the gradient norm

$$N_{\mathrm{gl/cf}} = |\mathrm{grad}\, F_{\mathrm{gl/cf}}| = \left(\left(\frac{\partial F_{\mathrm{gl/cf}}}{\partial x} \right)^2 + \left(\frac{\partial F_{\mathrm{gl/cf}}}{\partial y} \right)^2 \right)^{1/2} . \tag{5.24}$$

We assume that the functions $F_{\mathrm{gl/cf}}$ are chosen such that $\mathbf{n}$ points away from the ice shelf.

Formulating a suitable condition which describes the position of the grounding line (evolution of the function F_{gl}) constitutes a major problem in recent glaciological research. The easiest possibility is to simply prescribe its position. If this is not possible due to a lack of observational data, the position of the grounding line can be found by solving a contact problem for the coupled ice-sheet/ice-shelf problem, according to a recent suggestion by Durand et al. (2009b,a). This is based on the topological condition that the ice base cannot penetrate the lithosphere surface, that is,

$$\forall x, y, t : \quad b(x, y, t) \geq z_{\mathrm{l}}(x, y, t) \, . \tag{5.25}$$

For any given point (x, y) and time t, the ice is assumed to be grounded if it touches the lithosphere surface, and the basal normal stress N_{b} (which is positive for compression) is larger than the basal sea water pressure $p_{\mathrm{sw,b}}$ [$= \rho_{\mathrm{sw}} g (z_{\mathrm{sl}} - b)$, cf. Eq. (5.20)]:

$$b(x, y, t) = z_{\mathrm{l}}(x, y, t) \;\text{ and }\; N_{\mathrm{b}}(x, y, t) > p_{\mathrm{sw,b}}(x, y, t) \, . \tag{5.26}$$

By contrast, the ice is assumed to be floating if the ice base is above the lithosphere surface, or if it touches the lithosphere surface, but the basal normal stress is smaller than or equal to the basal sea water pressure:

$$\begin{aligned} & b(x, y, t) > z_{\mathrm{l}}(x, y, t) \, , \\ \text{or} \quad & b(x, y, t) = z_{\mathrm{l}}(x, y, t) \;\text{ and }\; N_{\mathrm{b}}(x, y, t) \leq p_{\mathrm{sw,b}}(x, y, t) \, . \end{aligned} \tag{5.27}$$

The position of the grounding line is the boundary of the two domains (grounded vs. floating ice) which result from the conditions (5.26) and (5.27). A further possibility will be discussed below (Sect. 5.3).

For determining the position of the calving front, a kinematic condition is well suited. As a direct consequence of Eq. (5.22), the time derivative of F_{cf} following the motion of the calving front with velocity $\mathbf{w} = w_x\mathbf{e}_x + w_y\mathbf{e}_y$ must vanish,

$$\frac{\mathrm{d}_w F_{\mathrm{cf}}}{\mathrm{d}t} = \frac{\partial F_{\mathrm{cf}}}{\partial t} + (\operatorname{grad} F_{\mathrm{cf}}) \cdot \mathbf{w} = 0 \tag{5.28}$$

[compare Eq. (4.18)]. Let $\mathbf{v}_{\mathrm{h}}$ be the horizontal component of the ice velocity at the calving front. We can then introduce the *calving rate* $c^{\perp}$,

$$c^{\perp} = (\mathbf{v}_{\mathrm{h}} - \mathbf{w}) \cdot \mathbf{n}\,, \tag{5.29}$$

and rewrite Eq. (5.28) as

$$\frac{\partial F_{\mathrm{cf}}}{\partial t} + (\operatorname{grad} F_{\mathrm{cf}}) \cdot \mathbf{v}_{\mathrm{h}} = N_{\mathrm{cf}} c^{\perp}\,. \tag{5.30}$$

This equation represents an evolution equation for the calving front, which can be solved provided that the calving rate $c^{\perp}$ is prescribed.

5.2 Hydrostatic Approximation

The hydrostatic approximation works the same way as for ice sheets. By neglecting the shear stresses t_{xz} and t_{yz} in the vertical momentum balance, one finds the hydrostatic distribution (4.59) for the vertical normal stress t_{zz}, and the relation (4.60) for the pressure p. This leads to the expressions (4.61) for the horizontal normal stresses t_{xx} and t_{yy}. By inserting them in the horizontal components of the momentum balance and applying Glen's flow law, one obtains the equations of motion (4.64), which replace the full-Stokes-flow equation (4.11).

5.3 Shallow Shelf Approximation

Similar to ice sheets, the interior regions of an ice shelf (that is, some 10 km away from the grounding line and the calving front) are characterised by a small aspect ratio [see Eq. (5.2)] and small slopes of the free surface and the ice base. The latter can be expressed as

$$\begin{aligned} \frac{\partial h}{\partial x},\, \frac{\partial h}{\partial y} &\sim \frac{[H]}{[L]} = \varepsilon\,, \\ \frac{\partial b}{\partial x},\, \frac{\partial b}{\partial y} &\sim \frac{[H]}{[L]} = \varepsilon\,. \end{aligned} \tag{5.31}$$

Since at the base of an ice shelf significant shear stresses cannot be maintained [see the stress condition (5.10); as mentioned at the end of Sect. 5.1, the contribution from the

water-flow-induced shear stress $\boldsymbol{\tau}_{\mathrm{sea}}$ is negligibly small in that context], the regime of bed-parallel shear flow found in grounded ice sheets cannot exist in floating ice shelves. By contrast, the typical situation is that of *plug flow*, whereby the horizontal velocities are essentially constant over depth. Naturally, in the immediate vicinity of the grounding line, a transitional state between these two limits will develop. The situation is illustrated in Fig. 5.2.

These considerations will now be used for deriving a further simplification of the hydrostatic approximation which is called the *shallow shelf approximation* (SSA) (Morland 1987). Mathematically, the regime of plug flow can be defined by

$$\frac{\partial v_x}{\partial z} \approx 0\,, \quad \frac{\partial v_y}{\partial z} \approx 0\,. \tag{5.32}$$

In other words, the horizontal velocities only depend on the horizontal coordinates and the time,

$$v_x = v_x(x, y, t)\,, \quad v_y = v_y(x, y, t)\,. \tag{5.33}$$

We go back to the horizontal components of the momentum balance of the hydrostatic approximation in the form (4.62). In order to make use of the fact that the shear stresses vanish at the surface and at the base, these equations are now integrated over depth:

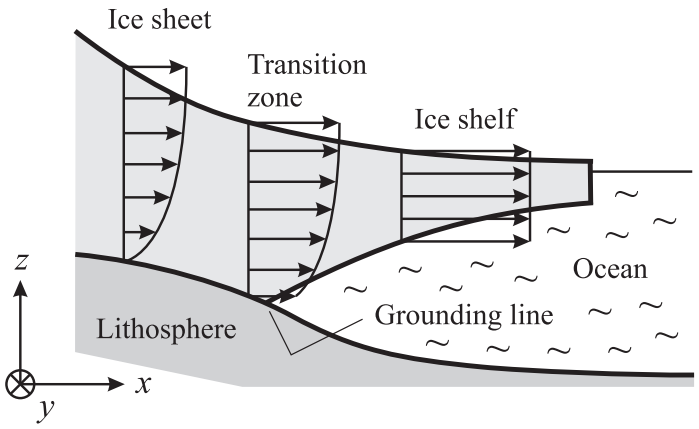

Figure 5.2: Flow regimes in an ice-sheet/ice-shelf system. In the grounded ice sheet, shear flow prevails, whereas in the floating ice shelf plug flow is present. The vicinity of the grounding line shows a transitional flow pattern.

$$2\int_b^h \frac{\partial t_{xx}^{\mathrm{D}}}{\partial x}\,\mathrm{d}z + \int_b^h \frac{\partial t_{yy}^{\mathrm{D}}}{\partial x}\,\mathrm{d}z + \int_b^h \frac{\partial t_{xy}}{\partial y}\,\mathrm{d}z + \int_b^h \frac{\partial t_{xz}}{\partial z}\,\mathrm{d}z = \rho g H \frac{\partial h}{\partial x}\,, \tag{5.34a}$$

$$2\int_b^h \frac{\partial t_{yy}^{\mathrm{D}}}{\partial y}\,\mathrm{d}z + \int_b^h \frac{\partial t_{xx}^{\mathrm{D}}}{\partial y}\,\mathrm{d}z + \int_b^h \frac{\partial t_{xy}}{\partial x}\,\mathrm{d}z + \int_b^h \frac{\partial t_{yz}}{\partial z}\,\mathrm{d}z = \rho g H \frac{\partial h}{\partial y}\,. \tag{5.34b}$$

The first three integrals of each equation can be modified by using Leibniz's rule (see also Sect. 4.1.3), whereas the last one simply gives the difference of t_{xz} or t_{yz} at the surface and at the base. One obtains

$$\begin{aligned} &2\frac{\partial}{\partial x}\int_b^h t_{xx}^{\mathrm{D}}\,\mathrm{d}z - 2t_{xx}^{\mathrm{D}}|_{z=h}\frac{\partial h}{\partial x} + 2t_{xx}^{\mathrm{D}}|_{z=b}\frac{\partial b}{\partial x} \\ &+ \frac{\partial}{\partial x}\int_b^h t_{yy}^{\mathrm{D}}\,\mathrm{d}z - t_{yy}^{\mathrm{D}}|_{z=h}\frac{\partial h}{\partial x} + t_{yy}^{\mathrm{D}}|_{z=b}\frac{\partial b}{\partial x} \\ &+ \frac{\partial}{\partial y}\int_b^h t_{xy}\,\mathrm{d}z - t_{xy}|_{z=h}\frac{\partial h}{\partial y} + t_{xy}|_{z=b}\frac{\partial b}{\partial y} \\ &+ t_{xz}|_{z=h} - t_{xz}|_{z=b} = \rho g H \frac{\partial h}{\partial x}\,, \end{aligned} \tag{5.35a}$$

$$
\begin{aligned}
&2\frac{\partial}{\partial y}\int_b^h t_{yy}^{\mathrm{D}}\,\mathrm{d}z - 2t_{yy}^{\mathrm{D}}|_{z=h}\frac{\partial h}{\partial y} + 2t_{yy}^{\mathrm{D}}|_{z=b}\frac{\partial b}{\partial y}\\
&+\frac{\partial}{\partial y}\int_b^h t_{xx}^{\mathrm{D}}\,\mathrm{d}z - t_{xx}^{\mathrm{D}}|_{z=h}\frac{\partial h}{\partial y} + t_{xx}^{\mathrm{D}}|_{z=b}\frac{\partial b}{\partial y}\\
&+\frac{\partial}{\partial x}\int_b^h t_{xy}\,\mathrm{d}z - t_{xy}|_{z=h}\frac{\partial h}{\partial x} + t_{xy}|_{z=b}\frac{\partial b}{\partial x}\\
&\qquad + t_{yz}|_{z=h} - t_{yz}|_{z=b} = \rho g H\frac{\partial h}{\partial y}\,. \qquad (5.35b)
\end{aligned}
$$

By introducing the *membrane stress* N as the vertically integrated deviatoric stress,

$$
\mathsf{N} = \int_b^h \mathsf{t}^{\mathrm{D}}\,\mathrm{d}z\,, \quad \text{or} \quad N_{ij} = \int_b^h t_{ij}^{\mathrm{D}}\,\mathrm{d}z\,, \qquad (5.36)
$$

and rearranging terms, this yields

$$
\begin{aligned}
&2\frac{\partial N_{xx}}{\partial x} + \frac{\partial N_{yy}}{\partial x} + \frac{\partial N_{xy}}{\partial y}\\
&-2t_{xx}^{\mathrm{D}}|_{z=h}\frac{\partial h}{\partial x} - t_{yy}^{\mathrm{D}}|_{z=h}\frac{\partial h}{\partial x} - t_{xy}|_{z=h}\frac{\partial h}{\partial y} + t_{xz}|_{z=h}\\
&+2t_{xx}^{\mathrm{D}}|_{z=b}\frac{\partial b}{\partial x} + t_{yy}^{\mathrm{D}}|_{z=b}\frac{\partial b}{\partial x} + t_{xy}|_{z=b}\frac{\partial b}{\partial y} - t_{xz}|_{z=b} = \rho g H\frac{\partial h}{\partial x}\,, \qquad (5.37a)\\
&2\frac{\partial N_{yy}}{\partial y} + \frac{\partial N_{xx}}{\partial y} + \frac{\partial N_{xy}}{\partial x}\\
&-2t_{yy}^{\mathrm{D}}|_{z=h}\frac{\partial h}{\partial y} - t_{xx}^{\mathrm{D}}|_{z=h}\frac{\partial h}{\partial y} - t_{xy}|_{z=h}\frac{\partial h}{\partial x} + t_{yz}|_{z=h}\\
&+2t_{yy}^{\mathrm{D}}|_{z=b}\frac{\partial b}{\partial y} + t_{xx}^{\mathrm{D}}|_{z=b}\frac{\partial b}{\partial y} + t_{xy}|_{z=b}\frac{\partial b}{\partial x} - t_{yz}|_{z=b} = \rho g H\frac{\partial h}{\partial y}\,. \qquad (5.37b)
\end{aligned}
$$

In order to further simplify this system, the stress conditions at the surface (4.23) and at the base (5.10) must be considered. With the unit normal vector (4.16), condition (4.23) reads, in component form,

$$
\begin{aligned}
\frac{1}{N_{\mathrm{s}}}\left(-t_{xx}|_{z=h}\frac{\partial h}{\partial x} - t_{xy}|_{z=h}\frac{\partial h}{\partial y} + t_{xz}|_{z=h}\right) &= 0\,,\\
\frac{1}{N_{\mathrm{s}}}\left(-t_{yy}|_{z=h}\frac{\partial h}{\partial y} - t_{xy}|_{z=h}\frac{\partial h}{\partial x} + t_{yz}|_{z=h}\right) &= 0\,, \qquad (5.38)\\
\frac{1}{N_{\mathrm{s}}}\left(-t_{xz}|_{z=h}\frac{\partial h}{\partial x} - t_{yz}|_{z=h}\frac{\partial h}{\partial y} + t_{zz}|_{z=h}\right) &= 0\,.
\end{aligned}
$$

In the last component, the shear stresses are negligible compared to the vertical normal stress, so that it simplifies to

$$t_{zz}|_{z=h} = 0\,, \tag{5.39}$$

in agreement with the hydrostatic distribution (4.59). In the first two components, we replace the normal stresses t_{xx} and t_{yy} by using the expressions (4.61) evaluated for $z = h$,

$$\begin{aligned} -2t^{\mathrm{D}}_{xx}|_{z=h}\frac{\partial h}{\partial x} - t^{\mathrm{D}}_{yy}|_{z=h}\frac{\partial h}{\partial x} - t_{xy}|_{z=h}\frac{\partial h}{\partial y} + t_{xz}|_{z=h} &= 0\,, \\ -2t^{\mathrm{D}}_{yy}|_{z=h}\frac{\partial h}{\partial y} - t^{\mathrm{D}}_{xx}|_{z=h}\frac{\partial h}{\partial y} - t_{xy}|_{z=h}\frac{\partial h}{\partial x} + t_{yz}|_{z=h} &= 0\,. \end{aligned} \tag{5.40}$$

As a consequence, the second and fifth lines of the vertically integrated momentum balance (5.37) vanish.

At the ice base, the component form of the stress condition (5.10), with the unit normal vector (4.26) and upon neglecting the shear stress $\boldsymbol{\tau}_{\mathrm{sea}}$, becomes

$$\begin{aligned} \frac{1}{N_{\mathrm{b}}}\left(t_{xx}|_{z=b}\frac{\partial b}{\partial x} + t_{xy}|_{z=b}\frac{\partial b}{\partial y} - t_{xz}|_{z=b}\right) &= -\frac{\rho_{\mathrm{sw}}g}{N_{\mathrm{b}}}(z_{\mathrm{sl}} - b)\,\frac{\partial b}{\partial x}\,, \\ \frac{1}{N_{\mathrm{b}}}\left(t_{yy}|_{z=b}\frac{\partial b}{\partial y} + t_{xy}|_{z=b}\frac{\partial b}{\partial x} - t_{yz}|_{z=b}\right) &= -\frac{\rho_{\mathrm{sw}}g}{N_{\mathrm{b}}}(z_{\mathrm{sl}} - b)\,\frac{\partial b}{\partial y}\,, \\ \frac{1}{N_{\mathrm{b}}}\left(t_{xz}|_{z=b}\frac{\partial b}{\partial x} + t_{yz}|_{z=b}\frac{\partial b}{\partial y} - t_{zz}|_{z=b}\right) &= \frac{\rho_{\mathrm{sw}}g}{N_{\mathrm{b}}}(z_{\mathrm{sl}} - b)\,. \end{aligned} \tag{5.41}$$

Again, in the last component the shear stresses can be neglected compared to the vertical normal stress, which yields

$$t_{zz}|_{z=b} = -\rho_{\mathrm{sw}}g(z_{\mathrm{sl}} - b)\,. \tag{5.42}$$

However, we can also obtain the value of $t_{zz}|_{z=b}$ by evaluating the hydrostatic distribution (4.59) for $z = b$,

$$t_{zz}|_{z=b} = -\rho g H\,. \tag{5.43}$$

Equating (5.42) and (5.43) relates the ice thickness H to the water column $z_{\mathrm{sl}} - b$,

$$\rho H = \rho_{\mathrm{sw}}(z_{\mathrm{sl}} - b)\,. \tag{5.44}$$

This result is called the *floating condition*. By replacing $b = h - H$, it can be rearranged into a relation for the *freeboard*, $h - z_{\mathrm{sl}}$, (part of the ice shelf above the water level),

$$\rho H = \rho_{\mathrm{sw}}(z_{\mathrm{sl}} - h + H) \;\Rightarrow\; h - z_{\mathrm{sl}} = H - \frac{\rho}{\rho_{\mathrm{sw}}}H = \frac{\rho_{\mathrm{sw}} - \rho}{\rho_{\mathrm{sw}}}H\,. \tag{5.45}$$

With the values $\rho = 910\,\mathrm{kg\,m^{-3}}$ and $\rho_{\mathrm{sw}} = 1028\,\mathrm{kg\,m^{-3}}$, the freeboard is approximately equal to 11.5% of the ice shelf thickness, so that the remaining 88.5% will be below the water level.

In the first two components of (5.41), we replace t_{xx} and t_{yy} again by using (4.61), now evaluated for $z = b$,

$$\begin{aligned} 2t^{\mathrm{D}}_{xx}|_{z=b}\frac{\partial b}{\partial x} + t^{\mathrm{D}}_{yy}|_{z=b}\frac{\partial b}{\partial x} - \rho g H\frac{\partial b}{\partial x} + t_{xy}|_{z=b}\frac{\partial b}{\partial y} - t_{xz}|_{z=b} & \\ = -\rho_{\mathrm{sw}} g (z_{\mathrm{sl}} - b)\,\frac{\partial b}{\partial x}\,, & \\ 2t_{yy}|_{z=b}\frac{\partial b}{\partial y} + t_{xx}|_{z=b}\frac{\partial b}{\partial y} - \rho g H\frac{\partial b}{\partial y} + t_{xy}|_{z=b}\frac{\partial b}{\partial x} - t_{yz}|_{z=b} & \\ = -\rho_{\mathrm{sw}} g (z_{\mathrm{sl}} - b)\,\frac{\partial b}{\partial y}\,. & \end{aligned} \tag{5.46}$$

Because of the floating condition (5.44), this simplifies to

$$\begin{aligned} 2t^{\mathrm{D}}_{xx}|_{z=b}\frac{\partial b}{\partial x} + t^{\mathrm{D}}_{yy}|_{z=b}\frac{\partial b}{\partial x} + t_{xy}|_{z=b}\frac{\partial b}{\partial y} - t_{xz}|_{z=b} &= 0\,, \\ 2t_{yy}|_{z=b}\frac{\partial b}{\partial y} + t_{xx}|_{z=b}\frac{\partial b}{\partial y} + t_{xy}|_{z=b}\frac{\partial b}{\partial x} - t_{yz}|_{z=b} &= 0\,. \end{aligned} \tag{5.47}$$

Thus, the terms on the left hand sides in the third and sixth lines of (5.37) vanish as well.

Application of the conditions (5.40) and (5.47) in the vertically integrated momentum balance (5.37) provides

$$\begin{aligned} 2\frac{\partial N_{xx}}{\partial x} + \frac{\partial N_{yy}}{\partial x} + \frac{\partial N_{xy}}{\partial y} &= \rho g H\frac{\partial h}{\partial x}\,, \\ 2\frac{\partial N_{yy}}{\partial y} + \frac{\partial N_{xx}}{\partial y} + \frac{\partial N_{xy}}{\partial x} &= \rho g H\frac{\partial h}{\partial y}\,, \end{aligned} \tag{5.48}$$

where h and H are related by the floating condition in the form (5.45). Vertically integrating the flow law (3.21) gives

$$\begin{aligned} N_{xx} &= 2\bar{\eta}\,D_{xx} = 2\bar{\eta}\,\frac{\partial v_x}{\partial x}\,, \\ N_{yy} &= 2\bar{\eta}\,D_{yy} = 2\bar{\eta}\,\frac{\partial v_y}{\partial y}\,, \\ N_{xy} &= 2\bar{\eta}\,D_{xy} = \bar{\eta}\left(\frac{\partial v_x}{\partial y} + \frac{\partial v_y}{\partial x}\right)\,, \end{aligned} \tag{5.49}$$

where the independence of v_x and v_y on z, Eq. (5.33), and the definition of the membrane stresses, Eq. (5.36), have been used, and the depth-integrated viscosity,

$$\bar{\eta} = \int_b^h \eta\,\mathrm{d}z = \int_b^h \frac{1}{2}B(T')\,d_{\mathrm{e}}^{-(1-1/n)}\,\mathrm{d}z\,, \tag{5.50}$$

has been introduced. The effective strain rate d_e, of which the general component form is given in Eq. (4.66), can be simplified for the plug flow regime [Eq. (5.32)] to

$$\begin{aligned} d_\mathrm{e} &= \left\{ \left(\frac{\partial v_x}{\partial x}\right)^2 + \left(\frac{\partial v_y}{\partial y}\right)^2 + \frac{\partial v_x}{\partial x}\,\frac{\partial v_y}{\partial y} \right. \\ &\qquad \left. + \frac{1}{4}\left(\frac{\partial v_x}{\partial y} + \frac{\partial v_y}{\partial x}\right)^2 + \frac{1}{4}\left(\frac{\partial v_z}{\partial x}\right)^2 + \frac{1}{4}\left(\frac{\partial v_z}{\partial y}\right)^2 \right\}^{1/2} . \end{aligned} \tag{5.51}$$

With the scaling (5.1) and the aspect ratio (5.2), we can estimate the orders of magnitude of the terms $(\partial v_x/\partial x)^2$ and $(\partial v_z/\partial x)^2$,

$$\left(\frac{\partial v_x}{\partial x}\right)^2 \sim \frac{[U]^2}{[L]^2}\,, \qquad \left(\frac{\partial v_z}{\partial x}\right)^2 \sim \frac{[W]^2}{[L]^2} = \varepsilon^2\frac{[U]^2}{[L]^2}\,. \tag{5.52}$$

Consequently, the term $(\partial v_z/\partial x)^2$ is negligible compared to $(\partial v_x/\partial x)^2$. The same holds for $(\partial v_z/\partial y)^2$ compared to $(\partial v_y/\partial y)^2$, and so we obtain a further simplified expression for the effective strain rate,

$$d_\mathrm{e} = \left\{ \left(\frac{\partial v_x}{\partial x}\right)^2 + \left(\frac{\partial v_y}{\partial y}\right)^2 + \frac{\partial v_x}{\partial x}\,\frac{\partial v_y}{\partial y} + \frac{1}{4}\left(\frac{\partial v_x}{\partial y} + \frac{\partial v_y}{\partial x}\right)^2 \right\}^{1/2} . \tag{5.53}$$

This relation is independent of the vertical coordinate z, which reduces the depth-integrated viscosity (5.50) to

$$\bar\eta = \frac{1}{2} d_\mathrm{e}^{-(1-1/n)} \int_b^h B(T')\,\mathrm{d}z\,. \tag{5.54}$$

Inserting the vertically integrated flow law, Eq. (5.49), in the vertically integrated momentum balance, Eq. (5.48), finally yields

$$\begin{aligned} 4\frac{\partial}{\partial x}\left(\bar\eta\frac{\partial v_x}{\partial x}\right) + 2\frac{\partial}{\partial x}\left(\bar\eta\frac{\partial v_y}{\partial y}\right) + \frac{\partial}{\partial y}\left(\bar\eta\Big(\frac{\partial v_x}{\partial y} + \frac{\partial v_y}{\partial x}\Big)\right) &= \rho g H\frac{\partial h}{\partial x}\,, \\ 4\frac{\partial}{\partial y}\left(\bar\eta\frac{\partial v_y}{\partial y}\right) + 2\frac{\partial}{\partial y}\left(\bar\eta\frac{\partial v_x}{\partial x}\right) + \frac{\partial}{\partial x}\left(\bar\eta\Big(\frac{\partial v_x}{\partial y} + \frac{\partial v_y}{\partial x}\Big)\right) &= \rho g H\frac{\partial h}{\partial y}\,, \end{aligned} \tag{5.55}$$

which is a system of non-linear elliptical differential equations for the horizontal velocities v_x and v_y.

This system must be complemented by boundary conditions along the lateral margin of the ice shelf. At the grounding line, the inflow $\mathbf{v}_\mathrm{gl}$ from the nourishing ice sheet is usually prescribed, which serves as a dynamic condition. The position of the grounding line can either be prescribed or determined by solving a contact problem (see Sect. 5.1.3). The shallow shelf approximation allows a simpler formulation of the contact problem by using the floating condition (5.44), which can be rearranged to

$$b = z_\mathrm{sl} - \frac{\rho}{\rho_\mathrm{sw}} H\,. \tag{5.56}$$

Combining this with the inequality (5.25) yields

$$z_{\mathrm{sl}} - \frac{\rho}{\rho_{\mathrm{sw}}} H \geq z_{\mathrm{l}} \quad \Rightarrow \quad H \leq \frac{\rho_{\mathrm{sw}}}{\rho}(z_{\mathrm{sl}} - z_{\mathrm{l}})\,. \tag{5.57}$$

For any point (x, y) and time t, the ice is assumed to be floating if the inequality (5.57) is fulfilled. Otherwise, for the case

$$H > \frac{\rho_{\mathrm{sw}}}{\rho}(z_{\mathrm{sl}} - z_{\mathrm{l}})\,, \tag{5.58}$$

the ice is assumed to be grounded, and the position of the grounding line is given by the boundary of the two domains.

At the calving front, the stress condition needs to be evaluated. Equation (5.19) reads in component form

$$\begin{aligned} (-p + t^{\mathrm{D}}_{xx})_{\mathrm{cf}}\, n_x + t_{xy}|_{\mathrm{cf}}\, n_y &= -p_{\mathrm{sw}}\, n_x\,, \\ t_{xy}|_{\mathrm{cf}}\, n_x + (-p + t^{\mathrm{D}}_{yy})_{\mathrm{cf}}\, n_y &= -p_{\mathrm{sw}}\, n_y\,, \\ t_{xz}|_{\mathrm{cf}}\, n_x + t_{yz}|_{\mathrm{cf}}\, n_y &= 0\,. \end{aligned} \tag{5.59}$$

With the relation (4.60) for the pressure p in the hydrostatic approximation, Eqs. $(5.59)_{1,2}$ yield

$$\begin{aligned} (2t^{\mathrm{D}}_{xx} + t^{\mathrm{D}}_{yy})_{\mathrm{cf}}\, n_x + t_{xy}|_{\mathrm{cf}}\, n_y &= -p_{\mathrm{sw}}\, n_x + \rho g(h - z) n_x\,, \\ t_{xy}|_{\mathrm{cf}}\, n_x + (2t^{\mathrm{D}}_{yy} + t^{\mathrm{D}}_{xx})_{\mathrm{cf}}\, n_y &= -p_{\mathrm{sw}}\, n_y + \rho g(h - z) n_y\,. \end{aligned} \tag{5.60}$$

Using Eq. (5.20) for the sea-water pressure and definition (5.36) for the membrane stresses, this is readily integrated,

$$\begin{aligned} &(2N_{xx} + N_{yy})_{\mathrm{cf}}\, n_x + N_{xy}|_{\mathrm{cf}}\, n_y \\ &\qquad = \left(\int_b^h \rho g(h - z)\,\mathrm{d}z - \int_b^{z_{\mathrm{sl}}} \rho_{\mathrm{sw}} g(z_{\mathrm{sl}} - z)\,\mathrm{d}z \right) n_x\,, \\ &N_{xy}|_{\mathrm{cf}}\, n_x + (2N_{yy} + N_{xx})_{\mathrm{cf}}\, n_y \\ &\qquad = \left(\int_b^h \rho g(h - z)\,\mathrm{d}z - \int_b^{z_{\mathrm{sl}}} \rho_{\mathrm{sw}} g(z_{\mathrm{sl}} - z)\,\mathrm{d}z \right) n_y\,. \end{aligned} \tag{5.61}$$

The integral terms on the right hand side yield

$$\begin{aligned} \Big(\cdots \Big) &= \frac{\rho g H^2}{2} - \frac{\rho_{\mathrm{sw}} g (z_{\mathrm{sl}} - b)^2}{2} \\ &\overset{(5.44)}{=} \frac{\rho g H^2}{2} - \left(\frac{\rho}{\rho_{\mathrm{sw}}} \right)^2 \frac{\rho_{\mathrm{sw}} g H^2}{2} \\ &= \frac{\rho}{\rho_{\mathrm{sw}}} (\rho_{\mathrm{sw}} - \rho) \frac{g H^2}{2}\,, \end{aligned} \tag{5.62}$$

so that for the stress condition at the calving front we obtain

$$\begin{aligned}(2N_{xx}+N_{yy})_{\mathrm{cf}}\,n_x+N_{xy}|_{\mathrm{cf}}\,n_y &= \frac{\rho}{\rho_{\mathrm{sw}}}(\rho_{\mathrm{sw}}-\rho)\frac{gH^2}{2}\,n_x\,,\\ N_{xy}|_{\mathrm{cf}}\,n_x+(2N_{yy}+N_{xx})_{\mathrm{cf}}\,n_y &= \frac{\rho}{\rho_{\mathrm{sw}}}(\rho_{\mathrm{sw}}-\rho)\frac{gH^2}{2}\,n_y\,.\end{aligned} \tag{5.63}$$

Inserting the vertically integrated flow law (5.49) yields the corresponding boundary condition for the velocities,

$$\begin{aligned}&4\bar{\eta}\left.\frac{\partial v_x}{\partial x}\right|_{\mathrm{cf}} n_x+2\bar{\eta}\left.\frac{\partial v_y}{\partial y}\right|_{\mathrm{cf}} n_x+\bar{\eta}\left(\frac{\partial v_x}{\partial y}+\frac{\partial v_y}{\partial x}\right)_{\mathrm{cf}} n_y\\ &\qquad=\frac{\rho}{\rho_{\mathrm{sw}}}(\rho_{\mathrm{sw}}-\rho)\frac{gH^2}{2}\,n_x\,,\\ &\bar{\eta}\left(\frac{\partial v_x}{\partial y}+\frac{\partial v_y}{\partial x}\right)_{\mathrm{cf}} n_x+4\bar{\eta}\left.\frac{\partial v_y}{\partial y}\right|_{\mathrm{cf}} n_y+2\bar{\eta}\left.\frac{\partial v_x}{\partial x}\right|_{\mathrm{cf}} n_y\\ &\qquad=\frac{\rho}{\rho_{\mathrm{sw}}}(\rho_{\mathrm{sw}}-\rho)\frac{gH^2}{2}\,n_y\,.\end{aligned} \tag{5.64}$$

The position of the calving front is governed by the kinematic condition (5.30), which does not simplify in the shallow shelf approximation. Note that it requires the calving rate $c^{\perp}$ as an input quantity.

The geometry and structure of the elliptical boundary-value problem for the horizontal velocity field, which consists of the system of differential equations (5.55) and its associated boundary conditions at the grounding line and at the calving front, are illustrated in Fig. 5.3.

The system of model equations in the shallow shelf approximation is completed by the vertically integrated mass balance, the ice thickness equation and the temperature evolution equation. The vertically integrated mass balance is essentially the same as Eq. (4.95); however, we formulate it with the sea level instead of the ice base as the reference horizon,

$$\begin{aligned}v_z &= v_z|_{z=z_{\mathrm{sl}}}-\int_{z_{\mathrm{sl}}}^{z}\left(\frac{\partial v_x}{\partial x}+\frac{\partial v_y}{\partial y}\right)\mathrm{d}\bar{z}\\ &= v_z|_{z=z_{\mathrm{sl}}}-(z-z_{\mathrm{sl}})\left(\frac{\partial v_x}{\partial x}+\frac{\partial v_y}{\partial y}\right)\,.\end{aligned} \tag{5.65}$$

Hence the vertical velocity is linear over depth. The ice thickness equation results from Eq. (4.55), with $N_{\mathrm{s}}\approx 1$ and $N_{\mathrm{b}}\approx 1$, so that due to (5.31) $a_{\mathrm{s}}\approx a_{\mathrm{s}}^{\perp}$ and $a_{\mathrm{b}}\approx a_{\mathrm{b}}^{\perp}$,

$$\begin{aligned}\frac{\partial H}{\partial t} &= -\mathrm{div}\,\mathbf{Q}+a_{\mathrm{s}}-a_{\mathrm{b}}\\ &= -\mathrm{div}\,(H\mathbf{v}_{\mathrm{h}})+a_{\mathrm{s}}-a_{\mathrm{b}}\,.\end{aligned} \tag{5.66}$$

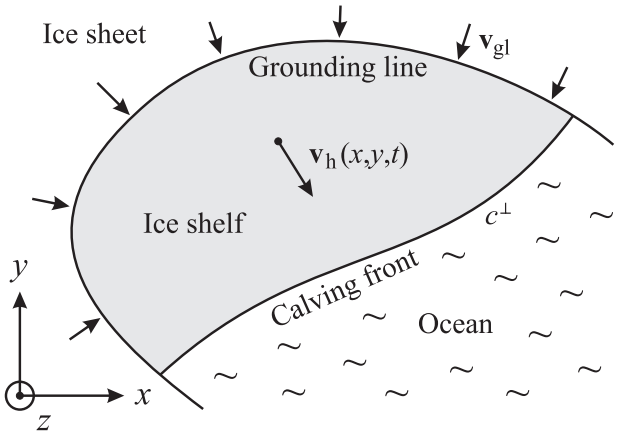

Figure 5.3: Ice shelf geometry in the horizontal map plane. The horizontal velocity field $\mathbf{v}_h$ is a solution of the elliptical differential equations (5.55) and the boundary conditions at the grounding line and at the calving front. Input quantities are the inflow velocity at the grounding line, $\mathbf{v}_{gl}$, and the calving rate at the calving front, $c^\perp$.

The temperature evolution equation [see Eq. (4.105)] is

$$\rho c\Big(\frac{\partial T}{\partial t} + v_x\frac{\partial T}{\partial x} + v_y\frac{\partial T}{\partial y} + v_z\frac{\partial T}{\partial z}\Big) = \frac{\partial}{\partial z}\Big(\kappa\frac{\partial T}{\partial z}\Big) + 2A(T')\,\sigma_e^{n+1}\,, \tag{5.67}$$

and is given simple Dirichlet boundary conditions (prescribed temperatures) at the surface, the ice base, the grounding line and the calving front as described above (Sect. 5.1).

It is instructive to compare the structure of the model equations of the shallow shelf approximation with that of the shallow ice approximation (Sect. 4.4). In the shallow ice approximation for ice sheets, the stresses, the horizontal velocity and the volume flux are *local* functions of the ice geometry and temperature. This means that information about the state of the ice sheet at other positions is not required in order to compute them. This is in strong contrast to the shallow shelf approximation, where the stresses, the horizontal velocity and the volume flux are determined by differential equations for the entire area of the ice shelf. Therefore, at any position they are influenced by the state of the whole ice shelf, or, in other words, they depend in a *non-local* way on the ice geometry and temperature. Of course, this makes the solution of the shallow shelf approximation more difficult.

5.4 Ice Shelf Ramp

Under certain conditions, it is possible to obtain analytical solutions for the equations of the shallow shelf approximation. Let us consider the following problem:

- Plane strain approximation (two-dimensional flow in the x-z plane).

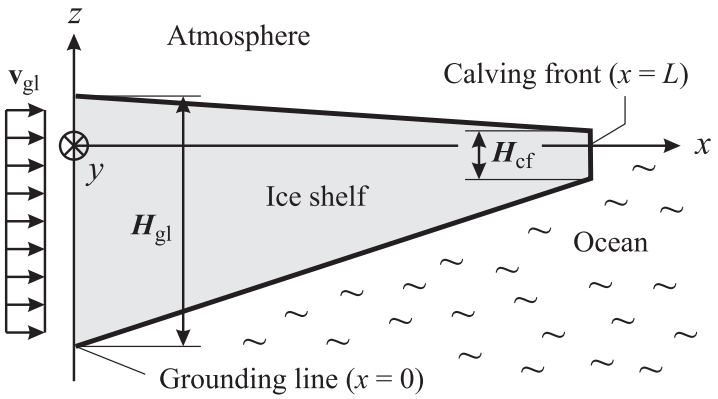

Figure 5.4: Ice shelf ramp of length L. The thickness is linearly decreasing from $H = H_{\mathrm{gl}}$ at the grounding line ($x = 0$) to $H = H_{\mathrm{cf}}$ at the calving front ($x = L$).

- Ice shelf extent between $x = 0$ and $x = L$, grounding line at $x = 0$, calving front at $x = L$.
- Thickness of the ice shelf linearly decreasing from $H = H_{\mathrm{gl}}$ at the grounding line to $H = H_{\mathrm{cf}}$ at the calving front.
- Mean sea level at $z = z_{\mathrm{sl}} = 0$.
- Inflow from attached ice sheet with velocity $\mathbf{v}_{\mathrm{gl}} = v_{\mathrm{gl}}\, \mathbf{e}_x$.
- Steady-state conditions: $\partial(\cdot)/\partial t = 0$ for all field quantities.
- Constant rate factor: $A(T') = A = \mathrm{const}$.

The geometry of this ice shelf ramp is illustrated in Fig. 5.4. The thickness $H(x)$ can be expressed as

$$H = H_{\mathrm{gl}} - \frac{H_{\mathrm{gl}} - H_{\mathrm{cf}}}{L}\, x\,. \tag{5.68}$$

With the floating condition in the alternative forms (5.44) and (5.45), the free surface and the ice base are given by

$$h = \frac{\rho_{\mathrm{sw}} - \rho}{\rho_{\mathrm{sw}}}\, H\,, \qquad b = -\frac{\rho}{\rho_{\mathrm{sw}}}\, H\,. \tag{5.69}$$

The velocity field consists of the two functions $v_x(x)$ and $v_z(x, z)$, so that the effective strain rate (5.53) is simply

$$d_{\mathrm{e}} = \left| \frac{\mathrm{d}v_x}{\mathrm{d}x} \right| = \frac{\mathrm{d}v_x}{\mathrm{d}x}\,. \tag{5.70}$$

The absolute value bars can be dropped because $\mathrm{d}v_x/\mathrm{d}x > 0$ for the ice shelf ramp. With this result, the depth-integrated viscosity (5.54) reads

$$\bar{\eta} = \frac{BH}{2}\left(\frac{\mathrm{d}v_x}{\mathrm{d}x}\right)^{-(1-1/n)} , \tag{5.71}$$

where the constant $B = A^{-1/n}$ (associated rate factor) has been introduced.

The horizontal velocity v_x is governed by Eq. $(5.55)_1$, whereas $(5.55)_2$ vanishes identically due to the plane strain approximation. Equation $(5.55)_1$ simplifies to

$$4\frac{\mathrm{d}}{\mathrm{d}x}\left(\bar{\eta}\frac{\mathrm{d}v_x}{\mathrm{d}x}\right) = \rho g H \frac{\mathrm{d}h}{\mathrm{d}x} , \tag{5.72}$$

and by inserting Eqs. $(5.69)_1$ and (5.71), we obtain

$$\begin{aligned} 2B\frac{\mathrm{d}}{\mathrm{d}x}\left[H\left(\frac{\mathrm{d}v_x}{\mathrm{d}x}\right)^{1/n}\right] &= \frac{\rho}{\rho_{\mathrm{sw}}}(\rho_{\mathrm{sw}}-\rho)gH\frac{\mathrm{d}H}{\mathrm{d}x} \\ &= \frac{\rho}{\rho_{\mathrm{sw}}}(\rho_{\mathrm{sw}}-\rho)g\frac{\mathrm{d}}{\mathrm{d}x}\left(\frac{H^2}{2}\right) . \end{aligned} \tag{5.73}$$

The first integral of this equation is

$$2BH\left(\frac{\mathrm{d}v_x}{\mathrm{d}x}\right)^{1/n} = \frac{\rho}{\rho_{\mathrm{sw}}}(\rho_{\mathrm{sw}}-\rho)\frac{gH^2}{2} + C_1 . \tag{5.74}$$

The integration constant C_1 can be determined by using the boundary condition (5.64) at the calving front. With $n_x = 1$ and $n_y = 0$, it yields

$$4\bar{\eta}\left.\frac{\mathrm{d}v_x}{\mathrm{d}x}\right|_{\mathrm{cf}} = \frac{\rho}{\rho_{\mathrm{sw}}}(\rho_{\mathrm{sw}}-\rho)\frac{gH^2}{2} , \tag{5.75}$$

or with the depth-integrated viscosity (5.71),

$$2BH\left.\left(\frac{\mathrm{d}v_x}{\mathrm{d}x}\right)^{1/n}\right|_{\mathrm{cf}} = \frac{\rho}{\rho_{\mathrm{sw}}}(\rho_{\mathrm{sw}}-\rho)\frac{gH^2}{2} . \tag{5.76}$$

Comparison of Eq. (5.74), taken at the calving front, and the boundary condition (5.76) yields $C_1 = 0$.

We proceed by solving Eq. (5.74) for the velocity derivative and integrating the result from the grounding line $x = 0$ to an arbitrary position x,

$$\begin{aligned} &\frac{\mathrm{d}v_x}{\mathrm{d}x} = \left(\frac{\rho}{\rho_{\mathrm{sw}}}(\rho_{\mathrm{sw}}-\rho)\frac{gH}{4B}\right)^n \\ &\Rightarrow\ v_x(x) = v_{\mathrm{gl}} + \left(\frac{\varrho g}{4B}\right)^n \mathcal{H}_n(x) , \end{aligned} \tag{5.77}$$

with the abbreviations

$$\varrho = \frac{\rho}{\rho_{\mathrm{sw}}}(\rho_{\mathrm{sw}} - \rho)\,, \qquad \mathcal{H}_n(x) = \int_0^x H^n(\tilde{x})\,\mathrm{d}\tilde{x}\,. \tag{5.78}$$

For the ice ramp defined by Eq. (5.68), the thickness integral reads

$$\begin{aligned} \mathcal{H}_n(x) &= \left[-\frac{L}{(n+1)(H_{\mathrm{gl}} - H_{\mathrm{cf}})} \left(H_{\mathrm{gl}} - \frac{H_{\mathrm{gl}} - H_{\mathrm{cf}}}{L}\,\tilde{x} \right)^{n+1} \right]_0^x \\ &= \frac{L}{(n+1)(H_{\mathrm{gl}} - H_{\mathrm{cf}})} \\ &\quad \times H_{\mathrm{gl}}^{n+1} \left[1 - \left(1 - \frac{H_{\mathrm{gl}} - H_{\mathrm{cf}}}{L H_{\mathrm{gl}}}\,x \right)^{n+1} \right]. \end{aligned} \tag{5.79}$$

Equations (5.77) and (5.79) describe the horizontal velocity for the ice shelf ramp. For the stress exponent $n = 3$, it is a quartic function of the position x.

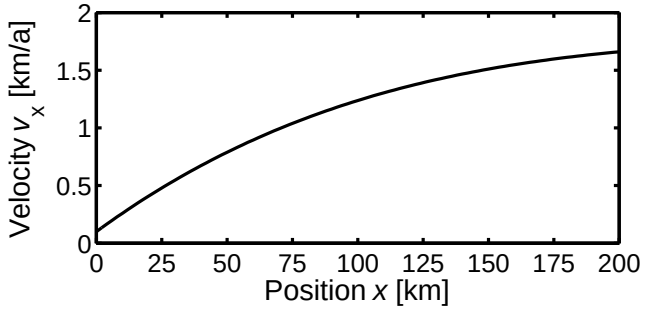

Figure 5.5: Ice shelf ramp: Horizontal velocity v_x according to Eqs. (5.77) and (5.79), for $H_{\mathrm{gl}} = 400\,\mathrm{m}$, $H_{\mathrm{cf}} = 200\,\mathrm{m}$, $L = 200\,\mathrm{km}$, $v_{\mathrm{gl}} = 100\,\mathrm{m\,a^{-1}}$, $n = 3$, $A = 4.9 \times 10^{-25}\,\mathrm{s^{-1}\,Pa^{-3}}$ (value for $T' = -10°\mathrm{C}$), $\rho = 910\,\mathrm{kg\,m^{-3}}$, $\rho_{\mathrm{sw}} = 1028\,\mathrm{kg\,m^{-3}}$ and $g = 9.81\,\mathrm{m\,s^{-2}}$.

An example is shown in Fig. 5.5. Even though the set-up is that of a rather small and thin ice shelf (see figure caption), a maximum velocity as large as $1.66\,\mathrm{km\,a^{-1}}$ is reached at the calving front. This is due to the fact that our two-dimensional, plane strain ice shelf does not feel any lateral drag, which would reduce the flow speed in a natural ice shelf.

The vertical velocity can be computed by inserting the horizontal velocity (5.77) into the vertically integrated mass balance (5.65),

$$\begin{aligned} v_z &= v_z|_{z=0} - \frac{\mathrm{d}v_x}{\mathrm{d}x}\,z = v_z|_{z=0} - \left(\frac{\varrho g}{4B} \right)^n \frac{\mathrm{d}\mathcal{H}_n}{\mathrm{d}x}\,z \\ &= v_z|_{z=0} - \left(\frac{\varrho g H}{4B} \right)^n z\,. \end{aligned} \tag{5.80}$$

The value of the integration constant $v_z|_{z=0}$ (vertical velocity at sea level) can be determined only if the distributions of the surface mass balance a_s and the basal mass balance a_b are known. For simplicity we assume instead that the ratio of a_s and a_b is such that $v_z|_{z=0} = 0$. The result for the vertical velocity is then

$$v_z(x,z) = -\left(\frac{\varrho g H(x)}{4B}\right)^n z\,. \tag{5.81}$$

It is illustrated in Fig. 5.6 for the center of the ice shelf described in the legend of Fig. 5.5.

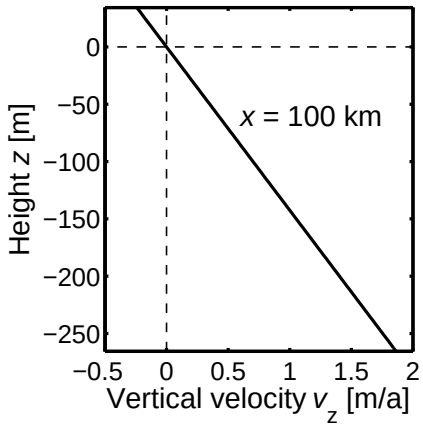

Figure 5.6: Ice shelf ramp: Profile of the vertical velocity v_z in the center of the ice shelf ($x = L/2 = 100\,\mathrm{km}$) according to Eq. (5.81). Parameters as in Fig. 5.5.

The total mass balance at the upper and lower interface, $a_\mathrm{s} - a_\mathrm{b}$ (where supply is positive and loss negative), can be obtained from the ice thickness equation (5.66) by employing the steady-state assumption,

$$a_\mathrm{s} - a_\mathrm{b} = \frac{\mathrm{d}(H v_x)}{\mathrm{d}x}\,. \tag{5.82}$$

With the horizontal velocity (5.77), this yields

$$\begin{aligned} a_\mathrm{s} - a_\mathrm{b} &= H\frac{\mathrm{d}v_x}{\mathrm{d}x} + v_x\frac{\mathrm{d}H}{\mathrm{d}x} \\ &= H\left(\frac{\varrho g}{4B}\right)^n \frac{\mathrm{d}\mathcal{H}_n}{\mathrm{d}x} + \frac{\mathrm{d}H}{\mathrm{d}x}\left[v_\mathrm{gl} + \left(\frac{\varrho g}{4B}\right)^n \mathcal{H}_n\right] \\ &= H\left(\frac{\varrho g H}{4B}\right)^n + \frac{\mathrm{d}H}{\mathrm{d}x}\left[v_\mathrm{gl} + \left(\frac{\varrho g}{4B}\right)^n \mathcal{H}_n\right], \end{aligned} \tag{5.83}$$

which is depicted in Fig. 5.7 for the set-up of Fig. 5.5. In this example, the total mass balance is positive in slightly more than the inner half of the ice shelf (until $x \approx 128\,\mathrm{km}$) and negative in the outer part towards the calving front.

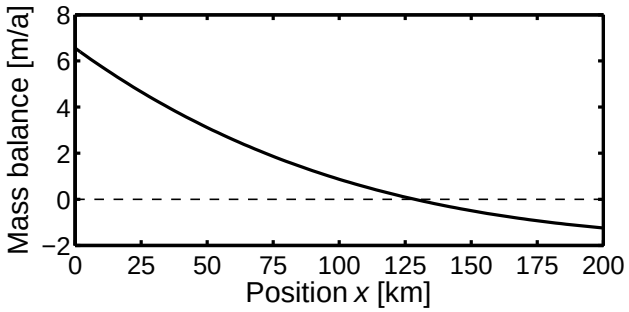

Figure 5.7: Ice shelf ramp: Total mass balance at the upper and lower interface, $a_\mathrm{s} - a_\mathrm{b}$, according to Eq. (5.83). Parameters as in Fig. 5.5.

It is also instructive to discuss the degenerate case of an *ice shelf with constant thickness*, which can be realised by setting $H_\mathrm{gl} = H_\mathrm{cf} = H = \text{const}$. One may intuitively conclude that for this situation there is no ice flow, because the forcing term $\rho g H(\mathrm{d}h/\mathrm{d}x)$ on the right-hand side of the momentum equation (5.72) vanishes. However, this is not the case. For a constant thickness H, the thickness integral $\mathcal{H}_n(x)$ defined in Eq. $(5.78)_2$ is given by $\mathcal{H}_n(x) = H^n x$. Inserting this into the velocity equation (5.77) yields the linearly increasing velocity distribution

$$v_x(x) = v_\mathrm{gl} + \left(\frac{\varrho g H}{4B}\right)^n x\,, \tag{5.84}$$

which corresponds to the constant horizontal dilatation rate

$$D_{xx} = \frac{\mathrm{d}v_x}{\mathrm{d}x} = \left(\frac{\varrho g H}{4B}\right)^n . \tag{5.85}$$

The vertical compression rate [due to Eq. (5.81)] is then

$$D_{zz} = \frac{\mathrm{d}v_z}{\mathrm{d}z} = -\left(\frac{\varrho g H}{4B}\right)^n . \tag{5.86}$$

Of course, the two strain rates add up to zero, which is a requirement of incompressibility.

The reason for this counterintuitive behaviour of horizontal stretching and vertical compression of the ice, despite constant ice thickness, is the existence of the calving front as a boundary of the system. Beyond the calving front, there is no more ice which could hinder the extension of the ice shelf, and the sea-water pressure at the calving front is not strong enough to buttress the ice shelf completely.

6 Dynamics of Glacier Flow

6.1 Glaciers Versus Ice Sheets

As mentioned in the introduction (Chapter 1), the size of land ice masses spans several orders of magnitude, from large ice sheets of a few thousand kilometres in diameter down to small glaciers of a few hundreds of metres in length. Consequently, the scaling given for ice sheets in Chapter 4 [Eqs. (4.5) and (4.102)] is not valid for smaller ice caps and glaciers, and needs to be modified. However, the Froude number (4.7) and Coriolis-force-to-pressure-gradient ratio (4.10) are always extremely small compared to unity, and therefore the Stokes flow problem formulated in Sect. 4.1 is applicable to land ice masses of all shapes and sizes. On the other hand, the applicability of the approximations defined in Sects. 4.2 to 4.4 is limited by the size of the ice masses. While the hydrostatic approximation and the first order approximation still provide reasonable accuracy for most problems of glacier flow, the shallow ice approximation is valid for the large-scale description of ice sheets and large ice caps only.

In addition to these dynamical issues, the thermal regime of ice sheets and glaciers shows important differences. Most ice in ice sheets is *cold ice*, i.e., its temperature is below the local pressure melting point. *Temperate ice*, with a temperature at the pressure melting point, exists only at the base or in thin, near-basal layers. While this behaviour is shared by glaciers at high latitudes, in glaciers at lower latitudes temperate ice occurs alongside cold ice, and many of them consist entirely of temperate ice except for a thin cold surface layer in winter. Glaciers that consist entirely of cold ice are called *cold glaciers*, glaciers that consist entirely of temperate ice are called *temperate glaciers*, and glaciers in which significant amounts of both temperate and cold ice occur are called *polythermal glaciers*. We will not expand further on glacier thermodynamics here and refer the interested reader to Greve and Blatter (2009, Sect. 9.3).

In the following, we will only consider the "parallel sided slab" as a simple, analytically solvable problem. More details on glacier-specific topics like two-dimensional flowline models, two-dimensional cross-section models etc., are discussed by Greve and Blatter (2009, Chapter 7).

6.2 Parallel Sided Slab

Depending on the exact geometry, the central part of a small valley glacier can sometimes be roughly approximated as a parallel sided slab on an inclined bed, similar to the gravity-driven thin-film flow discussed in Sect. 2.4.2. This is sketched in Fig. 6.1.

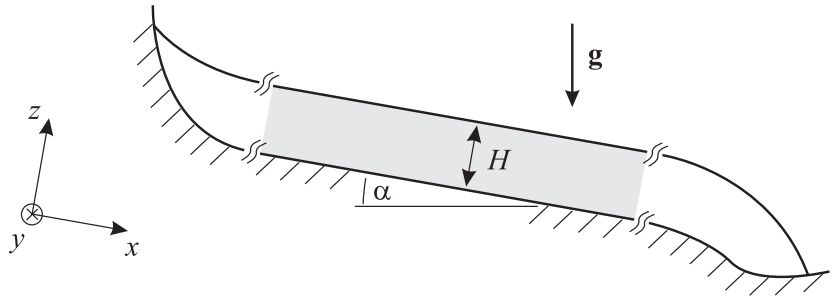

Figure 6.1: Approximation of the central part of a valley glacier (grey-shaded) as a parallel sided slab.

In order to formulate the ice-flow problem for the parallel sided slab as full Stokes flow, let us make the following assumptions:

- Plane strain approximation: purely two-dimensional flow in the vertical x-z plane, no dependencies on the transverse coordinate y.
- Constant thickness H and inclination angle α.
- Uniformity in the downslope (x) direction: $\partial(\cdot)/\partial x = 0$ for all field quantities.
- Steady-state conditions: $\partial(\cdot)/\partial t = 0$ for all field quantities.
- Flat, rigid bed: $b(x,t) = 0$ (in the inclined coordinate system). The free surface is therefore given by $h(x,t) = H$.
- No surface accumulation ($a_\mathrm{s}^\perp = 0$).
- No basal melting ($a_\mathrm{b}^\perp = 0$), no basal sliding ($C_\mathrm{b} = 0$).
- Glen's flow law (3.16) with stress exponent $n = 3$.
- Constant rate factor: $A(T') = A = \text{const}$.
- Constant heat conductivity: $\kappa(T) = \kappa = \text{const}$.

Thus, the mass balance (4.1) simplifies to

$$\frac{\partial v_z}{\partial z} = 0\,. \tag{6.1}$$

With the above assumptions, the kinematic conditions (4.21) at the free surface and (4.31) at the glacier bed imply

$$v_z|_{z=H} = 0\,, \quad v_z|_{z=0} = 0\,, \tag{6.2}$$

and so the solution of Eq. (6.1) is simply

$$v_z = 0\,. \tag{6.3}$$

Consequently, the velocity field is entirely described by the profile of the downslope velocity, $v_x(z)$.

With the evident decomposition $\mathbf{g} = g\sin\alpha\,\mathbf{e}_x - g\cos\alpha\,\mathbf{e}_z$, the x-component of the Stokes equation (4.11) reads

$$\begin{aligned} &-\frac{\partial p}{\partial x} + \eta\left(\frac{\partial^2 v_x}{\partial x^2} + \frac{\partial^2 v_x}{\partial y^2} + \frac{\partial^2 v_x}{\partial z^2}\right) \\ &+ 2\frac{\partial v_x}{\partial x}\frac{\partial \eta}{\partial x} + \left(\frac{\partial v_x}{\partial y} + \frac{\partial v_y}{\partial x}\right)\frac{\partial \eta}{\partial y} + \left(\frac{\partial v_x}{\partial z} + \frac{\partial v_z}{\partial x}\right)\frac{\partial \eta}{\partial z} \\ &+ \rho g\sin\alpha = 0\,, \end{aligned} \tag{6.4}$$

which simplifies to

$$\begin{aligned} &\eta\frac{\partial^2 v_x}{\partial z^2} + \frac{\partial v_x}{\partial z}\frac{\partial \eta}{\partial z} + \rho g\sin\alpha = 0 \\ &\Rightarrow\ \frac{\partial}{\partial z}\left(\eta\frac{\partial v_x}{\partial z}\right) + \rho g\sin\alpha = 0\,. \end{aligned} \tag{6.5}$$

The first integral of this equation is

$$\eta\frac{\partial v_x}{\partial z} = C_1 - \rho g z\sin\alpha\,, \tag{6.6}$$

where C_1 is an integration constant. Due to Glen's flow law in the form (3.21), the left-hand side is equal to the shear stress t_{xz},

$$t_{xz} = \eta\frac{\partial v_x}{\partial z} = C_1 - \rho g z\sin\alpha\,, \tag{6.7}$$

which vanishes at the free surface ($z = H$) due to the stress-free boundary condition (4.23). Hence, the integration constant can be determined,

$$t_{xz}|_{z=H} = C_1 - \rho g H\sin\alpha = 0 \quad\Rightarrow\quad C_1 = \rho g H\sin\alpha\,, \tag{6.8}$$

and we obtain the linear shear stress profile

$$t_{xz} = \eta\frac{\partial v_x}{\partial z} = \rho g(H - z)\sin\alpha\,. \tag{6.9}$$

In order to carry out the second integration, we insert the explicit form of the viscosity which results from Eq. (3.22),

$$\eta = \frac{1}{2}B\,d_{\mathrm{e}}^{-(1-1/n)}\,, \quad \text{where } B = A^{-1/n} \text{ and } d_{\mathrm{e}} = \frac{1}{2}\frac{\partial v_x}{\partial z}\,. \tag{6.10}$$

This yields from Eq. (6.9)

$$\begin{aligned}
&\frac{1}{2}A^{-1/n}\left(\frac{1}{2}\frac{\partial v_x}{\partial z}\right)^{-(1-1/n)}\frac{\partial v_x}{\partial z} = \rho g(H-z)\sin\alpha \\
&\Rightarrow\ A^{-1/n}\left(\frac{1}{2}\frac{\partial v_x}{\partial z}\right)^{1/n} = \rho g(H-z)\sin\alpha \\
&\Rightarrow\ \frac{\partial v_x}{\partial z} = 2A(\rho g\sin\alpha)^n(H-z)^n \\
&\Rightarrow\ v_x = -\frac{2A(\rho g\sin\alpha)^n}{n+1}(H-z)^{n+1} + C_2\,. \qquad (6.11)
\end{aligned}$$

The integration constant C_2 results from the no-slip condition $v_x|_{z=0} = 0$ (no basal sliding),

$$\begin{aligned}
&v_x|_{z=0} = -\frac{2A(\rho g\sin\alpha)^n}{n+1}H^{n+1} + C_2 = 0 \\
&\Rightarrow\ C_2 = \frac{2A(\rho g\sin\alpha)^n}{n+1}H^{n+1}\,. \qquad (6.12)
\end{aligned}$$

Therefore, we obtain the velocity profile

$$v_x = \frac{2A(\rho g\sin\alpha)^n}{n+1}\left[H^{n+1} - (H-z)^{n+1}\right]\,, \qquad (6.13)$$

which is a quartic function of z for the stress exponent $n = 3$.

Analogous to Eq. (6.4), the z-component of the Stokes equation (4.11) is

$$\begin{aligned}
&-\frac{\partial p}{\partial z} + \eta\left(\frac{\partial^2 v_z}{\partial x^2} + \frac{\partial^2 v_z}{\partial y^2} + \frac{\partial^2 v_z}{\partial z^2}\right) \\
&+ 2\frac{\partial v_z}{\partial z}\frac{\partial \eta}{\partial z} + \left(\frac{\partial v_x}{\partial z} + \frac{\partial v_z}{\partial x}\right)\frac{\partial \eta}{\partial x} + \left(\frac{\partial v_y}{\partial z} + \frac{\partial v_z}{\partial y}\right)\frac{\partial \eta}{\partial y} \\
&- \rho g\cos\alpha = 0\,, \qquad (6.14)
\end{aligned}$$

and simplifies, for the parallel-sided-slab problem, to

$$\frac{\partial p}{\partial z} = -\rho g\cos\alpha\,. \qquad (6.15)$$

The integral of this equation is

$$p = C_3 - \rho g z\cos\alpha\,. \qquad (6.16)$$

Owing to the stress-free boundary condition at the free surface (4.23), the pressure vanishes there, which yields the integration constant C_3,

$$p|_{z=H} = C_3 - \rho g H\cos\alpha = 0 \quad \Rightarrow \quad C_3 = \rho g H\cos\alpha\,. \qquad (6.17)$$

Thus, we obtain the hydrostatic pressure profile

$$p = \rho g (H - z) \cos\alpha \,. \tag{6.18}$$

It is interesting to note that the results for the pressure, Eq. (6.18), and the shear stress, Eq. (6.9), are identical to those for the thin-film flow of an incompressible Newtonian fluid (see Sect. 2.4.2). The nonlinearity of Glen's flow law affects only the velocity profile, which is quartic here [Eq. (6.13)], but parabolic for the Newtonian fluid [Eq. (2.108)].

It is also possible to compute the temperature profile analytically. The temperature equation (4.14) reads

$$\begin{aligned} &\rho c \left(\frac{\partial T}{\partial t} + v_x \frac{\partial T}{\partial x} + v_y \frac{\partial T}{\partial y} + v_z \frac{\partial T}{\partial z} \right) \\ &= \frac{\partial}{\partial x} \left(\kappa \frac{\partial T}{\partial x} \right) + \frac{\partial}{\partial y} \left(\kappa \frac{\partial T}{\partial y} \right) + \frac{\partial}{\partial z} \left(\kappa \frac{\partial T}{\partial z} \right) + 4\eta d_{\mathrm{e}}^2 \,, \end{aligned} \tag{6.19}$$

which simplifies to

$$\frac{\partial}{\partial z} \left(\kappa \frac{\partial T}{\partial z} \right) = -4\eta d_{\mathrm{e}}^2 \,. \tag{6.20}$$

By using Eq. (6.10), this can be rewritten as follows,

$$\begin{aligned} \frac{\partial}{\partial z} \left(\kappa \frac{\partial T}{\partial z} \right) &= -4 \times \frac{1}{2} A^{-1/n} \left(\frac{1}{2} \frac{\partial v_x}{\partial z} \right)^{-(1-1/n)} \times \left(\frac{1}{2} \frac{\partial v_x}{\partial z} \right)^2 \\ &= -(2A)^{-1/n} \left(\frac{\partial v_x}{\partial z} \right)^{1+1/n} . \end{aligned} \tag{6.21}$$

We substitute the term $\partial v_x / \partial z$ from (6.13) and obtain

$$\begin{aligned} \frac{\partial}{\partial z} \left(\kappa \frac{\partial T}{\partial z} \right) &= -(2A)^{-1/n} \left[2A (\rho g \sin\alpha)^n (H - z)^n \right]^{1+1/n} \\ &= -2A (\rho g \sin\alpha)^{n+1} (H - z)^{n+1} . \end{aligned} \tag{6.22}$$

The first integral of this equation is

$$\kappa \frac{\partial T}{\partial z} = \frac{2A (\rho g \sin\alpha)^{n+1}}{n+2} (H - z)^{n+2} + C_4 \,. \tag{6.23}$$

By assuming that the basal temperature does not reach the pressure melting point, the integration constant can be obtained from the basal boundary condition (4.38),

$$\begin{aligned} &-\kappa \left. \frac{\partial T}{\partial z} \right|_{z=0} = q_{\mathrm{geo}}^{\perp} \\ &\Rightarrow \; -\frac{2A (\rho g \sin\alpha)^{n+1}}{n+2} H^{n+2} - C_4 = q_{\mathrm{geo}}^{\perp} \\ &\Rightarrow \; C_4 = -q_{\mathrm{geo}}^{\perp} - \frac{2A (\rho g \sin\alpha)^{n+1}}{n+2} H^{n+2} \,, \end{aligned} \tag{6.24}$$

so that

$$\kappa\frac{\partial T}{\partial z} = -q_{\text{geo}}^{\perp} - \frac{2A(\rho g \sin\alpha)^{n+1}}{n+2}\left[H^{n+2} - (H-z)^{n+2}\right] . \tag{6.25}$$

Further integration yields

$$T = -\frac{q_{\text{geo}}^{\perp}}{\kappa}z - \frac{2A(\rho g \sin\alpha)^{n+1}}{\kappa(n+2)}\left[H^{n+2}z + \frac{(H-z)^{n+3}}{n+3}\right] + C_5 . \tag{6.26}$$

With the surface boundary condition (4.24), the integration constant can be computed,

$$\begin{aligned} & T|_{z=H} = T_{\text{s}} \\ \Rightarrow\ & -\frac{q_{\text{geo}}^{\perp}}{\kappa}H - \frac{2A(\rho g \sin\alpha)^{n+1}}{\kappa(n+2)}H^{n+3} + C_5 = T_{\text{s}} \\ \Rightarrow\ & C_5 = T_{\text{s}} + \frac{q_{\text{geo}}^{\perp}}{\kappa}H + \frac{2A(\rho g \sin\alpha)^{n+1}}{\kappa(n+2)}H^{n+3} . \end{aligned} \tag{6.27}$$

Thus, we obtain for the temperature profile the relation

$$\begin{aligned} T \;=\; & T_{\text{s}} + \frac{q_{\text{geo}}^{\perp}}{\kappa}(H-z) \\ & + \frac{2AH^{n+3}(\rho g \sin\alpha)^{n+1}}{\kappa(n+2)}\left[1 - \frac{z}{H} - \frac{1}{n+3}\left(\frac{H-z}{H}\right)^{n+3}\right] . \end{aligned} \tag{6.28}$$

The first line describes a linear profile due to heat conduction only, and the nonlinear modification in the second line is due to the dissipation term $4\eta d_{\text{e}}^2$ in the temperature equation (6.20).

For a glacier of 100 m thickness and 10° inclination, the results for the velocity profile, Eq. (6.13), and the temperature profile, Eq. (6.28), are depicted in Fig. 6.2. The simple-shear profile of the horizontal velocity with the largest shear rates ($\partial v_x/\partial z$) close to the base and smallest shear rates close to the surface is evident, and the surface velocity reaches a value of $18.6\,\text{m}\,\text{a}^{-1}$. The temperature increases from $-10°\text{C}$ at the surface to $-4.71°\text{C}$ at the base, and the profile is slightly curved due to viscous dissipation, which is also largest near the base. The importance of dissipation is further highlighted by comparison with the linear profile resulting from heat conduction only, for which the basal temperature reaches a mere $-7.62°\text{C}$.

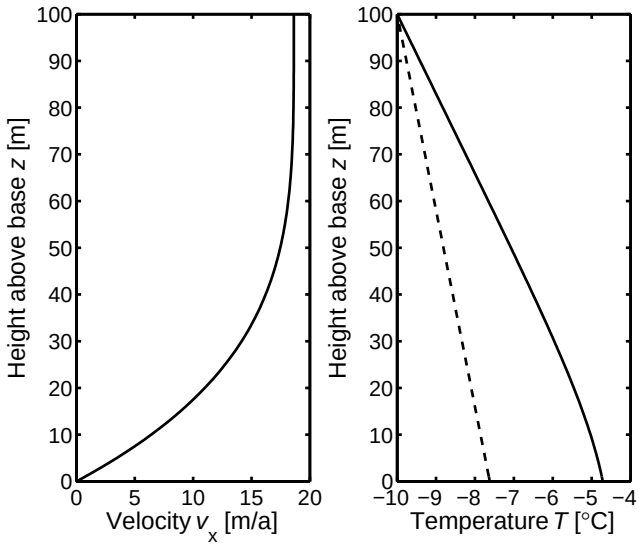

Figure 6.2: Parallel sided slab: Velocity and temperature profiles according to Eqs. (6.13) and (6.28), for $H = 100\,\mathrm{m}$, $\alpha = 10°$, $T_\mathrm{s} = -10°\mathrm{C}$, $q_\mathrm{geo}^\perp = 50\,\mathrm{mW\,m^{-2}}$, $n = 3$, $A = 10^{-16}\,\mathrm{a^{-1}\,Pa^{-3}}$, $\rho = 910\,\mathrm{kg\,m^{-3}}$, $\kappa = 2.1\,\mathrm{W\,m^{-1}\,K^{-1}}$ and $g = 9.81\,\mathrm{m\,s^{-2}}$ (solid lines). The dashed line in the temperature panel shows the linear profile that results from heat conduction only (dissipation neglected).

7 Glacial Isostasy

7.1 Structure of the Earth

From seismological studies it can be inferred that the interior of the Earth reveals a layered structure, the different layers being mutually separated by changes in the chemical composition and/or phase transitions (Fig. 7.1, left). The uppermost layer, the crust, has a mean thickness of 20 km (which, however, varies significantly from place to place; it is thickest below mountains and thinnest below oceans), a mineral composition and a mean density of 2900 $\mathrm{kg\,m^{-3}}$. The crust is underlain by a mineral mantle of 2900 km in thickness and a density varying from 3300 $\mathrm{kg\,m^{-3}}$ at the top to 5700 $\mathrm{kg\,m^{-3}}$ at the bottom. Below, the 3500 km thick, metallic core is found, which can be subdivided into an outer, liquid, and an inner, solid part. The density of the core increases from approximately 9400 $\mathrm{kg\,m^{-3}}$ at the top to 13500 $\mathrm{kg\,m^{-3}}$ at the center of the Earth.

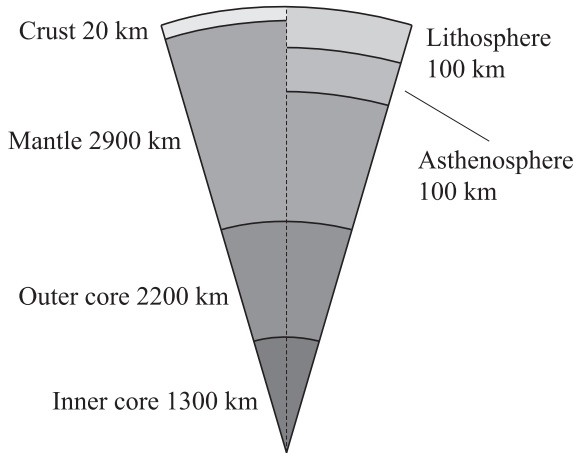

Figure 7.1: Layered structure of the Earth's interior. Left: Classification by chemical composition. Right: Classification by rheological properties.

However, from the point of view of rheological properties, this classification is not satisfactory for the upper regions. The crust and the uppermost part of the mantle behave mainly as an elastic solid; however, with increasing depth, viscous fluid properties become more dominant over geological periods due to the increasing temperature of the mantle material. Further down, the viscosity increases again due to the changing composition. Because of this, the crust and the uppermost part of the mantle comprise the $\sim$ 100 km

thick elastic lithosphere, underlain by a further $\sim$ 100 km thick layer of low viscosity, known as the asthenosphere (Fig. 7.1, right). By contrast, the remaining part of the mantle down to the outer core is characterised by a less pronounced, but nonetheless relevant, fluid behaviour.

Within this rheological classification, the well-known process of plate tectonics can be interpreted as the motion of solid lithosphere plates on the viscous asthenosphere layer, driven by internal convection currents. As we will see below, for the dynamics of glacial isostasy the rheological classification is also favourable and usually applied.

7.2 Simple Isostasy Models

In this section, simple models for the problem of glacial isostasy, based on a plane, two-layer, lithosphere/asthenosphere system, will be presented. Hereby, the lithosphere layer is treated in two different ways, either as a locally deforming plate (local lithosphere, "LL"), or as a thin elastic plate (elastic lithosphere, "EL"). For the asthenosphere, the relaxing asthenosphere ("RA") approach is employed where the viscous effects are parameterised by a constant time lag. The possible combinations lead to two different models, referred to as LLRA and ELRA.

7.2.1 LLRA Model

The most simple isostasy model combines the local lithosphere with the relaxing asthenosphere. The idea of the local lithosphere is that an ice load $q(x, y) = \rho g H(x, y)$, at a given position $(x,\, y)$, causes a steady-state displacement of the lithosphere, w_{ss}, in the vertical, z, direction at the position $(x,\, y)$ only (Fig. 7.2). Note that, in this chapter, we take z as positive *downward*, and identify the undisturbed position of the lithosphere base (in the absence of any ice loading) with $z = 0$. The value of w_{ss} (taken positive downward as well) is determined by the balance between the ice load and the buoyancy force which the lithosphere experiences in the underlying viscous asthenosphere,

$$\rho_{\mathrm{a}} g w_{\mathrm{ss}} = \rho g H \quad \Rightarrow \quad w_{\mathrm{ss}} = \frac{\rho}{\rho_{\mathrm{a}}} H \,, \tag{7.1}$$

where $\rho_{\mathrm{a}} = 3300\,\mathrm{kg\,m^{-3}}$ is the density of the asthenosphere.

Due to the viscous properties of the asthenosphere, for the case of time-dependent ice loads $q(x, y, t)$, the lithosphere cannot assume the steady-state displacement w_{ss} immediately. Instead, the response will have a time lag, and the relaxing asthenosphere parameterises this lag by a single time constant, τ_{a}, of the order of 1000s of years (a widely used value is $\tau_{\mathrm{a}} = 3\,\mathrm{ka}$). The evolution of the actual displacement, w, with time, t, is then determined by

$$\frac{\partial w}{\partial t} = -\frac{1}{\tau_{\mathrm{a}}}(w - w_{\mathrm{ss}}) \,, \tag{7.2}$$

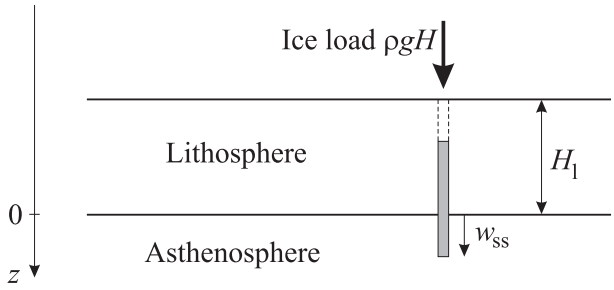

Figure 7.2: Local lithosphere: A localised ice load $q = \rho g H$ causes a vertical steady-state displacement of the lithosphere, w_{ss}, at the position of the load only. H_{l} denotes the lithosphere thickness.

which relates the vertical velocity of the lithosphere, $\partial w/\partial t$, linearly to the deviation of the displacement from the steady state, $w - w_{\mathrm{ss}}$. Provided the ice thickness H, and therefore the steady-state displacement w_{ss}, do not change with time, the solution of (7.2) is

$$w(x, y, t) = w_{\mathrm{ss}}(x, y) + [w_0(x, y) - w_{\mathrm{ss}}(x, y)]\, e^{-t/\tau_{\mathrm{a}}}\,, \tag{7.3}$$

so that any non-steady-state initial displacement w_0 relaxes exponentially into its steady-state value with the time constant τ_{a} (Fig. 7.3).

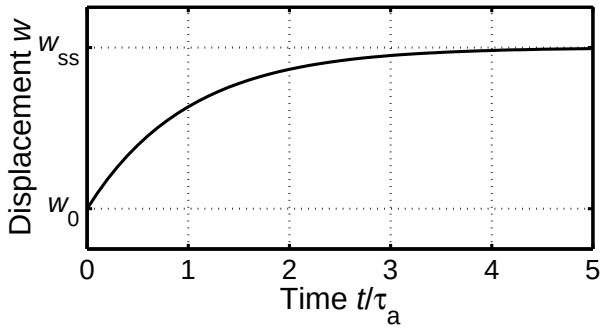

Figure 7.3: Vertical displacement of the lithosphere as a function of time for the relaxing asthenosphere, with an initial displacement w_0 and a steady-state displacement w_{ss} (assumed to be constant over time). Time is shown in units of the time lag τ_{a}.

The great strength of the LLRA model is its simplicity (only a single parameter, the time-lag constant τ_{a}, is needed) and easy implementation in numerical models. It feeds back to the ice sheet equations of Chapter 4 as follows. Let $z_{\mathrm{l},0}(x, y)$ be the reference position of the lithosphere surface in the coordinate system of Chapter 4 (vertical coordinate positive upward, see Fig. 4.1) for $w = 0$ (no displacement). The actual position of the lithosphere surface is then

$$z_{\mathrm{l}}(x, y, t) = z_{\mathrm{l},0}(x, y) - w(x, y, t)\,, \tag{7.4}$$

where the displacement w is governed by Eq. (7.3). Since the ice base b and the lithosphere surface z_l fall together under a grounded ice sheet, the time derivative reads

$$\frac{\partial z_\mathrm{l}}{\partial t} = \frac{\partial b}{\partial t} = -\frac{\partial w}{\partial t} \,. \tag{7.5}$$

This result enters the ice surface equation, for instance in its shallow ice form (4.100).

7.2.2 ELRA Model

The local lithosphere assumption, that the response to an ice load is a purely local displacement of the lithosphere, is certainly unrealistic. Instead, it is clear that the elasticity of the lithosphere layer must result in a non-local response, so that positions at some distance from an imposed ice load still suffer a displacement (Fig. 7.4).

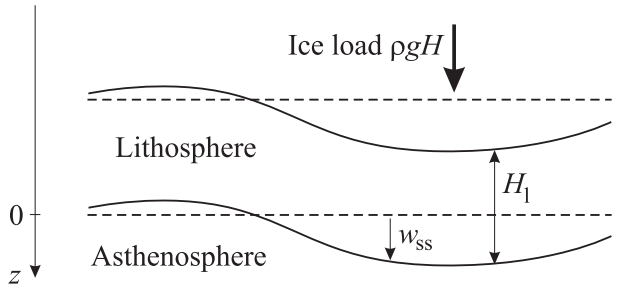

Figure 7.4: Elastic lithosphere: A localised ice load $q = \rho g H$ causes a horizontally distributed (non-local) vertical steady-state displacement of the lithosphere, w_ss. H_l denotes the lithosphere thickness.

A rather easy way to describe this behaviour more adequately is the thin elastic plate, governed by the biharmonic equation

$$K_\mathrm{l}\,\Delta^2 w_\mathrm{ss} + \rho_\mathrm{a} g w_\mathrm{ss} = \rho g H \,. \tag{7.6}$$

The parameter K_l is the flexural stiffness of the lithosphere,

$$K_\mathrm{l} = \frac{E_\mathrm{l} H_\mathrm{l}^3}{12(1-\nu_\mathrm{l}^2)} = \frac{\mu_\mathrm{l} H_\mathrm{l}^3}{6(1-\nu_\mathrm{l})} \,, \tag{7.7}$$

where H_l is the thickness, E_l Young's modulus, ν_l Poisson's ratio and μ_l the shear modulus of the lithosphere (indicated by the subscript "l").

Compared to the local lithosphere equation (7.1), the thin plate equation (7.6) contains an additional term of fourth order in the spatial derivative of the displacement which represents the flexural rigidity. Note that this term depends, apart from the elastic coefficients, on the lithosphere thickness H_l, whereas the simpler equation (7.1) is independent of H_l.

The Green's function of (7.6) is known and can be given analytically. Assume that the ice load is localised according to

$$q(x, y) = \rho g H(x, y) = F_0 \, \delta(x - \check{x}) \, \delta(y - \check{y}) \,, \tag{7.8}$$

which describes a single force F_0 imposed on the lithosphere surface at the position $(\check{x}, \check{y})$ [$\delta(\cdot)$ denotes Dirac's δ function], then the solution of (7.6) is

$$w_{\mathrm{ss}}(r) = -\frac{F_0 L_{\mathrm{r}}^2}{2\pi K_{\mathrm{l}}} \operatorname{kei}\left(\frac{r}{L_{\mathrm{r}}}\right) , \tag{7.9}$$

with

$$r = \sqrt{(x - \check{x})^2 + (y - \check{y})^2}, \quad L_{\mathrm{r}} = \left(\frac{K_{\mathrm{l}}}{\rho_{\mathrm{a}} g}\right)^{1/4} \tag{7.10}$$

(Brotchie and Silvester 1969). Here, $\operatorname{kei}(\cdot)$ is a Kelvin function of zero order, which can be derived from the general Bessel function, and whose values are tabulated in mathematical handbooks [e.g., Abramowitz and Stegun (1970)]. It is plotted in Fig. 7.5. Evidently, the radius of relative stiffness, L_{r}, determines the non-locality of the lithosphere displacement. The Kelvin function takes the value zero at approximately $r = 4L_{\mathrm{r}}$, followed by a slight forebulge (upward displacement) further away from the load.

The Green's function G of the thin plate equation (7.6) is given by Eq. (7.9) with the normalised force $F_0 = 1$,

$$G(r) = G(x, \check{x}, y, \check{y}) = -\frac{L_{\mathrm{r}}^2}{2\pi K_{\mathrm{l}}} \operatorname{kei}\left(\frac{r}{L_{\mathrm{r}}}\right) . \tag{7.11}$$

Since the differential equation (7.6) is linear, the Green's function can be used to construct its solution for a general distribution of the ice load $q(x, y) = \rho g H(x, y)$ by superposition,

$$w_{\mathrm{ss}}(x, y) = \int_{A_{\mathrm{ice}}} \rho g H(\check{x}, \check{y}) \, G(x, \check{x}, y, \check{y}) \, \mathrm{d}\check{x} \, \mathrm{d}\check{y} \,, \tag{7.12}$$

where A_{ice} denotes the ice-covered area. Note that the Green's function method is not restricted to the thin plate equation; however, it can be used to solve linear, inhomogeneous differential equations in general [see e.g. Bronshtein et al. (2004)].

The asthenosphere component in the ELRA model is the same as in the LLRA model described above. So once the steady-state displacement w_{ss} is computed by solving the thin plate equation (7.6), the actual displacement w follows from the relaxing asthenosphere evolution equation (7.2) as before. Also, the feedback to the ice sheet equations of Chapter 4 is as described by Eqs. (7.4) and (7.5).

For terrestrial conditions, a typical value for the radius of relative stiffness L_{r} is $\sim$ 100 km. It is much smaller than the typical horizontal extent $[L] = 1000$ km of a large ice sheet like Antarctica or Greenland [see Eq. (4.5)], and consequently the effect of a non-local lithosphere displacement is not too pronounced. For that reason, the simpler LLRA model still provides reasonable results. The differences between the two models will be

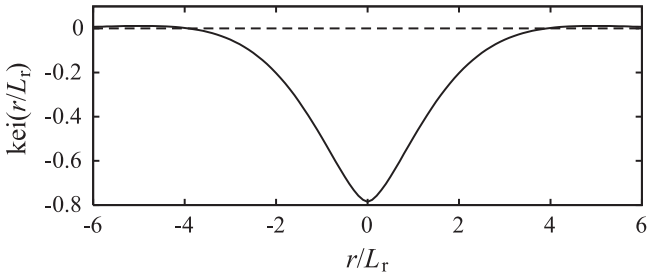

Figure 7.5: Normalised displacement of the elastic lithosphere under a point load. r/L_r is the normalised distance from the load, kei$(\cdot)$ a zero-order Kelvin function.

most significant in regions with large ice thickness gradients, which occur, in particular, close to the ice margins. By contrast, the extent of ice caps like Vatnajökull or Austfonna is similar to L_r, so that the non-locality of the elastic lithosphere approach is essential and must be accounted for. Glaciers are typically much smaller compared to L_r, which leads to an extreme spreading of the isostatic displacement and renders it negligible. Thus isostasy need not be considered for glaciers.

A On Vectors and Tensors

A.1 Definition of a Vector, Basic Properties

In mathematics, a *vector* is defined as an element of a vector space, and a vector space is a commutative (Abelian) group with a scalar multiplication. This is an abstract definition which has many possible realisations (numbers, functions, geometric objects and so on). For our purposes, it is sufficient to consider one of them, namely the geometric object of an *arrow* in the three-dimensional, Euclidian, physical space $\mathcal{E}$. Therefore, in our sense a vector $\mathbf{a} \in \mathcal{E}$ is an arrow which is characterised by a length and a direction. Physical quantities which can be described by such vectors are, for instance, velocity, acceleration, momentum and force. By contrast, *scalars* are simple numbers and characterise physical quantities without a direction, like mass, density, temperature etc.

We will usually denote vectors by bold-face symbols like $\mathbf{a}$, $\mathbf{b}$, $\mathbf{c}$, etc. The sum

$$\mathbf{s} = \mathbf{a} + \mathbf{b} \tag{A.1}$$

of two vectors is obtained by the parallelogram construction, and the scalar multiplication

$$\mathbf{p} = \lambda\mathbf{a}, \quad \lambda \in I\!R \tag{A.2}$$

($I\!R$ denotes the set of real numbers) is a vector parallel to $\mathbf{a}$ with length $\lambda|\mathbf{a}|$, where $|\mathbf{a}|$ is the length (absolute value, norm) of $\mathbf{a}$ (Fig. A.1).

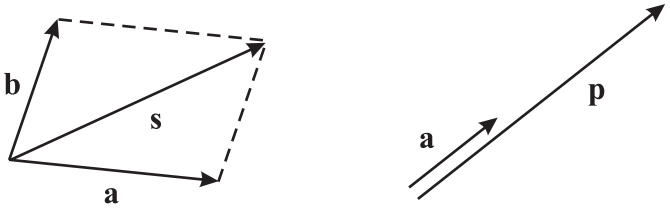

Figure A.1: Sum $\mathbf{s} = \mathbf{a} + \mathbf{b}$ and scalar multiplication $\mathbf{p} = \lambda\mathbf{a}$ of vectors.

The direction of a vector can be characterised by the unit vector (length equal to one) $\mathbf{e}_a = \mathbf{a}/|\mathbf{a}|$. Further, the dot product (inner product)

$$\delta = \mathbf{a} \cdot \mathbf{b} \tag{A.3}$$

of two vectors is equal to the scalar given by $|\mathbf{a}|\,|\mathbf{b}|\cos\varphi$ (where φ is the angle between the two vectors), and the cross product (vector product)

$$\mathbf{c} = \mathbf{a} \times \mathbf{b} \tag{A.4}$$

is equal to the vector with length $|\mathbf{a}|\,|\mathbf{b}|\sin\varphi$ and direction perpendicular to the plane spanned by $\mathbf{a}$ and $\mathbf{b}$, such that $\mathbf{a}$, $\mathbf{b}$ and $\mathbf{c}$ form a right-handed system (Fig. A.2). Note that

$$|\mathbf{a}| = \sqrt{\mathbf{a}\cdot\mathbf{a}}\,, \tag{A.5}$$

$$\mathbf{a}\cdot\mathbf{b} = 0 \quad \Leftrightarrow \quad \mathbf{a} \perp \mathbf{b} \;\text{ or }\; \mathbf{a} = \mathbf{0} \;\text{ or }\; \mathbf{b} = \mathbf{0}\,, \tag{A.6}$$

$$\mathbf{a} \times \mathbf{b} = -\mathbf{b} \times \mathbf{a} \tag{A.7}$$

and

$$\mathbf{a} \times \mathbf{a} = \mathbf{0}\,, \tag{A.8}$$

where $\mathbf{0}$ denotes the vector of length zero ("zero vector").

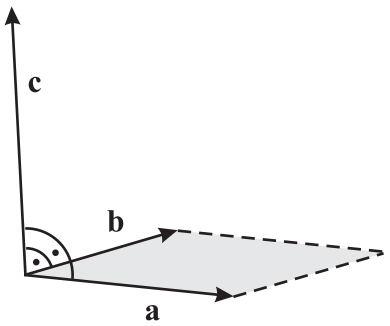

Figure A.2: Cross product $\mathbf{c} = \mathbf{a} \times \mathbf{b}$ of vectors.

Finally, the dyadic, outer or tensor product $\mathbf{a}\,\mathbf{b}$ (sometimes denoted as $\mathbf{a} \otimes \mathbf{b}$) is the linear transformation which, when applied to an arbitrary vector $\mathbf{x}$, obeys the relation

$$(\mathbf{a}\,\mathbf{b}) \cdot \mathbf{x} = \mathbf{a}(\mathbf{b}\cdot\mathbf{x})\,, \tag{A.9}$$

where $(\mathbf{b}\cdot\mathbf{x})$ means the dot product (A.3). In other words, the transformation $\mathbf{a}\,\mathbf{b}$ maps the vector $\mathbf{x}$ on the vector which has the direction of $\mathbf{a}$ and length $(\mathbf{b}\cdot\mathbf{x})\,|\mathbf{a}|$.

A.2 Representation of Vectors as Number Triples

Let $\{\mathbf{e}_i\}_{i=1,2,3}$ be a set of unit vectors which are perpendicular to each other and form a right-handed system. In other words,

$$\mathbf{e}_i \cdot \mathbf{e}_j = \delta_{ij}\,, \tag{A.10}$$

where δ_{ij} is the Kronecker symbol defined as

$$\delta_{ij} = \begin{cases} 1\,, & \text{for } i = j\,, \\ 0\,, & \text{for } i \neq j\,, \end{cases} \tag{A.11}$$

and

$$\mathbf{e}_i \times \mathbf{e}_j = \mathbf{e}_k\,, \quad (i,j,k) \in \{(1,2,3),(2,3,1),(3,1,2)\}\,. \tag{A.12}$$

We will refer to such a set $\{\mathbf{e}_i\}$ as an *orthonormal basis* (also *Cartesian basis*). An arbitrary vector $\mathbf{a}$ can then be uniquely written as

$$\mathbf{a} = a_1\mathbf{e}_1 + a_2\mathbf{e}_2 + a_3\mathbf{e}_3 = \sum_{i=1}^{3} a_i\mathbf{e}_i\,, \tag{A.13}$$

where the a_i are real numbers. With Einstein's summation convention, which says that double indices (here i) automatically imply summation, this can be written in compact form as

$$\mathbf{a} = a_i\mathbf{e}_i\,. \tag{A.14}$$

Since the coefficients a_i are unique for a given basis $\{\mathbf{e}_i\}$, it is possible to represent the vector $\mathbf{a}$ by these coefficients. It is usual to arrange them in a column (number triple) and write

$$\mathbf{a}_{\{\mathbf{e}_i\}} = \begin{pmatrix} a_1 \\ a_2 \\ a_3 \end{pmatrix}\,, \tag{A.15}$$

which is to say, the vector $\mathbf{a}$ is represented by the components a_i with respect to the basis $\{\mathbf{e}_i\}$. Of course, when a different orthonormal basis $\{\mathbf{e}_i^\star\}$ is used, the representation of the vector $\mathbf{a}$ will change:

$$\mathbf{a} = a_i^\star\mathbf{e}_i^\star\,, \tag{A.16}$$

or

$$\mathbf{a}_{\{\mathbf{e}_i^\star\}} = \begin{pmatrix} a_1^\star \\ a_2^\star \\ a_3^\star \end{pmatrix}\,. \tag{A.17}$$

Note that the vector $\mathbf{a}$ is still the same object (arrow in space), whereas its components have changed. It is therefore of great importance to distinguish between vectors themselves and their representation as number triples. Mixing up these two different things is a notorious source of confusion. Only when a single basis $\{\mathbf{e}_i\}$ is defined from the outset, is $\mathbf{a}$ uniquely expressed by

$$\mathbf{a} = \begin{pmatrix} a_1 \\ a_2 \\ a_3 \end{pmatrix}\,. \tag{A.18}$$

In components with respect to a given basis $\{\mathbf{e}_i\}$, the dot product (A.3) can be evaluated as

$$\mathbf{a} \cdot \mathbf{b} = a_i b_i\,, \tag{A.19}$$

and the ith component of the cross product (A.4) is

$$(\mathbf{a} \times \mathbf{b})_i = \varepsilon_{ijk}\, a_j b_k \tag{A.20}$$

(summation over j and k). In the latter expression, ε_{ijk} is called the Levi-Civita symbol or alternator, defined as

$$\varepsilon_{ijk} = \begin{cases} 1\,, & \text{for } (i,j,k) \in \{(1,2,3),\,(2,3,1),\,(3,1,2)\}\,, \\ -1\,, & \text{for } (i,j,k) \in \{(1,3,2),\,(3,2,1),\,(2,1,3)\}\,, \\ 0\,, & \text{otherwise (at least two indices are equal)}\,. \end{cases} \tag{A.21}$$

The dyadic product defined in Eq. (A.9) is expressed as

$$\mathbf{a}\,\mathbf{b} = (a_i \mathbf{e}_i)\,(b_j \mathbf{e}_j) = a_i b_j\, \mathbf{e}_i\, \mathbf{e}_j\,, \tag{A.22}$$

(summation over i and j), where $\mathbf{e}_i\, \mathbf{e}_j$ is the dyadic product of the respective basis vectors.

A.3 Tensors of Order 2

A *tensor* A of order 2 (often simply called a tensor) is defined as a linear transformation which maps vectors on vectors:

$$\mathbf{y} = \mathsf{A} \cdot \mathbf{x}\,. \tag{A.23}$$

Tensors will generally be denoted by sans-serif symbols like A, B, C, etc. We have already encountered special tensors of order 2, namely the dyadic products between two vectors introduced in Eq. (A.9). Their expression with respect to an orthonormal basis $\{\mathbf{e}_i\}$ was given by Eq. (A.22), and similarly a general tensor of order 2 can be written as

$$\mathsf{A} = A_{ij}\, \mathbf{e}_i\, \mathbf{e}_j\,. \tag{A.24}$$

Evidently, the tensor A is represented by the components A_{ij}, and analogous to Eq. (A.15) this can be denoted by

$$\mathsf{A}_{\{\mathbf{e}_i\}} = \begin{pmatrix} A_{11} & A_{12} & A_{13} \\ A_{21} & A_{22} & A_{23} \\ A_{31} & A_{32} & A_{33} \end{pmatrix}\,, \tag{A.25}$$

where the components have been arranged into a square matrix. Again, if a different basis $\{\mathbf{e}_i^\star\}$ is used, the representation will change,

$$\mathsf{A}_{\{\mathbf{e}_i^\star\}} = \begin{pmatrix} A_{11}^\star & A_{12}^\star & A_{13}^\star \\ A_{21}^\star & A_{22}^\star & A_{23}^\star \\ A_{31}^\star & A_{32}^\star & A_{33}^\star \end{pmatrix}\,, \tag{A.26}$$

so that tensors and matrices must be distinguished in the same way as vectors and number triples. Only when a single, fixed basis $\{\mathbf{e}_i\}$ is used, is A uniquely expressed by the square matrix

$$\mathsf{A} = \begin{pmatrix} A_{11} & A_{12} & A_{13} \\ A_{21} & A_{22} & A_{23} \\ A_{31} & A_{32} & A_{33} \end{pmatrix}\,. \tag{A.27}$$

With the representation of Eq. (A.24), the linear transformation (A.23) is given by

$$\begin{aligned} \mathbf{y} &= (A_{ij}\,\mathbf{e}_i\,\mathbf{e}_j)\cdot(x_k\,\mathbf{e}_k) = A_{ij}x_k\,\mathbf{e}_i\,(\mathbf{e}_j\cdot\mathbf{e}_k) \\ &= A_{ij}x_k\,\mathbf{e}_i\,\delta_{jk} = A_{ij}x_j\,\mathbf{e}_i\,, \end{aligned} \tag{A.28}$$

or

$$y_i = A_{ij}x_j\,. \tag{A.29}$$

Evidently, this is nothing else but the matrix-column product

$$\begin{pmatrix} y_1 \\ y_2 \\ y_3 \end{pmatrix} = \begin{pmatrix} A_{11} & A_{12} & A_{13} \\ A_{21} & A_{22} & A_{23} \\ A_{31} & A_{32} & A_{33} \end{pmatrix} \cdot \begin{pmatrix} x_1 \\ x_2 \\ x_3 \end{pmatrix} \tag{A.30}$$

expressed in (Cartesian) *index notation*. Index notation is a very efficient method of carrying out computations in vector/tensor algebra and analysis [see also the expressions (A.19) and (A.20) for the dot product and the cross product, respectively], and we will use it frequently.

The transpose of a tensor A is the unique tensor A^{T} defined by

$$\mathsf{A}^{\mathrm{T}} = A_{ji}\,\mathbf{e}_i\,\mathbf{e}_j\,. \tag{A.31}$$

In matrix form, this reads

$$\mathsf{A}^{\mathrm{T}}_{\{\mathbf{e}_i\}} = \begin{pmatrix} A_{11} & A_{21} & A_{31} \\ A_{12} & A_{22} & A_{32} \\ A_{13} & A_{23} & A_{33} \end{pmatrix}; \tag{A.32}$$

that is, the elements of the original matrix $\mathsf{A}_{\{\mathbf{e}_i\}}$ [Eq. (A.25)] have been mirrored along the main diagonal A_{11}-A_{22}-A_{33}. In index notation, this is expressed by the relation

$$A^{\mathrm{T}}_{ij} = A_{ji}\,. \tag{A.33}$$

A symmetric tensor is defined by

$$\mathsf{A}^{\mathrm{T}} = \mathsf{A} \qquad (A_{ij} = A_{ji})\,, \tag{A.34}$$

whereas for an antisymmetric tensor

$$\mathsf{A}^{\mathrm{T}} = -\mathsf{A} \qquad (A_{ij} = -A_{ji}) \tag{A.35}$$

holds. The latter case implies that all main-diagonal elements (A_{11}, A_{22}, A_{33}) are equal to zero.

An important example for a tensor of order 2 is the unit tensor I, which provides the identity transformation $\mathbf{x} = \mathsf{I}\cdot\mathbf{x}$. Its components in *any* orthonormal basis $\{\mathbf{e}_i\}$ are given by the Kronecker symbol δ_{ij}, that is,

$$\mathsf{I} = \delta_{ij}\,\mathbf{e}_i\,\mathbf{e}_j\,, \tag{A.36}$$

so that its matrix representation is given by the unit matrix,

$$\mathsf{I}_{\{\mathbf{e}_i\}} = \begin{pmatrix} 1 & 0 & 0 \\ 0 & 1 & 0 \\ 0 & 0 & 1 \end{pmatrix} . \tag{A.37}$$

The multiplication of two tensors A and B yields the tensor $\mathsf{A} \cdot \mathsf{B}$ defined by successive application of first B and then A on an arbitrary vector $\mathbf{x}$,

$$(\mathsf{A} \cdot \mathsf{B}) \cdot \mathbf{x} = \mathsf{A} \cdot (\mathsf{B} \cdot \mathbf{x}) . \tag{A.38}$$

By expressing the two tensors according to Eq. (A.24), we find

$$\begin{aligned} \mathsf{A} \cdot (\mathsf{B} \cdot \mathbf{x}) &= (A_{ij}\, \mathbf{e}_i\, \mathbf{e}_j) \cdot [(B_{kl}\, \mathbf{e}_k\, \mathbf{e}_l) \cdot (x_m\, \mathbf{e}_m)] \\ &= (A_{ij}\, \mathbf{e}_i\, \mathbf{e}_j) \cdot (B_{kl} x_l\, \mathbf{e}_k) \\ &= A_{ij} B_{kl} x_l\, \mathbf{e}_i\, (\mathbf{e}_j \cdot \mathbf{e}_k) \\ &= A_{ij} B_{kl} x_l\, \mathbf{e}_i\, \delta_{jk} \\ &= A_{ij} B_{jl} x_l\, \mathbf{e}_i \\ \Rightarrow\ \mathsf{A} \cdot \mathsf{B} &= A_{ij} B_{jl}\, \mathbf{e}_i\, \mathbf{e}_l , \quad \text{or} \quad (\mathsf{A} \cdot \mathsf{B})_{il} = A_{ij} B_{jl} . \end{aligned} \tag{A.39}$$

This represents the familiar matrix multiplication

$$(\mathsf{A} \cdot \mathsf{B})_{\{\mathbf{e}_i\}} = \begin{pmatrix} A_{11} & A_{12} & A_{13} \\ A_{21} & A_{22} & A_{23} \\ A_{31} & A_{32} & A_{33} \end{pmatrix} \cdot \begin{pmatrix} B_{11} & B_{12} & B_{13} \\ B_{21} & B_{22} & B_{23} \\ B_{31} & B_{32} & B_{33} \end{pmatrix} . \tag{A.40}$$

The above rules can be extended to the multiplication of more than two tensors (e.g., $\mathsf{A} \cdot \mathsf{B} \cdot \mathsf{C}$), and powers of a tensor A are defined by

$$\mathsf{A}^2 = \mathsf{A} \cdot \mathsf{A} , \quad \mathsf{A}^3 = \mathsf{A} \cdot \mathsf{A} \cdot \mathsf{A} , \quad \text{etc.} \tag{A.41}$$

Note that the multiplication of tensors is associative, but in general not commutative.

An order 2 tensor A in three-dimensional space has three independent scalar invariants. If A is represented by the matrix $\mathsf{A}_{\{\mathbf{e}_i\}}$ [Eq. (A.25)], the invariants are

$$\begin{aligned} I_{\mathsf{A}} &= \operatorname{tr} \mathsf{A} = A_{11} + A_{22} + A_{33} , \\ II_{\mathsf{A}} &= \tfrac{1}{2} [\operatorname{tr} (\mathsf{A}^2) - (\operatorname{tr} \mathsf{A})^2] \\ &= A_{12}A_{21} + A_{13}A_{31} + A_{23}A_{32} - A_{11}A_{22} - A_{11}A_{33} - A_{22}A_{33} , \\ III_{\mathsf{A}} &= \det \mathsf{A} = \tfrac{1}{6} [2 \operatorname{tr} (\mathsf{A}^3) - 3 \operatorname{tr} \mathsf{A} \operatorname{tr} (\mathsf{A}^2) + (\operatorname{tr} \mathsf{A})^3] \\ &\qquad = A_{11}A_{22}A_{33} + A_{12}A_{23}A_{31} + A_{13}A_{21}A_{32} \\ &\qquad - A_{11}A_{23}A_{32} - A_{12}A_{21}A_{33} - A_{13}A_{22}A_{31} . \end{aligned} \tag{A.42}$$

The important point is that these scalar invariants do not depend on the particular basis; that is, the same values are obtained when they are computed with a different matrix representation $\mathsf{A}_{\{\mathbf{e}_i^\star\}}$. The first ($I_\mathsf{A}$) and third ($III_\mathsf{A}$) invariants are also called the trace and determinant of the tensor A, respectively. For the determinant, a useful expression in index notation is

$$\det \mathsf{A} = \tfrac{1}{6}\varepsilon_{ijk}\varepsilon_{lmn}A_{il}A_{jm}A_{kn}\,, \tag{A.43}$$

which involves a sixfold summation and the Levi-Civita symbol defined in Eq. (A.21).

The inverse A^{-1} of the tensor A is defined by the relations

$$\mathsf{A}\cdot\mathsf{A}^{-1} = \mathsf{A}^{-1}\cdot\mathsf{A} = \mathsf{I}\,. \tag{A.44}$$

It only exists if the determinant of A is not equal to zero:

$$\det \mathsf{A} \neq 0 \quad \Leftrightarrow \quad \exists \mathsf{A}^{-1}: \text{ Eq. (A.44) fulfilled}\,. \tag{A.45}$$

When expressed in component form, a tensor of order 2 is a quantity with two indices [see Eq. (A.24)]. As we have seen in Sect. A.2, the expression of a vector in component form leads to a quantity with one index (for instance, a_i), and a scalar quantity, of course, does not have any indices at all. Therefore, vectors and scalars are also referred to as tensors of order 1 and 0, respectively.

A.4 Higher Order Tensors

As a generalisation of Eq. (A.23), tensors $\mathsf{A}^{[r]}$ of order $r > 2$ can be defined inductively as linear transformations which map vectors $\mathbf{x}$ on tensors $\mathsf{Y}^{[r-1]}$ of order $r-1$,

$$\mathsf{Y}^{[r-1]} = \mathsf{A}^{[r]}\cdot\mathbf{x}\,. \tag{A.46}$$

Such tensors can be written in component form as

$$\mathsf{A}^{[r]} = A_{i_1 i_2 \ldots i_r}\,\mathbf{e}_{i_1}\,\mathbf{e}_{i_2}\ldots\mathbf{e}_{i_r} \tag{A.47}$$

(summation over the r indices i_1, i_2, ..., i_r). As an example, the Levi-Civita symbol (A.21) can be interpreted as the components of an order 3 tensor $\epsilon^{[3]}$,

$$\epsilon^{[3]} = \varepsilon_{ijk}\,\mathbf{e}_i\,\mathbf{e}_j\,\mathbf{e}_k\,, \tag{A.48}$$

which is known as the epsilon or permutation tensor. Tensors of order 4 play a role in the theories of elasticity and visco-elasticity.

The tensor multiplication introduced in Eq. (A.39) can be generalised to tensors of arbitrary orders $\mathsf{A}^{[r]}$ and $\mathsf{B}^{[s]}$, and the result is a tensor of order $r+s-2$,

$$\begin{aligned}
\mathsf{A}^{[r]}\cdot\mathsf{B}^{[s]} &= (A_{i_1 i_2\ldots i_r}\,\mathbf{e}_{i_1}\,\mathbf{e}_{i_2}\ldots\mathbf{e}_{i_r})\cdot(B_{j_1 j_2\ldots j_s}\,\mathbf{e}_{j_1}\,\mathbf{e}_{j_2}\ldots\mathbf{e}_{j_s}) \\
&= A_{i_1 i_2\ldots i_r}B_{j_1 j_2\ldots j_s}\,\mathbf{e}_{i_1}\,\mathbf{e}_{i_2}\ldots\mathbf{e}_{i_{r-1}}\,(\mathbf{e}_{i_r}\cdot\mathbf{e}_{j_1})\,\mathbf{e}_{j_2}\ldots\mathbf{e}_{j_s} \\
&= A_{i_1 i_2\ldots i_r}B_{j_1 j_2\ldots j_s}\delta_{i_r j_1}\,\mathbf{e}_{i_1}\,\mathbf{e}_{i_2}\ldots\mathbf{e}_{i_{r-1}}\,\mathbf{e}_{j_2}\ldots\mathbf{e}_{j_s} \\
&= A_{i_1 i_2\ldots i_r}B_{i_r j_2\ldots j_s}\,\mathbf{e}_{i_1}\,\mathbf{e}_{i_2}\ldots\mathbf{e}_{i_{r-1}}\,\mathbf{e}_{j_2}\ldots\mathbf{e}_{j_s}\,.
\end{aligned} \tag{A.49}$$

This operation is called tensor contraction. The dot product (A.3) between two vectors, the tensor-vector multiplications (A.23) and (A.46) as well as the tensor multiplication (A.39) can all be considered as special cases of the general tensor contraction (A.49).

Further, the dyadic product between two vectors [Eqs. (A.9), (A.22)] can be readily generalised to arbitrary tensors $\mathsf{A}^{[r]}$ and $\mathsf{B}^{[s]}$,

$$\begin{aligned} \mathsf{A}^{[r]}\,\mathsf{B}^{[s]} &= (A_{i_1 i_2 \ldots i_r}\,\mathbf{e}_{i_1}\,\mathbf{e}_{i_2}\ldots\mathbf{e}_{i_r})\,(B_{j_1 j_2 \ldots j_s}\,\mathbf{e}_{j_1}\,\mathbf{e}_{j_2}\ldots\mathbf{e}_{j_s}) \\ &= A_{i_1 i_2 \ldots i_r} B_{j_1 j_2 \ldots j_s}\,\mathbf{e}_{i_1}\,\mathbf{e}_{i_2}\ldots\mathbf{e}_{i_r}\,\mathbf{e}_{j_1}\,\mathbf{e}_{j_2}\ldots\mathbf{e}_{j_s}\,, \end{aligned} \tag{A.50}$$

which is called tensor product. The result is a tensor of order $r + s$.

A.5 Vector and Tensor Analysis

In physical applications like the continuum-mechanical modelling of ice sheets and glaciers, we are often concerned with scalar, vector or tensor *fields*, in which the respective quantities depend on space and time. Let us assume a fixed orthonormal basis $\{\mathbf{e}_1, \mathbf{e}_2, \mathbf{e}_3\}$ (or $\{\mathbf{e}_x, \mathbf{e}_y, \mathbf{e}_z\}$), then space can be described by the Cartesian coordinates x_1, x_2, x_3 (or x, y, z), and time is designated by the variable t.

Partial derivatives of a scalar field $\lambda(x_1, x_2, x_3, t)$ will be denoted by the alternative notations

$$\frac{\partial\lambda}{\partial t} = \lambda_{,t}\,, \qquad \frac{\partial\lambda}{\partial x_1} = \frac{\partial\lambda}{\partial x} = \lambda_{,1} = \lambda_{,x}\,, \qquad \text{etc.} \tag{A.51}$$

For a vector field $\mathbf{a}(x_1, x_2, x_3, t)$,

$$\begin{aligned} \frac{\partial\mathbf{a}}{\partial t} = \mathbf{a}_{,t} &= \frac{\partial(a_i\,\mathbf{e}_i)}{\partial t} = \frac{\partial a_i}{\partial t}\,\mathbf{e}_i = a_{i,t}\,\mathbf{e}_i\,, \\ \frac{\partial\mathbf{a}}{\partial x_1} = \frac{\partial\mathbf{a}}{\partial x} = \mathbf{a}_{,1} = \mathbf{a}_{,x} &= \frac{\partial(a_i\,\mathbf{e}_i)}{\partial x_1} = \frac{\partial a_i}{\partial x_1}\,\mathbf{e}_i = a_{i,1}\,\mathbf{e}_i\,, \\ &\text{etc.}\,, \end{aligned} \tag{A.52}$$

and analogous for order 2 and higher order tensor fields.

The nabla operator ∇ is defined in terms of spatial partial derivative operators as

$$\nabla = \mathbf{e}_x\frac{\partial}{\partial x} + \mathbf{e}_y\frac{\partial}{\partial y} + \mathbf{e}_z\frac{\partial}{\partial z} = \mathbf{e}_i\frac{\partial}{\partial x_i}\,. \tag{A.53}$$

It is useful in order to introduce the gradient of a scalar field,

$$\operatorname{grad}\lambda = \nabla\lambda = \frac{\partial\lambda}{\partial x}\,\mathbf{e}_x + \frac{\partial\lambda}{\partial y}\,\mathbf{e}_y + \frac{\partial\lambda}{\partial z}\,\mathbf{e}_z = \frac{\partial\lambda}{\partial x_i}\,\mathbf{e}_i = \lambda_{,i}\,\mathbf{e}_i\,, \tag{A.54}$$

the divergence of a vector field,

$$\operatorname{div}\mathbf{a} = \nabla\cdot\mathbf{a} = \frac{\partial a_x}{\partial x} + \frac{\partial a_y}{\partial y} + \frac{\partial a_z}{\partial z} = \frac{\partial a_i}{\partial x_i} = a_{i,i}\,, \tag{A.55}$$

the curl of a vector field,

$$\begin{aligned}\operatorname{curl}\mathbf{a} &= \nabla\times\mathbf{a}\\ &= \left(\frac{\partial a_z}{\partial y}-\frac{\partial a_y}{\partial z}\right)\mathbf{e}_x+\left(\frac{\partial a_x}{\partial z}-\frac{\partial a_z}{\partial x}\right)\mathbf{e}_y+\left(\frac{\partial a_y}{\partial x}-\frac{\partial a_x}{\partial y}\right)\mathbf{e}_z\\ &= \varepsilon_{ijk}\,\frac{\partial a_k}{\partial x_j}\,\mathbf{e}_i=\varepsilon_{ijk}\,a_{k,j}\,\mathbf{e}_i\,,\end{aligned}\tag{A.56}$$

and the Laplacian of a scalar field,

$$\begin{aligned}\Delta\lambda &= \operatorname{div}\operatorname{grad}\lambda=\nabla^2\lambda\\ &= \frac{\partial^2\lambda}{\partial x^2}+\frac{\partial^2\lambda}{\partial y^2}+\frac{\partial^2\lambda}{\partial z^2}=\frac{\partial}{\partial x_i}\left(\frac{\partial\lambda}{\partial x_i}\right)=\lambda_{,ii}\,.\end{aligned}\tag{A.57}$$

These expressions can be generalised to tensor fields

$$\mathsf{A}^{[r]}(x_1,x_2,x_3,t)=A_{i_1i_2\ldots i_r}(x_1,x_2,x_3,t)\,\mathbf{e}_{i_1}\,\mathbf{e}_{i_2}\ldots\mathbf{e}_{i_r}\tag{A.58}$$

of order $r\geq 1$ as follows:

$$\begin{aligned}\operatorname{grad}\mathsf{A}^{[r]} &= \frac{\partial A_{i_1i_2\ldots i_r}}{\partial x_j}\,\mathbf{e}_{i_1}\,\mathbf{e}_{i_2}\ldots\mathbf{e}_{i_r}\,\mathbf{e}_j\\ &= A_{i_1i_2\ldots i_r,j}\,\mathbf{e}_{i_1}\,\mathbf{e}_{i_2}\ldots\mathbf{e}_{i_r}\,\mathbf{e}_j \qquad (\text{order } r+1)\,,\end{aligned}\tag{A.59}$$

$$\begin{aligned}\operatorname{div}\mathsf{A}^{[r]} &= \frac{\partial A_{i_1i_2\ldots i_{r-1}j}}{\partial x_j}\,\mathbf{e}_{i_1}\,\mathbf{e}_{i_2}\ldots\mathbf{e}_{i_{r-1}}\\ &= A_{i_1i_2\ldots i_{r-1}j,j}\,\mathbf{e}_{i_1}\,\mathbf{e}_{i_2}\ldots\mathbf{e}_{i_{r-1}} \qquad (\text{order } r-1)\,,\end{aligned}\tag{A.60}$$

$$\begin{aligned}\operatorname{curl}\mathsf{A}^{[r]} &= \varepsilon_{ijk}\,\frac{\partial A_{i_1i_2\ldots i_{r-1}k}}{\partial x_j}\,\mathbf{e}_{i_1}\,\mathbf{e}_{i_2}\ldots\mathbf{e}_{i_{r-1}}\,\mathbf{e}_i\\ &= \varepsilon_{ijk}\,A_{i_1i_2\ldots i_{r-1}k,j}\,\mathbf{e}_{i_1}\,\mathbf{e}_{i_2}\ldots\mathbf{e}_{i_{r-1}}\,\mathbf{e}_i \quad (\text{order } r)\,,\end{aligned}\tag{A.61}$$

$$\begin{aligned}\Delta\mathsf{A}^{[r]} &= \frac{\partial}{\partial x_j}\left(\frac{\partial A_{i_1i_2\ldots i_r}}{\partial x_j}\right)\mathbf{e}_{i_1}\,\mathbf{e}_{i_2}\ldots\mathbf{e}_{i_r}\\ &= A_{i_1i_2\ldots i_r,jj}\,\mathbf{e}_{i_1}\,\mathbf{e}_{i_2}\ldots\mathbf{e}_{i_r} \qquad (\text{order } r)\,.\end{aligned}\tag{A.62}$$

For the sake of simplicity, we refrain from giving the corresponding expressions for curvilinear coordinates like cylindrical coordinates, spherical coordinates etc., and refer the interested reader to the mathematical literature (e.g., Heinbockel 1996) instead.

Let us finally note two important integral theorems. The divergence theorem relates the integral of the divergence of a vector field $\mathbf{a}$ over a volume ω and the integral of the "flux" of $\mathbf{a}$ through the surface $\partial\omega$,

$$\int_\omega(\operatorname{div}\mathbf{a})\,\mathrm{d}v=\oint_{\partial\omega}\mathbf{a}\cdot\mathbf{n}\,\mathrm{d}a\,,\tag{A.63}$$

where $\mathrm{d}v$ is the volume increment, $\mathrm{d}a$ the surface increment and $\mathbf{n}$ the outer unit normal vector on $\partial\omega$. The curl theorem states that the integral of the curl of a vector field $\mathbf{a}$ over a surface σ equals the line integral of $\mathbf{a}$ over the curve $\partial\sigma$ bounding the surface,

$$\int_{\sigma} (\operatorname{curl} \mathbf{a}) \cdot \mathbf{n} \, \mathrm{d}a = \oint_{\partial\sigma} \mathbf{a} \cdot \, \mathrm{d}\mathbf{l} \,, \tag{A.64}$$

where $\mathrm{d}\mathbf{l}$ is the vectorial line increment along the curve $\partial\sigma$.

B Basic Numerics

Methods for Numerical Solution of Differential Equations

- Finite Differences. ←
- Finite Elements.
- Finite Volumes.

Idea of the Finite Difference Method

- Introduce a discrete grid.
- Approximate derivatives by difference quotients at grid points.

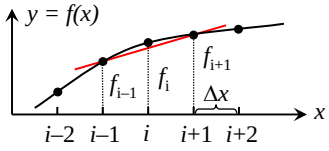

$$\left.\frac{\mathrm{d}f}{\mathrm{d}x}\right|_i \sim \frac{f_{i+1}-f_{i-1}}{2\Delta x}$$

Types of Difference Quotients

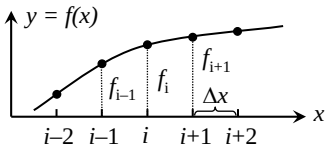

Central:

$$\left.\frac{\mathrm{d}f}{\mathrm{d}x}\right|_i \sim \frac{f_{i+1}-f_{i-1}}{2\Delta x}, \qquad \left.\frac{\mathrm{d}f}{\mathrm{d}x}\right|_i \sim \frac{f_{i+1/2}-f_{i-1/2}}{\Delta x}$$

One-sided:

$$\left.\frac{\mathrm{d}f}{\mathrm{d}x}\right|_i \sim \frac{f_{i+1}-f_i}{\Delta x}, \qquad \left.\frac{\mathrm{d}f}{\mathrm{d}x}\right|_i \sim \frac{f_i-f_{i-1}}{\Delta x}$$

Central, second derivative:

$$\left.\frac{\mathrm{d}^2 f}{\mathrm{d}x^2}\right|_i = \left.\frac{\mathrm{d}}{\mathrm{d}x}\frac{\mathrm{d}f}{\mathrm{d}x}\right|_i \sim \frac{\left.\frac{\mathrm{d}f}{\mathrm{d}x}\right|_{i+1/2} - \left.\frac{\mathrm{d}f}{\mathrm{d}x}\right|_{i-1/2}}{\Delta x} \sim \frac{\frac{f_{i+1}-f_i}{\Delta x} - \frac{f_i-f_{i-1}}{\Delta x}}{\Delta x}$$

$$= \frac{f_{i+1}-2f_i+f_{i-1}}{\Delta x^2}$$

Example: 1-D Heat-Conduction Equation

Partial differential equation:

$$\frac{\partial T}{\partial t} = k \frac{\partial^2 T}{\partial x^2}$$

→ requires discrete grid in space (index *i*) and time (index *m*).

Forward-time central-space (FTCS) scheme:

$$\left.\frac{\partial T}{\partial t}\right|_{i,m} \sim \frac{T_{i,m+1} - T_{i,m}}{\Delta t}, \quad \left.\frac{\partial^2 T}{\partial x^2}\right|_{i,m} \sim \frac{T_{i+1,m} - 2T_{i,m} + T_{i-1,m}}{\Delta x^2}$$

$$\Rightarrow \frac{T_{i,m+1} - T_{i,m}}{\Delta t} = \frac{k}{\Delta x^2} \left(T_{i+1,m} - 2T_{i,m} + T_{i-1,m}\right)$$

$$\Rightarrow T_{i,m+1} = T_{i,m} + \frac{k\Delta t}{\Delta x^2} \left(T_{i+1,m} - 2T_{i,m} + T_{i-1,m}\right)$$

The FTCS scheme can be integrated time step by time step, provided that initial conditions for $t = t_{\text{init}}$ ($m = 1$) and boundary conditions for $x = x_{\text{min}}$ ($i = 1$) and $x = x_{\text{max}}$ ($i = i_{\text{max}}$) are known.

Courant-Friedrichs-Lewy (CFL) condition:

$$\Delta t < \frac{\Delta x^2}{2k}$$

Necessary condition for numerical stability. If violated, the FTCS scheme will produce wildly incorrect results!

References

Abramowitz, M. and I. A. Stegun. 1970. *Handbook of Mathematical Functions with Formulars, Graphs, and Mathematical Tables*. Dover Publications, New York, NY, USA.

Bindoff, N. L., J. Willebrand, V. Artale, A. Cazenave, J. Gregory, S. Gulev, K. Hanawa, C. Le Quéré, S. Levitus, Y. Nojiri, C. K. Shum, L. D. Talley and A. Unnikrishnan. 2007. Observations: Oceanic climate change and sea level. In: S. Solomon, D. Qin, M. Manning, Z. Chen, M. Marquis, K. B. Averyt, M. Tignor and H. L. Miller (Eds.), *Climate Change 2007: The Physical Science Basis. Contribution of Working Group I to the Fourth Assessment Report of the Intergovernmental Panel on Climate Change*, pp. 385–432. Cambridge University Press, Cambridge, UK, and New York, NY, USA. URL `http://ipcc-wg1.ucar.edu/wg1/wg1-report.html`.

Bronshtein, I. N., K. A. Semendyayev, G. Musiol and H. Muehlig. 2004. *Handbook of Mathematics*. Springer, Berlin, Germany etc., 4th ed.

Brotchie, J. F. and R. Silvester. 1969. On crustal flexure. *Journal of Geophysical Research*, **74** (22), 5240–5252.

Bueler, E. 2003. Construction of steady state solutions for isothermal shallow ice sheets. Tech. Rep. 03-02, Department of Mathematics and Statistics, University of Alaska, Fairbanks.

Bueler, E., C. S. Lingle, J. A. Kallen-Brown, D. N. Covey and L. N. Bowman. 2005. Exact solutions and verification of numerical models for isothermal ice sheets. *Journal of Glaciology*, **51** (173), 291–306.

Durand, G., O. Gagliardini, B. de Fleurian, T. Zwinger and E. Le Meur. 2009a. Marine ice sheet dynamics: Hysteresis and neutral equilibrium. *Journal of Geophysical Research*, **114** (F3), F03009. doi:10.1029/2008JF001170.

Durand, G., O. Gagliardini, T. Zwinger, E. Le Meur and R. C. A. Hindmarsh. 2009b. Full Stokes modeling of marine ice sheets: influence of the grid size. *Annals of Glaciology*, **50** (52), 109–114.

Faria, S. H. 2003. *Mechanics and thermodynamics of mixtures with continuous diversity*. Doctoral thesis, Department of Mechanics, Darmstadt University of Technology, Germany. URL `http://tuprints.ulb.tu-darmstadt.de/307/`.

Glen, J. W. 1955. The creep of polycrystalline ice. *Proceedings of the Royal Society London A*, **228** (1175), 519–538. doi:10.1098/rspa.1955.0066.

Greve, R. and H. Blatter. 2009. *Dynamics of Ice Sheets and Glaciers*. Springer, Berlin, Germany etc. ISBN 978-3-642-03414-5.

Heinbockel, J. H. 1996. *Introduction to Tensor Calculus and Continuum Mechanics*. Trafford Publishing, Victoria, BC, Canada and Oxford, UK. ISBN 1-55369-133-4. Free online version available at http://www.math.odu.edu/∼jhh/counter2.html (retrieved 2009-03-11).

Hooke, R. L. 2005. *Principles of Glacier Mechanics*. Cambridge University Press, Cambridge, UK and New York, NY, USA, 2nd ed.

Hutter, K. 1983. *Theoretical Glaciology; Material Science of Ice and the Mechanics of Glaciers and Ice Sheets*. D. Reidel Publishing Company, Dordrecht, The Netherlands.

Hutter, K. and K. Jöhnk. 2004. *Continuum Methods of Physical Modeling*. Springer, Berlin, Germany etc.

Huybrechts, P., A. J. Payne and EISMINT Intercomparison Group. 1996. The EISMINT benchmarks for testing ice-sheet models. *Annals of Glaciology*, **23**, 1–12.

Lemke, P., J. Ren, R. B. Alley, I. Allison, J. Carrasco, G. Flato, Y. Fujii, G. Kaser, P. Mote, R. H. Thomas and T. Zhang. 2007. Observations: Changes in snow, ice and frozen ground. In: S. Solomon, D. Qin, M. Manning, Z. Chen, M. Marquis, K. B. Averyt, M. Tignor and H. L. Miller (Eds.), *Climate Change 2007: The Physical Science Basis. Contribution of Working Group I to the Fourth Assessment Report of the Intergovernmental Panel on Climate Change*, pp. 337–383. Cambridge University Press, Cambridge, UK, and New York, NY, USA. URL `http://ipcc-wg1.ucar.edu/wg1/wg1-report.html`.

Liu, I.-S. 2002. *Continuum Mechanics*. Springer, Berlin, Germany etc.

Morland, L. W. 1984. Thermomechanical balances of ice sheet flows. *Geophysical and Astrophysical Fluid Dynamics*, **29**, 237–266.

Morland, L. W. 1987. Unconfined ice-shelf flow. In: C. J. van der Veen and J. Oerlemans (Eds.), *Dynamics of the West Antarctic Ice Sheet*, pp. 99–116. D. Reidel Publishing Company, Dordrecht, The Netherlands.

Nye, J. F. 1957. The distribution of stress and velocity in glaciers and ice sheets. *Proceedings of the Royal Society London A*, **239** (1216), 113–133. doi:10.1098/rspa.1957.0026.

Paterson, W. S. B. 1994. *The Physics of Glaciers*. Pergamon Press, Oxford, UK etc., 3rd ed.

Ritz, C. 1987. Time dependent boundary conditions for calculation of temperature fields in ice sheets. In: E. D. Waddington and J. S. Walder (Eds.), *The Physical Basis of Ice Sheet Modelling*, IAHS Publication No. 170, pp. 207–216. IAHS Press, Wallingford, UK.

van der Veen, C. J. 1999. *Fundamentals of Glacier Dynamics*. A. A. Balkema, Rotterdam, The Netherlands.

Vialov, S. S. 1958. Regularities of glacial shields movement and the theory of plastic viscous flow. In: *Physics of the Motion of Ice*, IAHS Publication No. 47, pp. 266–275. IAHS Press, Wallingford, UK.